EXPERIMENTS IN A ROTATING SOURCE-SINK ANNULUS

by

RICHARD GRANT INGRAM

B.S., McGill University
(1965)

M.S., McGill University
(1967)

SUBMITTED IN PARTIAL FULFILLMENT OF THE
REQUIREMENTS FOR THE DEGREE OF
DOCTOR OF PHILOSOPHY

at the

MASSACHUSETTS INSTITUTE OF TECHNOLOGY

and the

WOODS HOLE OCEANOGRAPHIC INSTITUTION

August, 1971

Signature of Author _____
Joint Program in Oceanography, Massachusetts
Institute of Technology - Woods Hole Oceano-
graphic Institution, Department of Earth and
Planetary Sciences, and Department of Meteor-
ology, Massachusetts Institute of Technology,
August, 1971

Certified by_ _____
Thesis Supervisor

Accepted by_____
Chairman, Joint Oceanography Committee in the
Earth Sciences, Massachusetts Institute of
Technology - Woods Hole Oceanographic Institution

EXPERIMENTS IN A ROTATING SOURCE-SINK ANNULUS

by

Richard Grant Ingram

ABSTRACT

An experimental investigation of the different flow regimes in
a rotating source-sink annulus is described. Both the steady and
transient velocities are measured over a large range of Ekman Rey-
nolds number and Rossby number. Differing probe configurations are
used to investigate the corresponding motions in spatially separated
regions of the annulus.

The steady interior circulation field exhibits a strong depen-
dence on the imposed flux values. The non-dimensional circulation
increases with radius over a certain radial range for higher system
Rossby number. The observed profile changes are related to the ex-
istence of an unstable Ekman layer at some inner radial position.

The thickness of the observed Ekman layers is typically 85% of
the theoretical. . For higher local Reynolds number (Re_L),
the thickness is generally much smaller. The width of the sidewall
boundary layer adjacent to the sink increases with larger system
Rossby number. Adjacent to the source, the radial boundary layer
is wider than that at the sink wall.

Observed oscillations are separable into three types. For Re_L
> 50, instability waves are observed in the Ekman layer flow.
In the same Re_L range, inertial oscillations are detected in the in-
terior region of the annulus. The observed inertial wave frequency
at differing radial positions is explained by incorporating Doppler
shift corrections and taking account of the steady circulation pro-
files. The radial wavelength of the inertial waves corresponds to
the length of the Class A Ekman layer instability. For small values
of Re_L and local Rossby number, an axisymmetric disturbance, with
a characteristic frequency slightly greater than the rotation rate,
is observed at the outer radial positions.

Thesis Supervisor: Erik Mollo-Christensen
Title: Professor of Meteorology

2.

ACKNOWLEDGEMENTS

3.

TABLE OF CONTENTS

4.

LIST OF FIGURES

LIST OF FIGURES (Cont.)

LIST OF FIGURES (Cont.)

CHAPTER I

Introduction

The motions observed in both the seas and the atmosphere exhibit a wide range of scales, and are found to depend on an interplay of many factors. In order to avoid an inordinate degree of complexity most investigators isolate a single process to study in detail. The synthesis of independent works may then bring greater understanding to the overall picture. The present work will focus on mean geostrophic flows, the inherent boundary layers, and the structure of waves emitted into the interior through the use of a laboratory model. Concurrent characteristics of stratification and turbulence, found in nature, will not be examined. As with most laboratory simulations of a geophysical process, the model itself evolves peripheral problems, which, in the opinion of the present writer, are interesting in themselves, but seemingly have little relevance to the original phenomena. The aim remains throughout, to relate the experimental findings to analogous geophysical effects.

The structure of the boundary layers formed at the air-sea interface and the ocean's bottom was first described theoretically by Ekman (1905). This important work showed the significant role played by the earth's rotation in influencing large scale ocean circulation. It was also in Ekman's paper that the existence of a skewed boundary layer of uniform thickness at the ocean's top and bottom was postulated. These boundary layers, which result from a balance of viscous and Coriolis forces, are known as "Ekman layers". Ekman also found that the transient response of a rotating system to a change in forcing was the generation of inertial waves in the interior portion of the flow. This concept resembles earlier theories of Kelvin (1880).

Since Ekman's time, the concept of a steady Ekman layer has been used as a tool in explaining many of the features observed in oceanic phenomena. In general, the observational evidence showing the existence of such layers on a local scale has been difficult to come by. There is little doubt that a skewed boundary layer exists; Brennecke (1921) in the Weddell Sea, and Swallow and Bruce (1966) in the area of the Somali current have both observed it. More recently, Gonella (1968) found a clearly defined Ekman-like spiral in the wind mixed layer, at large wind speeds from a fixed buoy in the Mediterranean. The discrepancies usually arise in the comparison of vertical structure, with the actual spiral showing only a slight resemblance to theory. The reasons why this lack exists is readily found in the nature of the driving forces - such as the wind, the spectra of which usually shows most of its energy at frequencies much higher than that of inertial (Ingram, 1967). To date, Hunkin's (1966) observations under Drift Station Alpha in the Arctic Ocean, provide the best fit between nature and classical theory; whereby the massive inertia of the ice island damps out smaller scale transients, so that the forcing appears quasi-steady.

The inertial oscillations mentioned by Ekman and others were unobserved in the open oceans for many years. However, their existence has been detected in smaller seas (Gustafson & Kullenberg, 1933). Only in the last decade has a large amount of information been compiled about their structure in the deep ocean, resulting mainly from the implementation of long term moored current meters. Hunkins (1966), Knauss (1964), Webster (1963), Day and Webster (1965), and Pollard and Millard (1970) are amongst those who have both observed, and in some cases, attempted to explain the amplitude and spatial coherence of these motions.

During the last three decades, experimental and theoretical work on

"laboratory" Ekman layers has been advancing at a rate chronologically similar to the observational program. Two models have been used; a rotating disk in still air, and a rotating annulus with an axisymmetric peripheral source and sink.

. The annular configuration produces an interior potential vortex bounded by non-divergent Ekman layers on the horizontal solid boundaries. It was hypothesized that in such an experimental set-up, both the steady and unsteady boundary layers could be observed, and perhaps, the dynamical features could be compared to analogous structure in nature. However, the experimental and natural environments differ substantially in their viscous properties. Since in the laboratory, the viscous action is predominantly of a laminar form, whereas in the sea, "turbulent eddy" viscosity dominates. Furthermore, stratification, which plays a significant role in the ocean, is a difficult parameter to model experimentally in a source sink annulus.

Using a source sink annulus, as indicated above, it is possible to study the transfer of energy from boundary layers to the interior. This energy transfer is accomplished by the Reynolds stresses generated through instabilities of the Ekman layer. The occurence of these instabilities has been studied (Faller, 1963), and found to be the function of the Ekman layer, rotational Reynolds number. Since a mechanism exists for exciting interior wave motions it would seem appropriate to inquire if analogous oceanic phenomena may be explained similarly. The energies produced by similar dynamics in the ocean are small when compared to the competing mechanisms; nevertheless, their contribution may be important under optimum conditions (see Faller [1963]).

Early annulus experimenters, employing mainly dye techniques in water were able to observe qualitative features of the steady flow and some quasi-steady disturbances. In most cases, these experiments employed equipment having a free surface. More recently a quantitative approach has been used in annuli having a rigid top and bottom. These latter findings have introduced many more queries as to the dynamics of source sink annulus flows. Until the underlying physics is explained, it is difficult to compare experimental results to geophysical observations. With this in mind, the present work is an attempt to both observe and explain the transient and steady motions in all regions of the annulus.

The study of vortices is not a new one to M.I.T., as in the 1860's, William Barton Rogers, founder of the school, was involved in this work and published a paper in the field. With such an ancestry, it is appropriate that some of the above aims should be furthered at this institution.

CHAPTER II

Background Literature

The experimental work done previously in the field of Ekman layer in-stabilities has followed two paths, both from a configurational and a chronological sense. Earlier work, which resulted from an interest in the dynamics of flow over a delta wing and quickly rotating objects, focused on the motions produced by a disk rotating in still air. Later, source-sink rotating annuli, with the sink located peripherally on the inner cylinder and the source likewise on the outer wall, were used to study laminar Ekman layers and their inherent instabilities.

The early experiments in rotating boudary layers were those of Theodorsen and Regier (1944), using a fixed hot wire anemometer probe located over a rotating disk in air. They found a transition Reynolds number for the boundary flow at which sinusoidal oscillations were gen-erated. In a similar manner, Smith (1945) made hot wire anemometer measurements over a rotating disk, but at different radii and with a double probe. He found a range of critical Reynolds number, for insta-bility onset, slightly lower, but comparable to the values of Therodor-sen and Regier. Using the double probe, Smith was able to measure the phase velocity and orientation of the disturbances. It was found that they propagated inward at an angle of 14° from the azimuthal direction with a speed of order 0.2 of the azimuthal velocity. Although the results shown are similar to those depicted by Tatro (1966), the insta-bility structure Smith found has characteristics of both the Class A and B waves mentioned by Greenspan (1968, sect. 6.3).

Later, Gregory, Stuart and Walker (1955) studied the onset of boundary layer instabilities using two techniques: china clay streaks and a sonic probe. In this paper, Stuart solved the inviscid stability problem for a rotating disk, by postulating that the instability was centered near the inflection point in the vertical velocity profile. He indicated that the instabilities took the form of a series of horizontal roll vortices in spiral bands and whose velocity, orientation and spacing were predictable theoretically. But for the lateral spacing, his results were well matched with experimental evidence.

The china clay techniques of observation allowed Gregory and Walker to view the disturbances as a group of equiangular spiral vortices distributed azimuthally on the disk, which would alternately provide regions of convergence and divergence. The critical Reynolds number ($Re^1 = \frac{\Omega r \delta}{\nu} = \frac{r}{\delta}$, where δ = Ekman layer depth) was found to be 435, lower than those reported by previous workers. In another series of experiments, using a sonic probe to sense small pressure fluctuations, they obtained a range of 408 to 445 for the critical Reynolds number and a series of spectra showing a prevalence of rotation rate harmonics.

More recently, the path chosen by both theorists and experimenters has been a study of rotating source-sink annuli as seen in figure 2.1
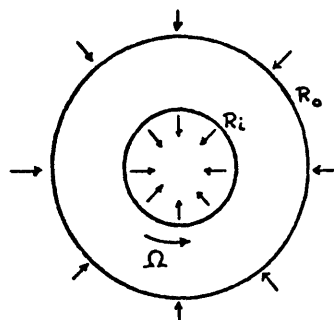
Figure 2.1. Horizontal cross-section of annulus, showing imposed mass flux through vertical walls.

The rationale for choosing this container is readily seen in the result-
ing flows. To ascertain the nature of these flows, we assume a geomet-
ry as shown in fig. 2.1, with the horizontal top and bottom walls
separated by a distance H, and a constant flux Q imposed radially in-
ward. Scaling velocity by $\frac{Q}{2\pi R_i H}$, where R_i= inner wall radius, and
with axial symmetry, the dimensionless linear equations of motion in
cylindrical coordinates (Greenspan [1968] sect. 1.2 and 2.3; also
Lewellen [1965]) yields an interior azimuthal velocity proportional to
$1/_r E^{1/2}$ (where r = radius and E = $\nu/_{\Omega H^2}$) and zero interior radial
and vertical velocities. The resulting potential vortex is adjusted
at the top and bottom walls by non-divergent Ekman layers, their pas-
sivity resulting from the zero vorticity interior. The radial flow
takes place solely through the Ekman layers, similar to that shown in
fig. 2.2 (Lewellen [1965]). The radial adjustment of the zonal vel-
ocity field near the source and sink areas is accomplished by the side
wall boundary layers (Sterwartson [1957]). From fig. 2.2 one sees
that the flux transported though the Ekman layer is a convergent flow
with its velocity increasing proportionally to the reciprocal of the
radius. Defining an Ekman layer Reynolds number Re = $\frac{U\delta}{\nu}$ (as
previously defined), the value of which increases with decreasing
radius, the possibility of Re reaching sufficient size as to produce
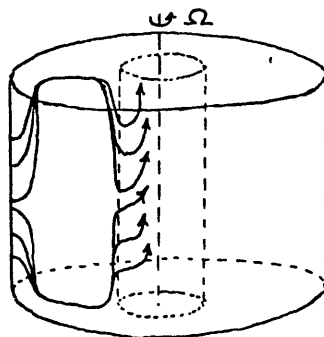
Figure 2.2
Idealized Flow Pattern

an instability at some inner radius becomes realizable. Due mainly to the simplicity of these relations and the freedom of parameter choice, much attention was turned to annular models.

· Stern (1960) first looked at the instability of laminar Ekman layers in a source sink annulus having a free surface (the rotational Froude number was assumed small as compared to unity). His analysis was mainly of a theoretical nature, although some crude experiments were performed. The occurrence of some "body-boundary" modes of in- · stability, as he named them, was dependent on a critical Taylor (Ta = $\Omega H^2/\nu$) and assumed to result from a shear instability which drew its energy from a coupling with the ageostrophic perturbation velocity. These waves differ from the "pure boundary" species (Faller [1963]), as they are found throughout the interior of the fluid. Stern found a lower limit of Ta equal to 2500 (and a Re of not more than 80) for the lowest mode. Although higher modes exist for larger Taylor number and lower Reynolds numbers, he was not able to predict their characteristics.

Arons, Ingersoll and Green (1961) found instabilities somewhat similar to those discussed by Stern. However, the observed critical Taylor number differed with the predicted value. Using a wide range of both Taylor and Reynolds number, in a partially water-filled annulus, they found a highly organized pattern of concentric cylindrical sheets of fluid. These sheets permeated the entire interior and boundary layer regions of the "critical" zone. The waves appeared in a Taylor number range of 1,290 to 19 x 10^3 and an Ekman Reynolds number

range of 1.6 to 3.6. The instability wavelength was estimated to be proportional to a product of Ekman depth and the Taylor number to the one quarter power, as predicted by Stern.

Since the studies of Stern and Arons, et al, the low Reynolds number instability work has been superceded by an interest in the "pure" boundary instabilities (at higher critical Re#). This has been done to such an extent, that the influence of the "body-boundary" waves exper-iments (although often at similar Ta#) has been neglected, and no ob-servations of their occurrence reported. Specifically, Tatro (1966) states that the mechanism mentioned by Stern is not relevant to his observational results.

Faller (1963) was the first to look at the boundary layer species of instability with a pertially water-filled rotating annulus. Using dye techniques to observe boundary layer motions, he estimated criti-cal Reynolds number be varying both the flux and rotation rates. The Reynolds number was calculated assuming all flux was transported through an ideal Ekman layer of thickness, $(\frac{\nu}{\Omega})^{1/2}$. By photographing the insta-bilities, which converged towards the sink, Faller was ble to estimate both the wavelengths (9.6 to 12.6 δ) and the wave front orientation (approx. 14.5° to the left of the azimuthal flow.) The critical Reynolds number for wave onset was approximately 125, after which, slowly moving spiral-like roll vortices appeared. A numerical study of the circulation, employing a power series expansion in Rossby number, predicted no radial interior flow to second order.

Barcilon (1965) obtained analytic solutions of the perturbation

equations for a non-divergent Ekman layer. He was unable to estimate

accurately the critical Reynolds numbers, since his method of solution

required an assumption of large Reynolds number for closure.

Lilly (1966) investigated Ekman instabilities by a perturbation

analysis and numerically solved the resultant eigenvalue problem for

the complete and a truncated set of equations. Both solutions showed

an instability, the former at a Reynolds number 55, the latter at 93.

Furthermore, stationary waves were found to be unstable for Reynolds

numbers greater than 115. This instability (class B, Greenspan [1961])

disappears at higher flow rates and is thus viscous in nature. Having

a greater wavelength and phase velocity than those of the class B, the

predicted class A waves are more difficult to observe by dye techniques

than the former. The influence of these waves was found to extend

well into the interior (5 or 6δ). Lilly's analysis played a signi-

ficant role in both confirming experimental, and furthering theoretical

studies of the pure boundary instabilities.

At the same time, Faller and Kaylor (1966) derived numerical sol-

utions for the time dependent non-linear equations of motion with per-

turbations on an initially laminar Ekman layer. They confirmed Lilly's

finding of the class A waves' critical Reynolds number, their range

being 50 to 70. The class B waves occurred for Reynolds numbers in the

range of 110 to 130. Their work also.predicted the previously obser-

ved wavelength and orientation of the waves. As Lilly (1966) stated,

the chief merit of this non-linear solution was to allow a study of

finite amplitude disturbances.

The presence of the two instability mechanisms predicted by Lilly[19] at Reynolds numbers of the same order of magnitude had led to some confusion in analyzing qualitative results. These shortcomings were alleviated when Tatro (1966) conducted the first quantitative measurements in a rotating source-sink annulus, using air as the ambient fluid. In contrast to earlier work with free surfaces, this model used a plexglass tank having a rigid top. By employing a silk screen baffle as the peripheral source, Tatro varied the flux (by vacuum cleaner suction) and the rotation rate to produce the desired variability in flow parameters. Using hot wire anemometers he was able to describe the velocity profile of the interior as well as of the top and bottom boundary layers. The results showed a marked discrepancy between the actual geostrophic interior and that predicted theoretically (Faller [1963]). Also, Tatro observed that the class A waves occurred at a local Reynolds number equal to 56.3 plus a factor equal to 58.4 times the local Rossby number. Their wavelength was 25 to 33 δ , a phase-speed of 0.16 times the local interior geostrophic flow, and the orientation of the wave fronts 0 to (-)8° from the interior azimuthal flow. Similarly, the class B wavelength is 11.8 δ , phase speed of 0.034 times the interior flow, orientation of 14.6° from the geostrophic flow, and a critical Reynolds number equal to 124.5 plus a small factor dependent on Rossby number. He also observed some inertial wave-like disturbances in the interior and a somewhat indefinite transition to turbulence at higher Reynolds numbers of order 200.

Green and Mollo-Christensen (1970) carried on work similar to
that of Tatro (1966) but with a larger tank and greater flexibility
in probe positioning. Their emphasis was on the exchange of energy
between unstable Ekman layers (presence of class A, and at times class
B waves) and the interior flow. Some spectra at different radii in
the interior, for constant flux and rotation rate, showed inertial
wave energy at dominant frequencies which were not readily explain-
able. By comparing some of the predicted inertial mode frequencies
to those observed, an equivalence was established. This is not un-
expected, as the inertial modes of a rotating cylinder are denum-
erably infinite in the range of 0 to 2Ω (Greenspan [1968]). The
generated inertial waves are found to be important in altering the
Ekman layer structure and vice versa, such that an equilibrium flow
configuration evolves. A linear increase of the non-dimensional dom-
inant wave frequency for a limited range of system Rossby number was
attributed to Doppler effects. Their observations of the steady in-
terior flow show circulation profiles differing greatly from the
idealized potential vortex flow and a mean Ekman layer thickness of
1.7 δ . In contrast to Tatro (1966) the authors found no dependence
of the boundary layer thickness on radious (i.e., local Rossby and
Reynolds number). Green and Mollo-Christensen feel that the unstead-
iness of the Ekman layers, due to the impingement of inertial waves,
alters the existing theoretical predictions, which neglect wave radi-
ation. No critical Reynolds' numbers are given for instability on-
set, although Green (1968) suggested that the class A waves were
responsible for the disturbances observed.

In a recent paper, Caldwell and Van Atta (1970) using tehcniques similar to Tatro and Mollo-Christensen (1967) investigated the onset of the class A waves and their spectral characteristics. In close agreement with Tatro (1966), the critical Reynolds number was found to be 56.7. Both of the observed values agree well with the value predicted numerically by Lilly (1966). The wave frequencies found by Caldwell and Van Atta are much higher than those alluded to by Tatro (1966). The class B waves are not observed. Caldwell and Van Atta also present mean zonal velocity profiles for the interior (radially) and the horizontal boundary layers (vertically). The latter are found to match the ideal Ekman layer with amazing similarity and exhibit no radial dependence for Reynolds numbers below critical values. They observed a sudden onset of turbulence in the boundary layer at a Reynolds number of 148.

The mean circulations obtained by Caldwell and Van Atta in the interior somewhat resemble those of Green and Mollo-Christensen, although the former are much smoother (Caldwell and Van Atta do not show actual points of observation). No interior spectra are presented. Caldwell and Van Atta give a chart summarizing the pertinent experimental and theoretical Ekman layer instability (high Re#) work in rotating annuli, which serves as an excellent history of the field to this time.

The diversity and similarity of work in rotating annuli leads to much speculation about extraneous influences on the flow observations and conditions. As Lilly (1966) states, the initial dye studies inadvertently but effectively filtered out evidence of the quickly moving class A disturbances. The china clay technique used by Gregory, et al

(1955) on a rotating disk was only sensitive to stationary bands. Differences in the results of quantitative studies of the annulus are due mainly to the influence of apparatus configuration in altering the basic flow.

• On surveying the similar onset criteria found by these workers (hot wire methods in annuli) for the class A waves, Lilly's (1966) assertion that this instability will always find suitable shear conditions in the lower part of the Ekman layer, is substantiated. However, non-linear modifications of the Ekman layer structure, mentioned by Barcilon (1970) may in some cases inhibit the formation of class B waves, which are generated in the upper part of the boundary layer.

The large discrepancy in critical Reynolds numbers between annulus and disk experiments is attributable only to its means of computation. The value of Re^1 for the class B waves found by Tatro (1966) is of order 370 and by Faller (1963), of order 450. These compare favorably with Smith (1945), who observed 483 and Gregory, et al, (1955) who found 435 as their critical Reynolds number (Re^1). The prime denotes the difference in its calculation.

Hide (1968) studied the non-linear modifications to source-sink flows of various geometries and carried out some interesting qualitative experiments. He predicted that the side wall boundary layer adjacent the source was liable to be thicker at higher Rossby numbers. No equivalent change was expected in the sink region. Recently, Dudis and Davis (1971) have re-examined Ekman layer instabilities by appealing to the energy theory. Their numerical solution (Re_c=

18.3) differs greatly from the linear results (Re$_c$ = 55) of Lilly (1966).

This range allows for the onset of sub-critical instabilities. Dudis

and Davis are unable to confirm existence in the literature; however,

they comment that similar problems have shown experimental verifica-

tion

CHAPTER III

Experimental Equipment

3.1   The Rotating Annulus

The annular configuration used in the present work is pictured schematically in figure 3.1. Dimensionally , the tank was 24 cm. high and had an inner and outer radius of 8.5 and 61.8 cm., respectively. For most of the experiments, the source was at the outer radial position and the sink at the inner location. These boundaries were composed of one inch thick reticulated polymethane foam. A negative radial pressure gradient was imposed between these vertical walls by a vacuum system connected to the central hub. The tank was rotated about its center by a variable speed motor.

The resulting flows in the annulus were monitored by constant temperature hot wire anemometer probes. The relative positioning of the sensors allowed a thorough analysis of the velocity structure. Figure 3.2 gives a flow chart description of the associated electronic equipment. A complete discussion of the experimental setup and methods is found in Appendix I.

3.2   New Techniques

A number of the experimental methods used in this work are different from those employed previously. This section gives a brief account of these innovative techniques. However, the individual topics are covered in much greater detail in Appendix I.
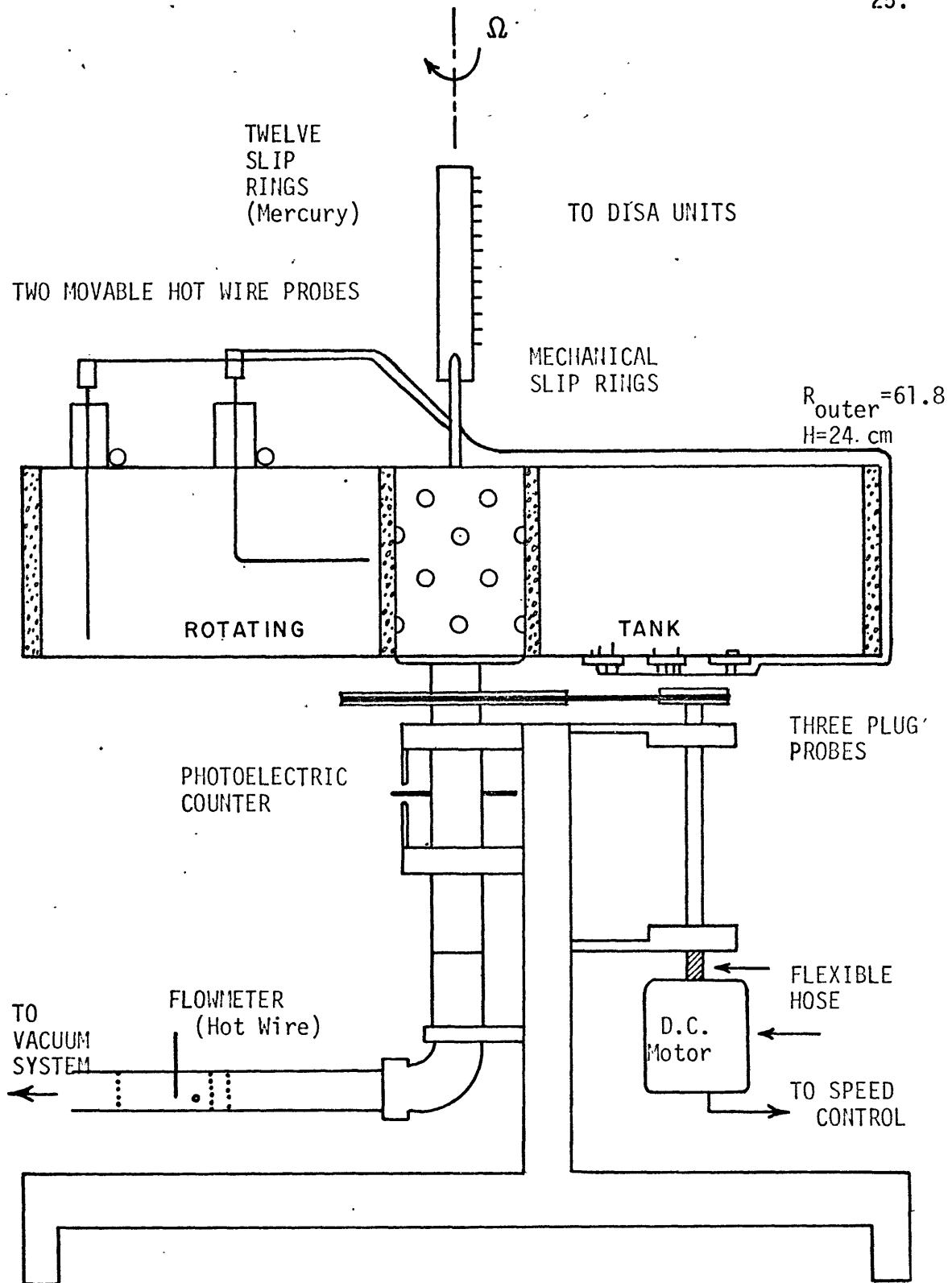
Figure 3.1
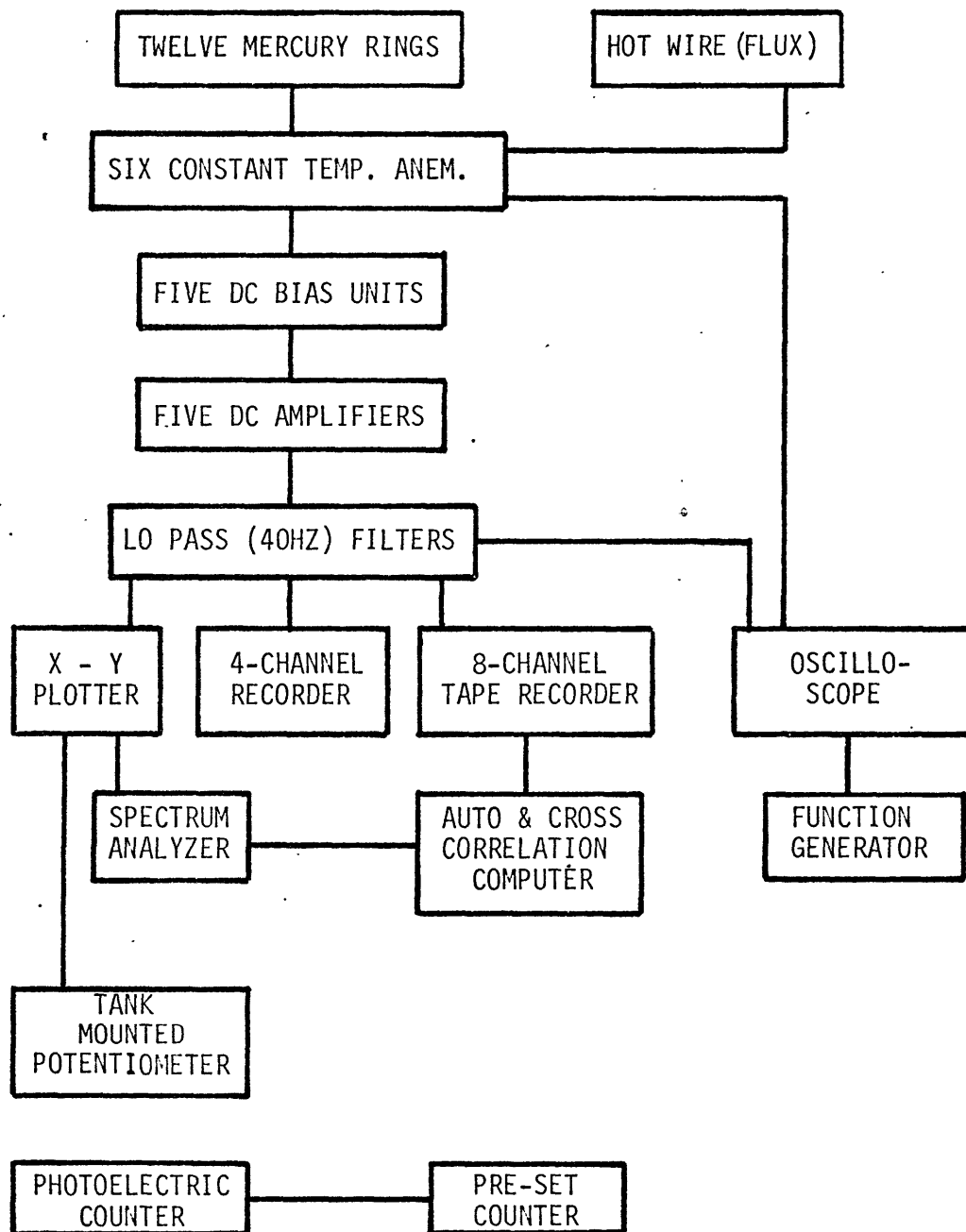
SCHEMATIC OF CIRCUITRY.

FIGURE 3.2

a. Rotation Rate. Through utilization of a photoelectric
    counter to measure rotation rate, a significantly higher
    degree of accuracy (10 times greater) was obtained, than
    in earlier, similar experiments.

b. Probe design. A single (extended) probe was constructed
    with the capability to measure interior velocities at all
    radial positions, within a short time. The resultant
    scatter in the circulation profiles was shown to be minimal.
    Previously reported observations, with single fixed sen-
    sors, were subject to ambient temperature changes, which
    distorted individual velocity distributions for a constant
    flux and rotation rate. Furthermore, uniform conditions of
    flux and rotation rate were not always assured when using
    the latter technique. Past measurements of velocity with-
    in the Ekman layer have been subject to errors in-probe
    height determination. To overcome this difficulty, a
    sensor with a third leg was manufactured. This leg was
    longer than the probe needles and served as an accurate
    measure for the vertical distance. An added advantage of
    this design was the elimination of possible probe damage
    from impact with the lower wall.

       Small plexiglass mounted probes were used for
    some of the cross-correlation work in the Ekman layer.
    Similar hot wires used for the interior measurements allow-
    ed a more detailed view of the flow than possible with the
    top-mounted probes. Figure AI.1 shows the probe configu-
    rations employed in this work.

c. Wall Proximity Effects.   In the past, Tatro (1966) and
Green (1968) have observed anomalous hot wire response, for
measurements close to the top and bottom walls. This dis-
tortion resulted in an observed increase in velocity for
decreasing height in the Ekman layer. The effect has led to
some errors in estimating onset criteria for the Ekman
layer instabilities (Green and Mollo-Christensen [1970]).
By calibrating the heat losses under conditions of "no
flow", Dryden's (1936) method was used to correct the obser-
ved voltages. This technique gave a vertical distribution
of velocity comparable to theoretical prediction.

d. Low Velocity Work.   Past experimenters using hot wires,
have assumed a linear relationship between the square of re-
corded voltage and the square root of the perpendicularly im-
pinging flow velocity. This simple dependence fails for vel-
ocities below 25cm/sec. Linear extrapolation into the vel-
ocity range of 0 - 25cm/sec. has been a source of much exper-
imental error. No calibrations were possible in this range
since previous workers used vortex shedding methods, which
fail below 25cm/sec. Presently, a new low velocity wind
tunnel was designed employing an entirely different calibra-
tion technique. Using this method, accurate calibration
curves from 1 to 100 cm/sec. were possible. No linearization
was necessary.

A detailed account of observation techniques is in-
cluded in Appendix II. The present experimental set-up was

not amenable to flow visualization using smoke, dyes, etc.

The aluminum plates and the necessity of having a baffle

on the outer radial wall gives little opportunity for using

any combination of mirrors and cameras. A clear plexiglass

insert would be one solution, if sufficient lighting was av-

ailable. Tatro (1966) has conducted some smoke experiments

in a similar tank, which had plexiglass discs as top and

bottom walls. Numerous experiments using dye techniques in

water-filled annuli have been reported.

CHAPTER IV

Mean Velocity Structure in the Annulus

In general, each observation was composed of a mean velocity, with a variety of superimposed wave motions. The time-averaged mean velocity of this signal was found to be independent of the azimuthal coordinate, and exhibited a vertical and radial structure in the boundary regions, similar to the theoretical predictions. Although, the results presented in this section are simply averages of the actual flow, the role played by the transients in altering this mean structure may be an important one.

As discussed in Chapter III, the influence of ambient temperature changes and non-uniform conditions can explain the irregularity of some profiles in the literature. By utilization of the extended probe (see section 3.2), this inconsistency was eliminated in the present work. Having removed this important source of error, the changes resulting from viscous and non-linear modifications were more readily seen. A thorough discussion of the observation methods used for the mean velocity work is given in Appendix II.

4.1   Radial Structure of Vertically Independent Flows

       4.1.1   Theoretical Predictions

Given the geometry, pictured in figure 2.2, with a peripheral source and sink, one expects on theoretical grounds, that an inviscid potential vortex is formed in the interior (Lewellen [1965]). The interior in this case is a region excluding the top and bottom Ekman layers, and the side wall layers adjacent to the source and sink. As

found in Chapter II, the steady linear dynamics supports only a zonally-directed geostrophic interior flow, with the radial transport being accommodated solely in the Ekman layers. The idealized interior velocity field takes the following form (Greenspan [1968]):

$$V_I = \frac{S}{2 R \pi \delta}$$ (equation 4.1)

where V_I = theoretical zonal flow (relative to tank)

S = volume flux

R = local radius

δ = Ekman layer thickness ($[\nu/\Omega]^{1/2}$)

Employing this relation, one readily finds that the dimensional circulation, ($\Gamma' = V_I R$), is independent of radius, for a fixed flux and rotation. However, a majority of the results shown in this chapter will compare the non-dimensional circulation (Γ) with radius. Using equation 4.1, we define Γ as follows:

$$\Gamma = \frac{(V_M R)}{(V_I R)} = \frac{2 \pi V_M \delta R}{S}$$ (equation 4.2)

where Γ = non-dimensional circulation

V_M = observed zonal velocity (rotating frame)

A closer look at equation 4.2 shows that Γ also gives the non-dimensional zonal velcoity field (V_M/V_I). If Γ is assumed equal to one, we expect the azimuthal velocity V_M to vary inversely as R, and the Ekman boundary layers to be non-divergent. However, by including both the top and bottom Ekman layers, we might expect the theoretically predicted Γ to be 0.5. Adjacent to the source and sink regions Γ decreases as a result of the sidewall boundary layers (Stewartson [1957]).

4.1.2   Observed Velocity and Circulation Profiles

Figure 4.1 shows dimensional zonal velocity versus radius for

seven increasing values of flux at a constant rotation. Although the radial dependence of this velocity field is similar to theoretical prediction, a further interpretation is difficult. The non-dimensional circulation profiles Γ (r) are more suitable for comparison with theory. Graphs 4.2 - 4.11 show Γ (with error bars), as obtained from equation 4.2, versus non-dimensional radius (r=R/R$_0$). In terms of this radial coordinate, the sink and source are located at 0.13 and 1.0, respectively. The asymmetry of the error bars results from rounding off the circulation values to the nearest one-hundreth.

The circulation profiles show a noticeably lower value than predicted theoretically. Typical values of Γ at mid-radial positions range from 0.55 to 0.75. However, adjacent to both the source and sink a marked decrease in Γ is apparent. Within the range of r= 0.35 to 0.75, Γ is found to increase with radius at the higher flux rates. This is in contrast to the lower fluxes, where a nearly constant distribution of Γ is obtained.

4.1.3 Comparison and Discussion

A comparison of the present and previous work to theoretical prediction shows a definite difference from the relation determined in equation 4.1. This discrepancy can be related to the influence of non-linearities, and also to viscous action adjacent to the tank walls. Since Γ is found to vary with radius, divergences in the Ekman layer are produced. A calculation of the resulting induced vertical mass flux (Greenspan [1968]), shows typical velocities of order 1% of the mean zonal flow, for the relative interior vorticities present. To the present time, the influence of wave radiation in altering the mean flow has not been included in any theoretical model.

V_M
cm/sec

Ω = 5.02 rad/sec
z = 12 cm

S= 2136 cc/sec

S= 1314 cc/sec

S= 766 cc/sec

r
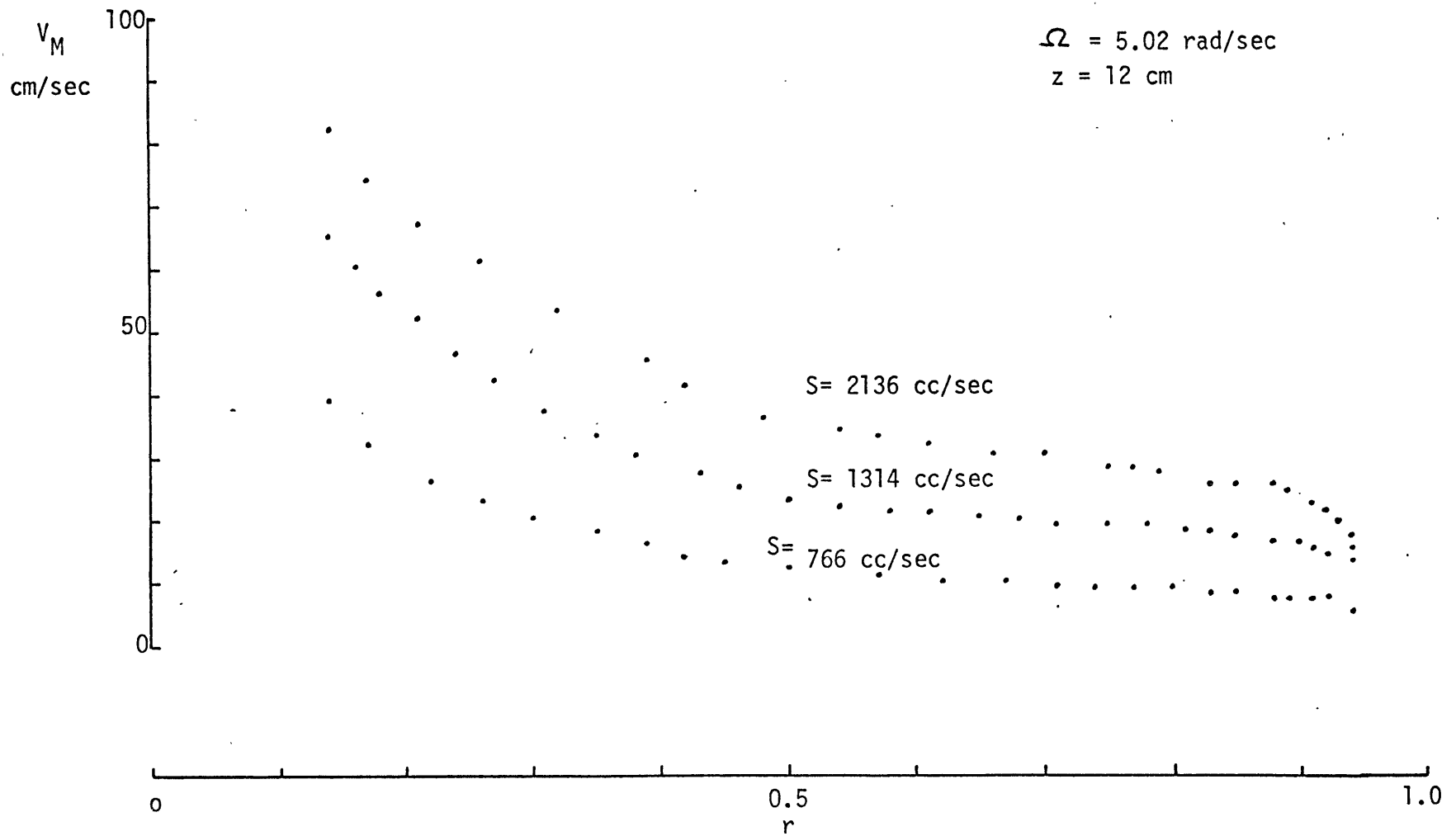
FIGURE 4.1 - ZONAL VELOCITY PROFILES
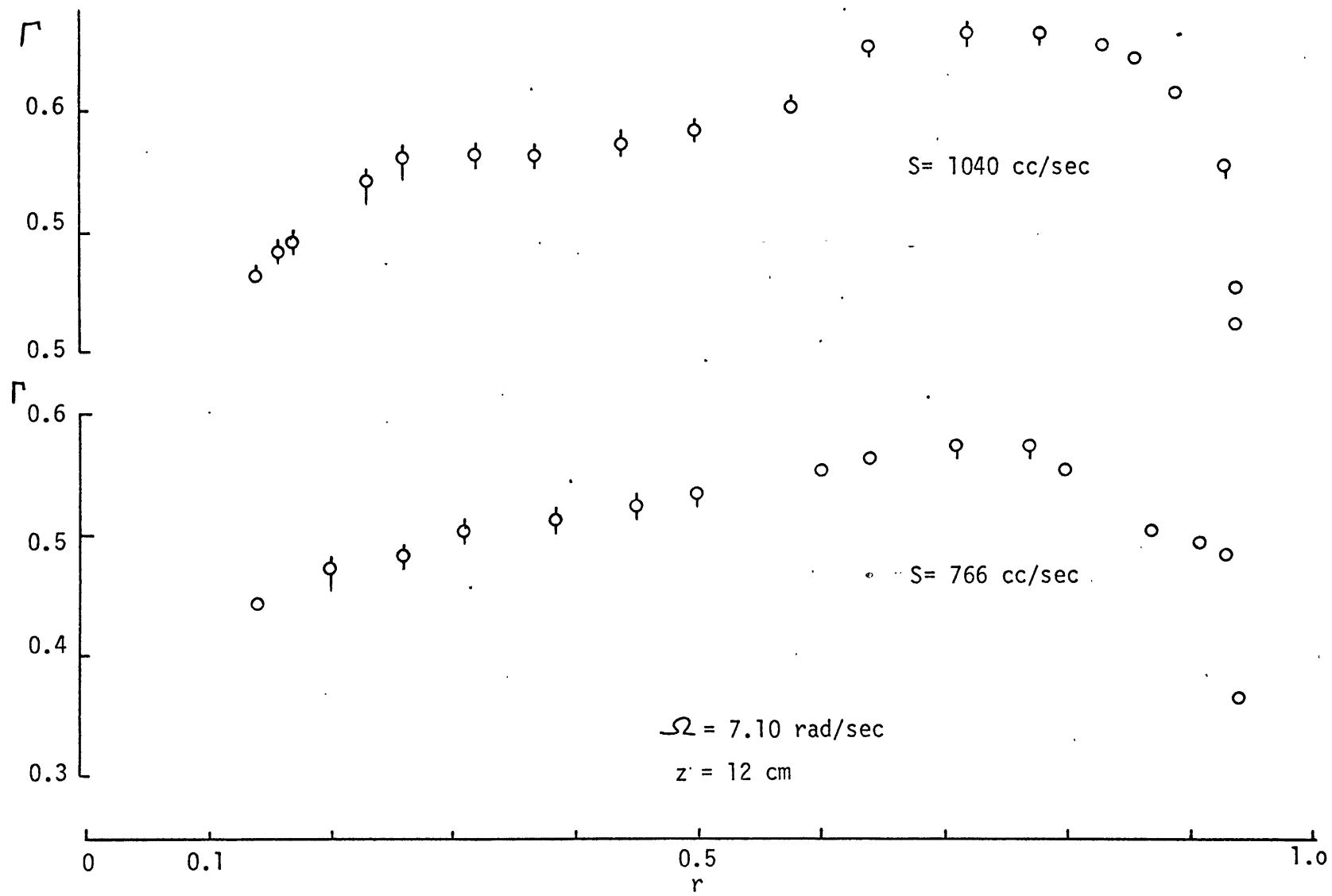
FIGURE 4.2 - CIRCULATION PROFILE

Γ

0.6

0.5

0.5

S= 1040 cc/sec

Γ

0.6

0.5

0.4

0.3

S= 766 cc/sec

Ω = 7.10 rad/sec

z = 12 cm

0   0.1   0.5   1.0

r
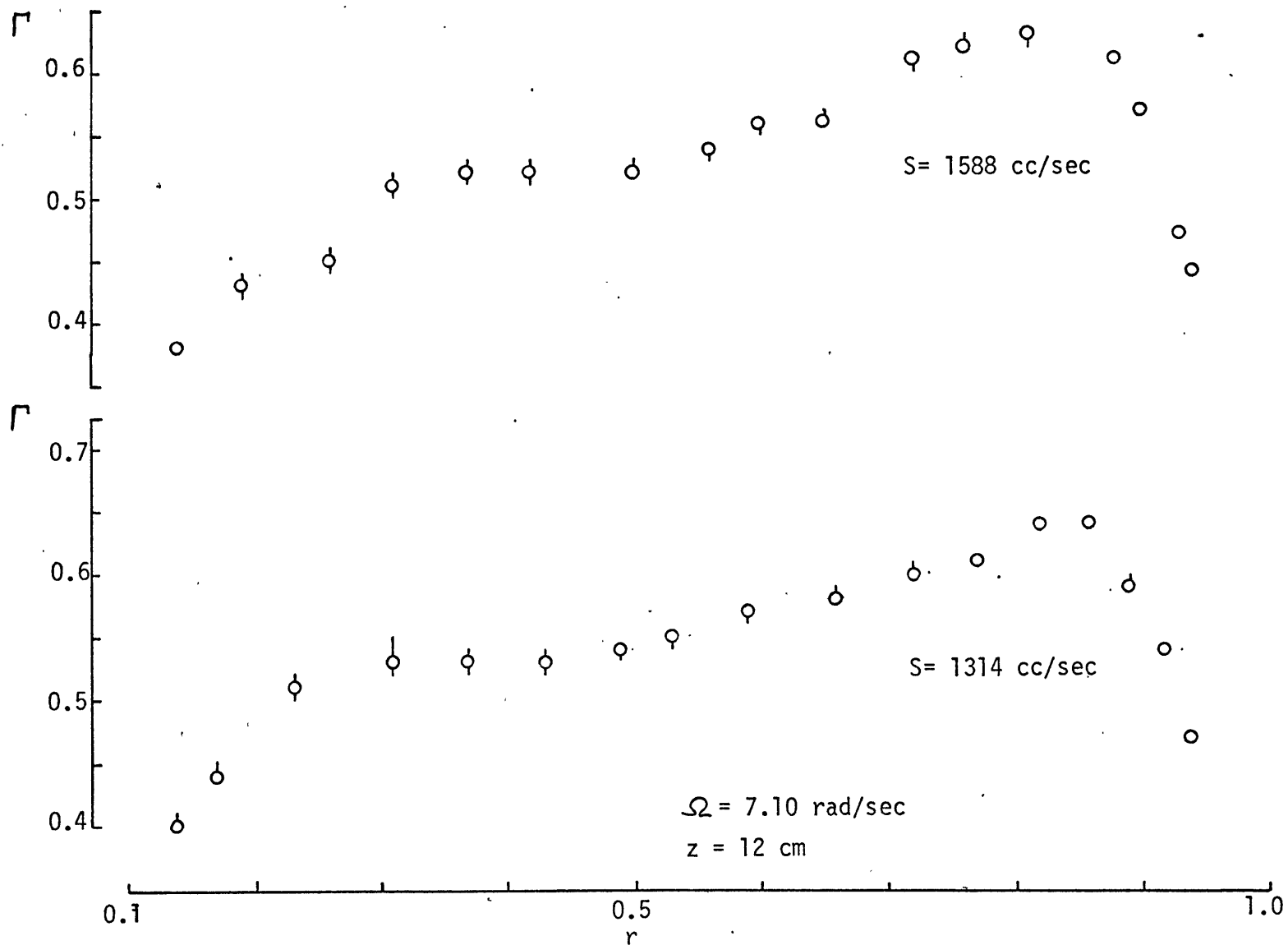
FIGURE 4.3 - CIRCULATION PROFILE

S= 1588 cc/sec

S= 1314 cc/sec

Ω = 7.10 rad/sec

z = 12 cm
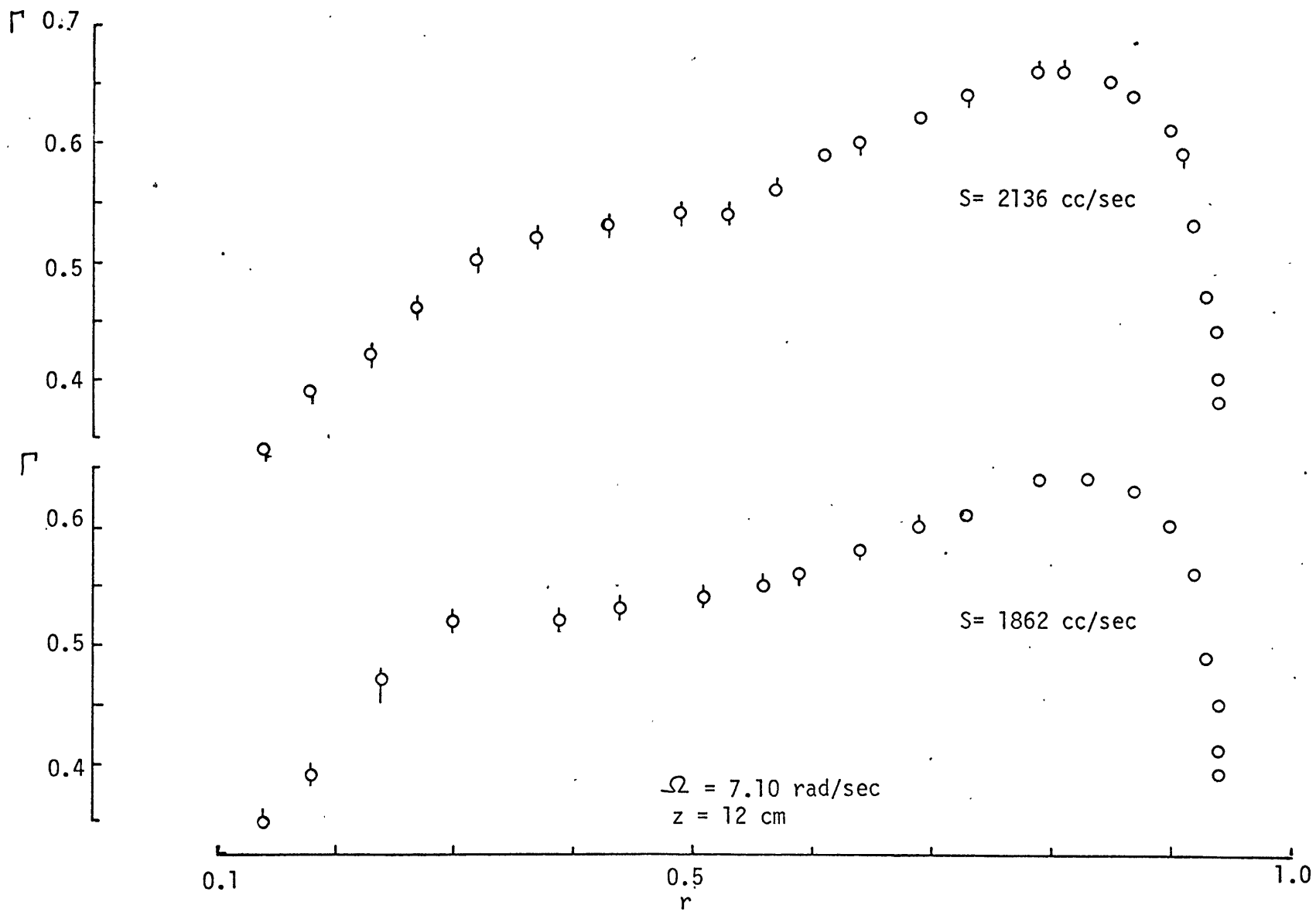
FIGURE 4.4 - CIRCULATION PROFILE
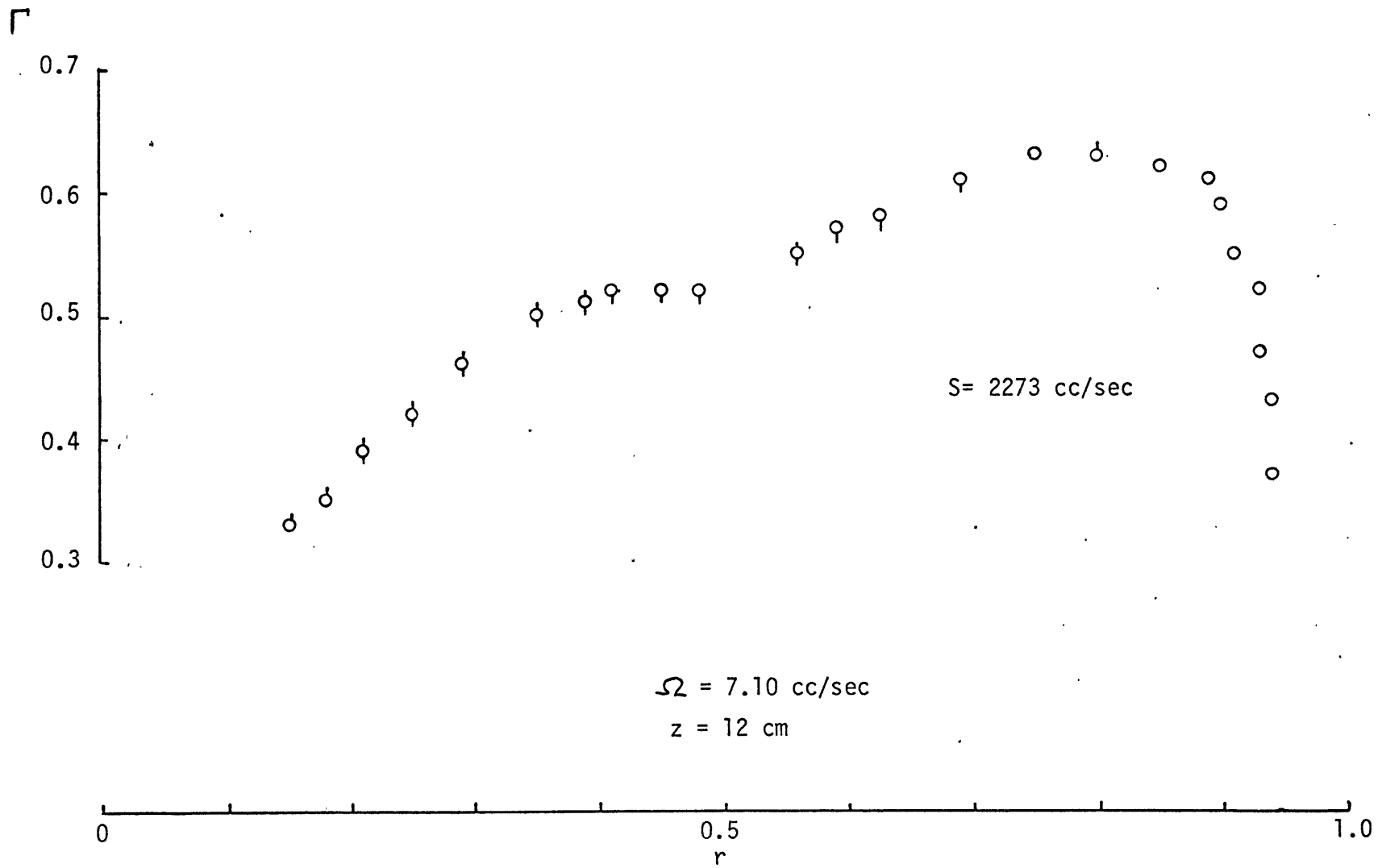
FIGURE 4.5 - CIRCULATION PROFILE

S= 2273 cc/sec

Ω = 7.10 cc/sec

z = 12 cm
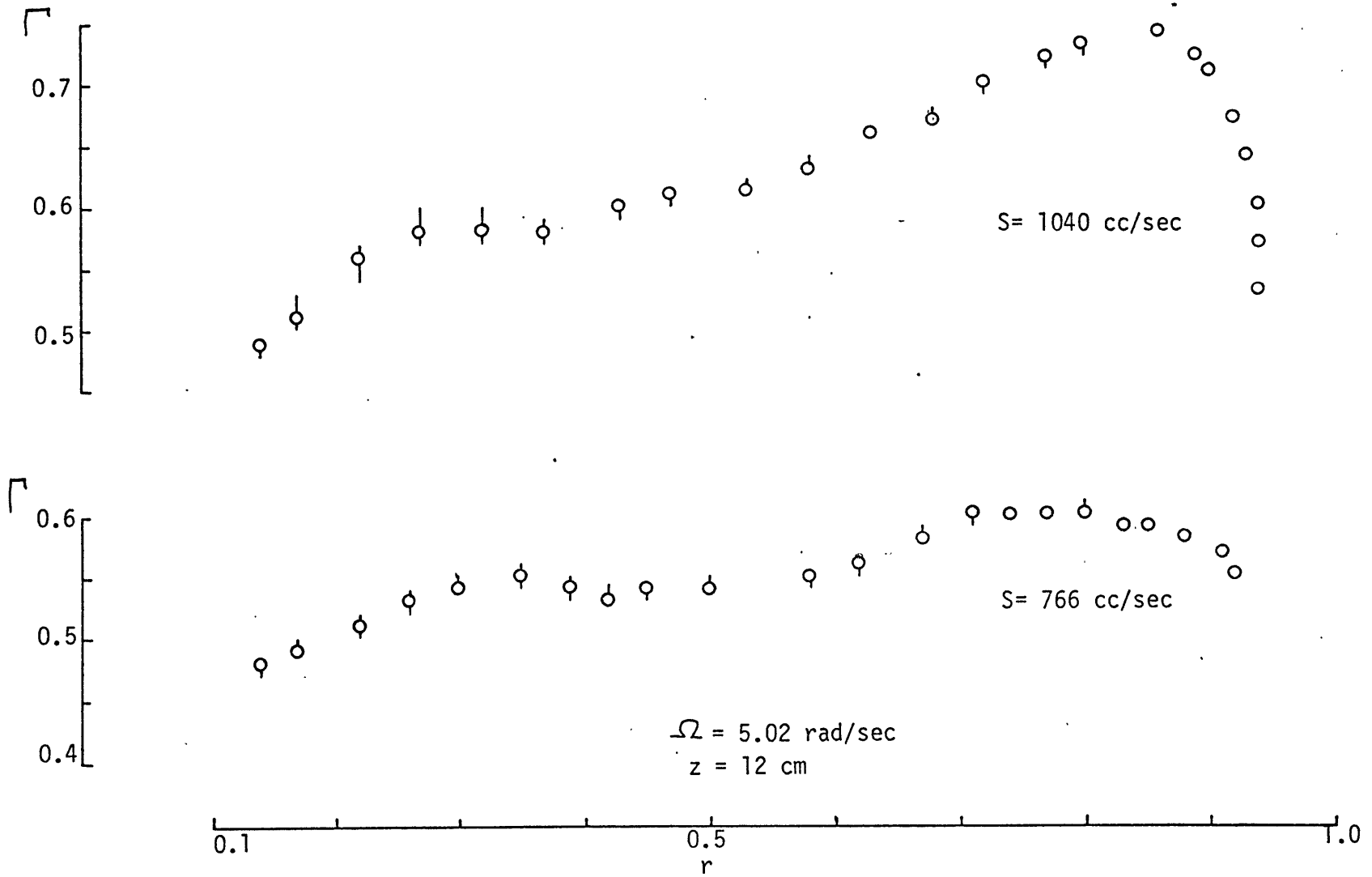
FIGURE 4.6 - CIRCULATION PROFILE

S= 1040 cc/sec

S= 766 cc/sec

Ω = 5.02 rad/sec
z = 12 cm
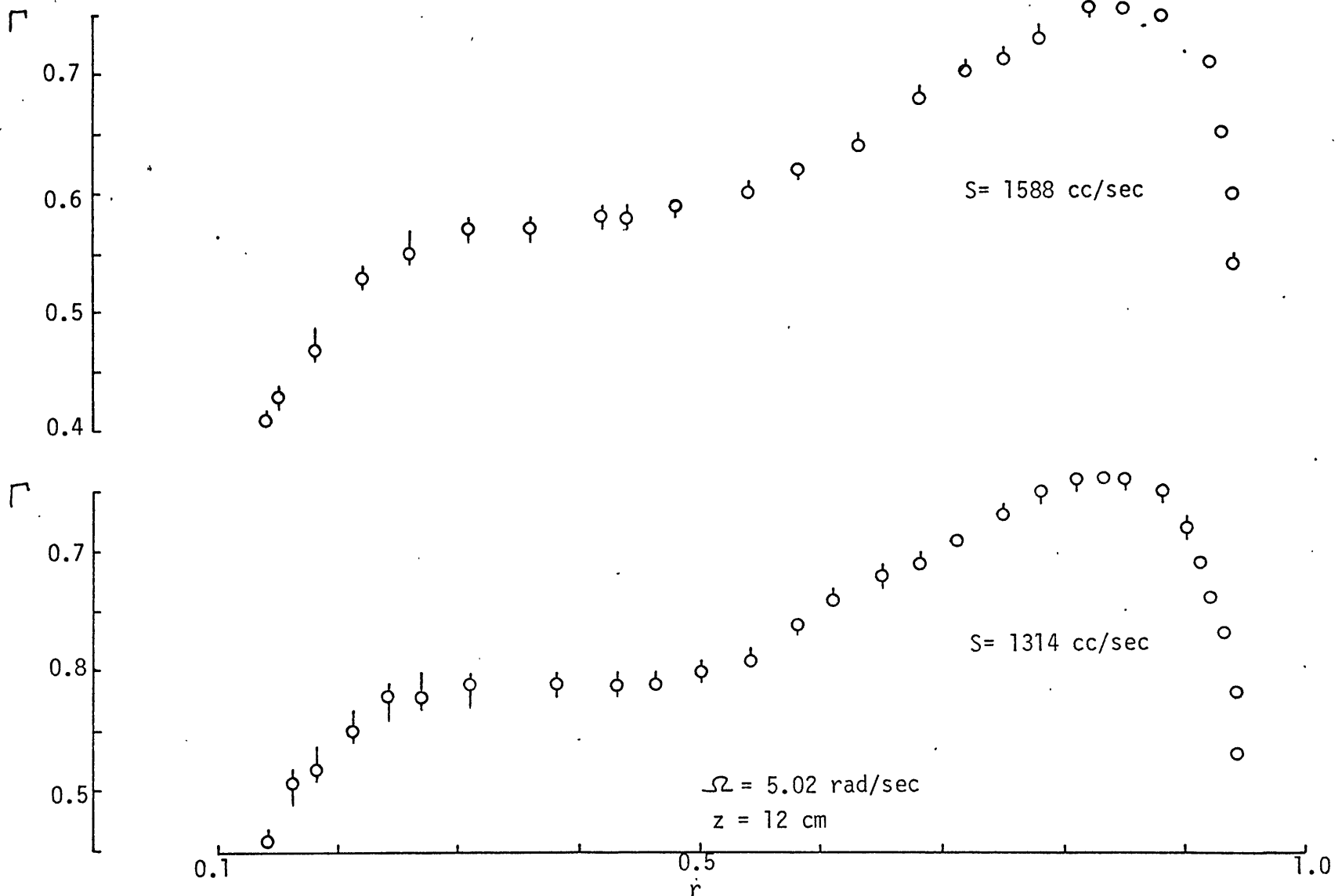
FIGURE 4.7 - CIRCULATION PROFILE
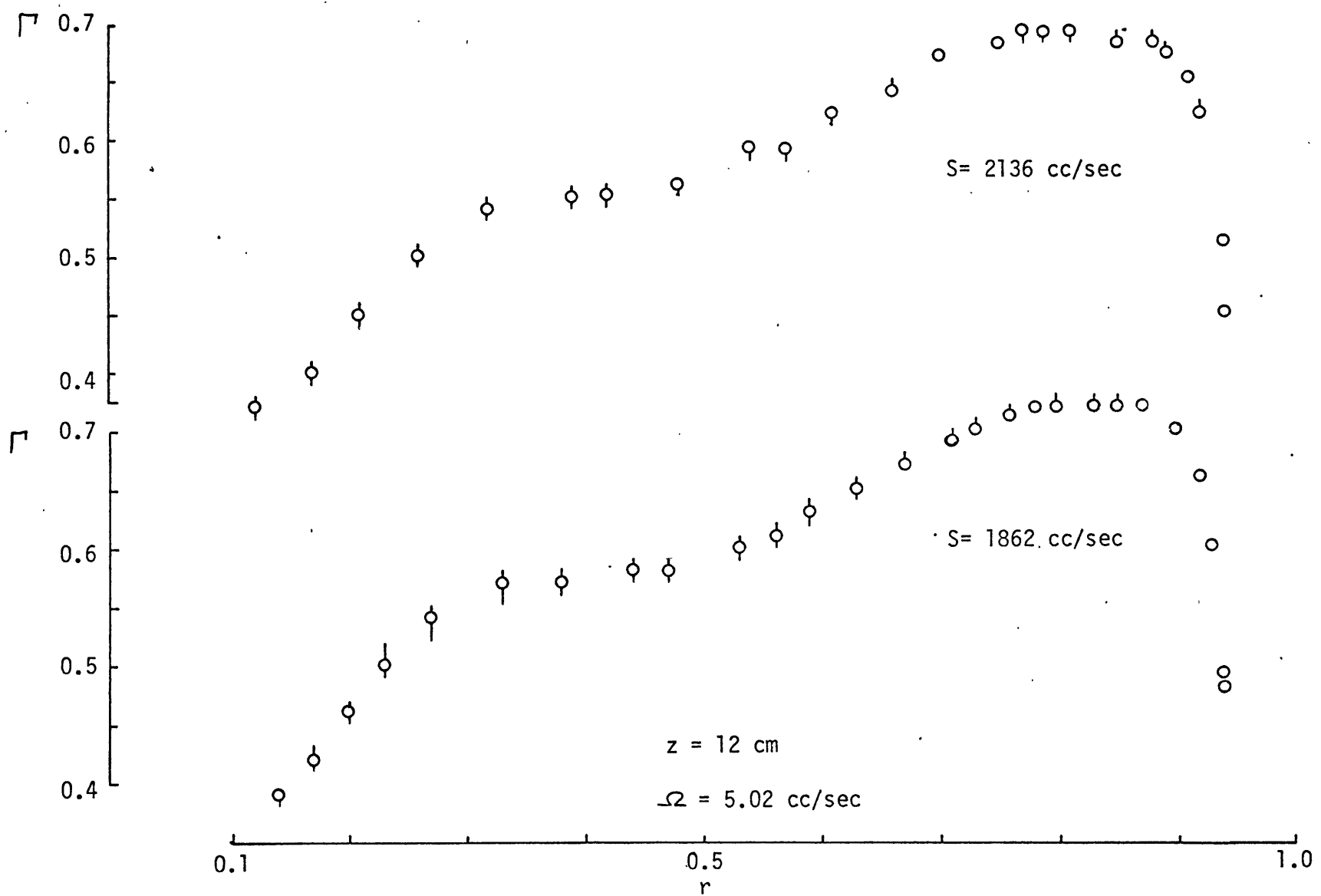
FIGURE 4.8 - CIRCULATION PROFILE

S= 2136 cc/sec

S= 1862 cc/sec

z = 12 cm

Ω = 5.02 cc/sec

40.
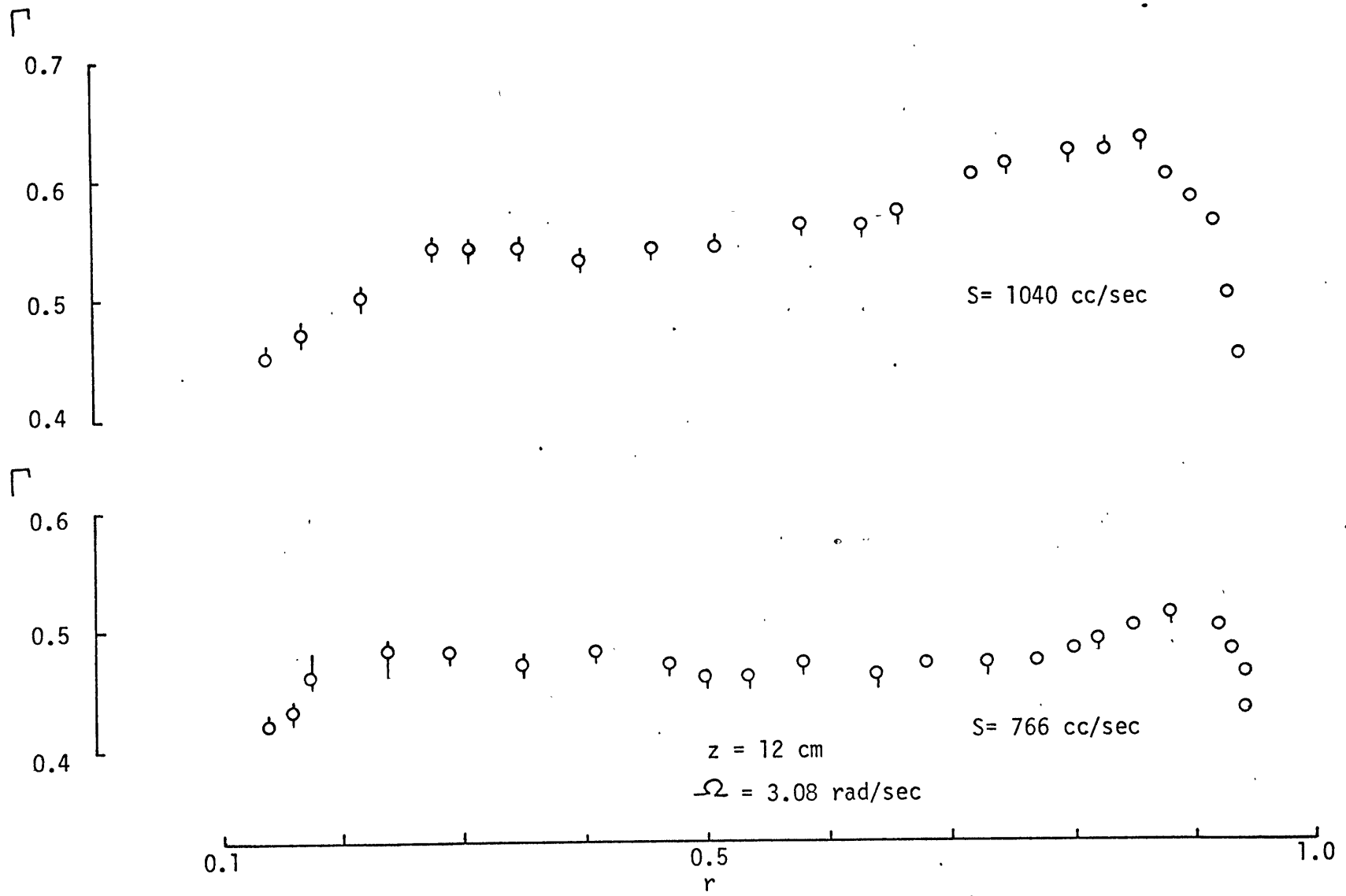
FIGURE 4.9 - CIRCULATION PROFILE

S= 1040 cc/sec

S= 766 cc/sec

z = 12 cm

Ω = 3.08 rad/sec

41.
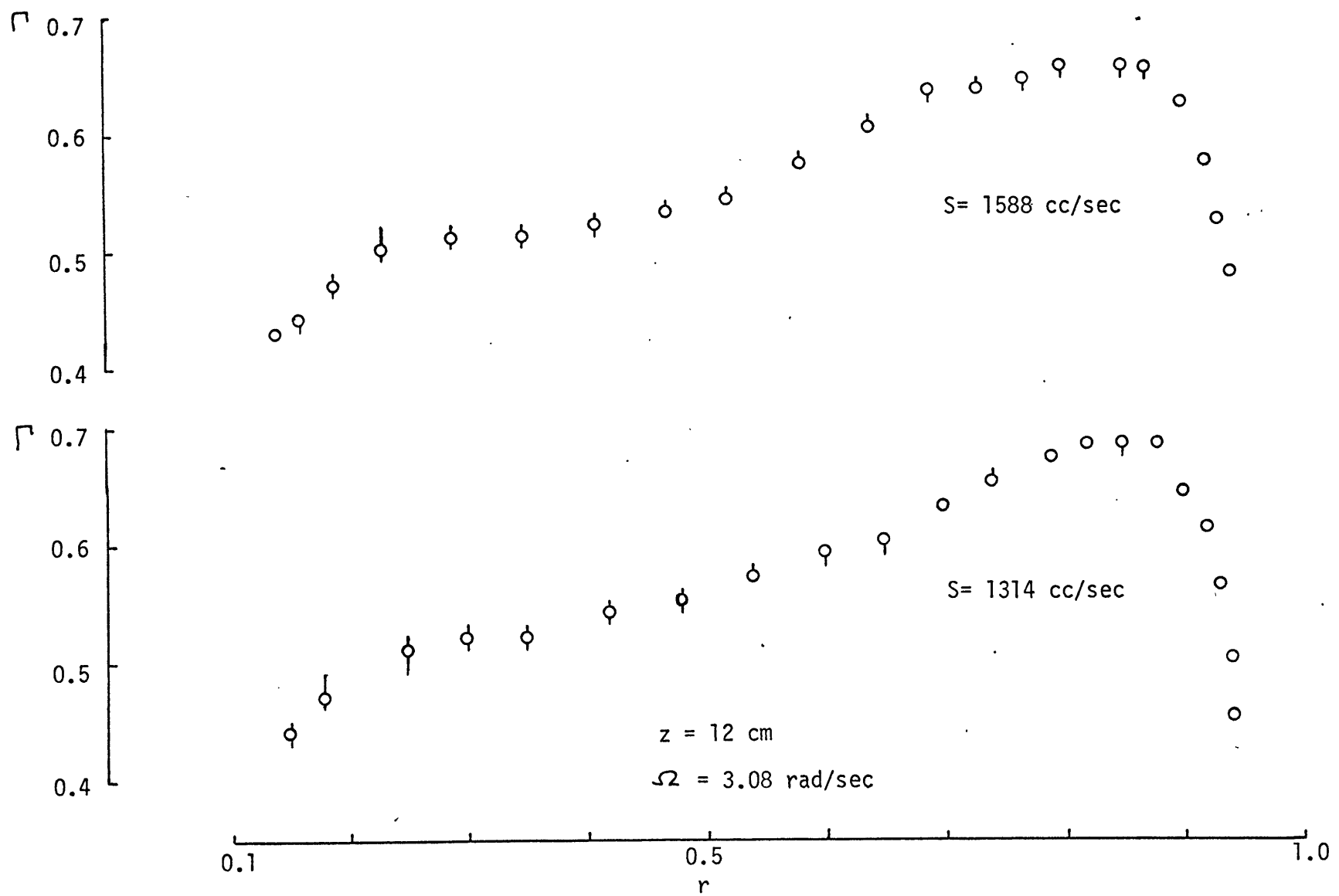
FIGURE 4.10 - CIRCULATION PROFILE

S= 1588 cc/sec

S= 1314 cc/sec

z = 12 cm

Ω = 3.08 rad/sec

42.
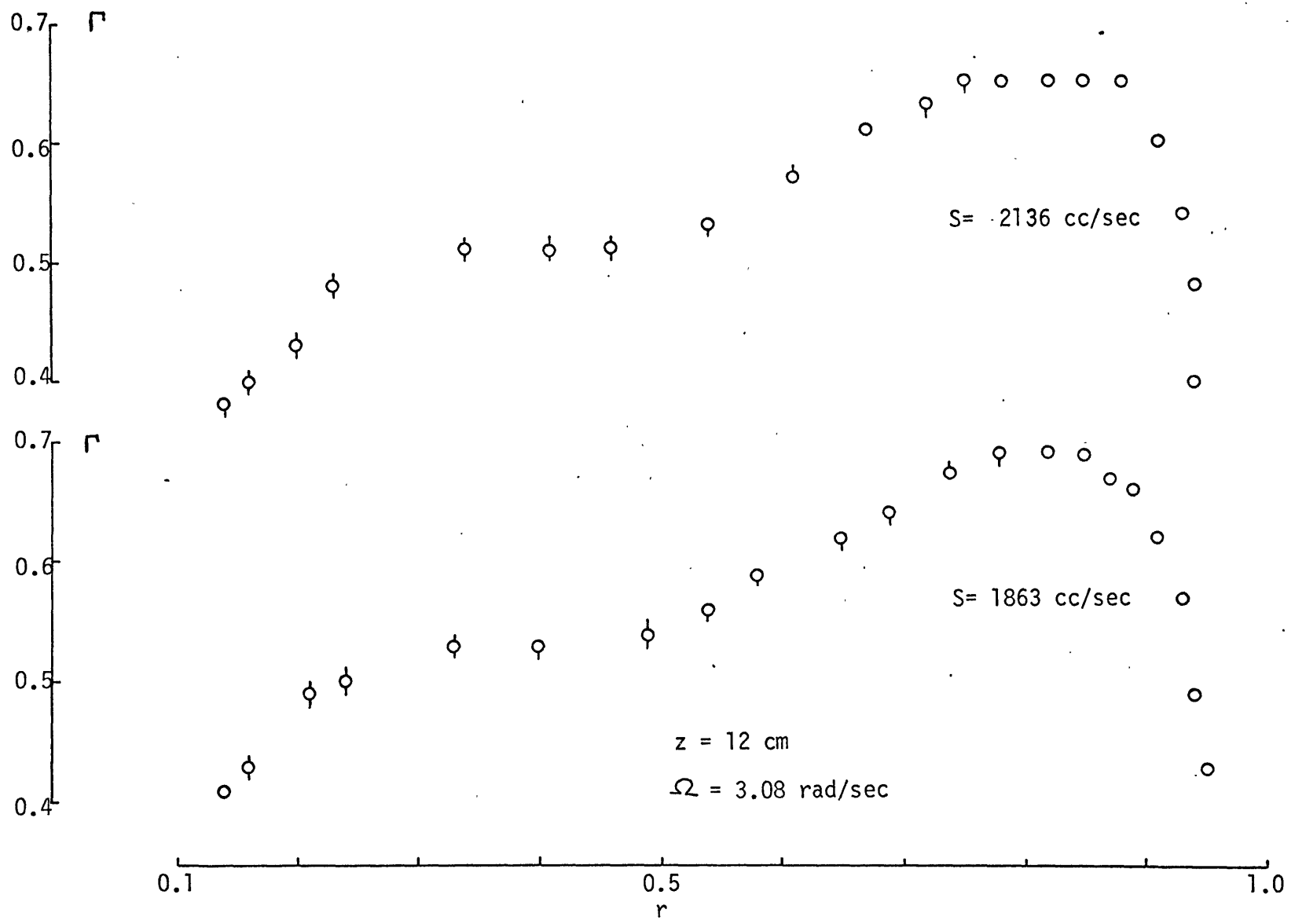
FIGURE 4.11 - CIRCULATION PROFILE

S= 2136 cc/sec

S= 1863 cc/sec

z = 12 cm

Ω = 3.08 rad/sec

Past observations of the circulation profile have been of a somewhat sketchy nature. Generally, results have been obtained over a limited range of flux and rotation. Tatro (1966) published only a single profile of velocity (dimensional) against radius. However, by using his results, it was possible to compute a mean value of Γ as 0.7, and also show that Γ increased over a certain radial range. Tatro's work focused on the interior region, excluding the sidewall boundary layer regions.

From a limited number of profiles, Green (1968) obtained radial dependence of circulation in marked contrast to the present findings. For the lowest flux value (680 cc/sec.), Green observed a large increase in Γ with radius from r=0.2 to 0.92, whereas at the higher flux (1310 cc/sec.), his profile was flat from r=0.2 to 0.5 and showed only a gradual increase over the remaining radial range. He attempted to explain this Γ distribution by the existence of unstable Ekman layers in regions of constant circulation. Figures 4.2 - 4.11 reveal a completely opposite response than Green's to changes of flux. At the lower fluxes (766 cc/sec.), the profile is almost flat, while at the higher values (2000 cc/sec.), Γ is found to increase with radius over certain ranges. In replotting Green's (1968) results, Green and Mollo-Christensen (1970) obtained a large amount of scatter in their profiles. None of the structure observed by Green is found in the circulation profiles of the later report. This discrepancy is unexplained. Figure 4.12 shows a comparison of the circulation profiles from the three aforementioned works.

The scatter in Green and Mollo-Christensen's results is explained by the small differences in operating conditions encountered when using single fixed probes (see Section 3.2). Although
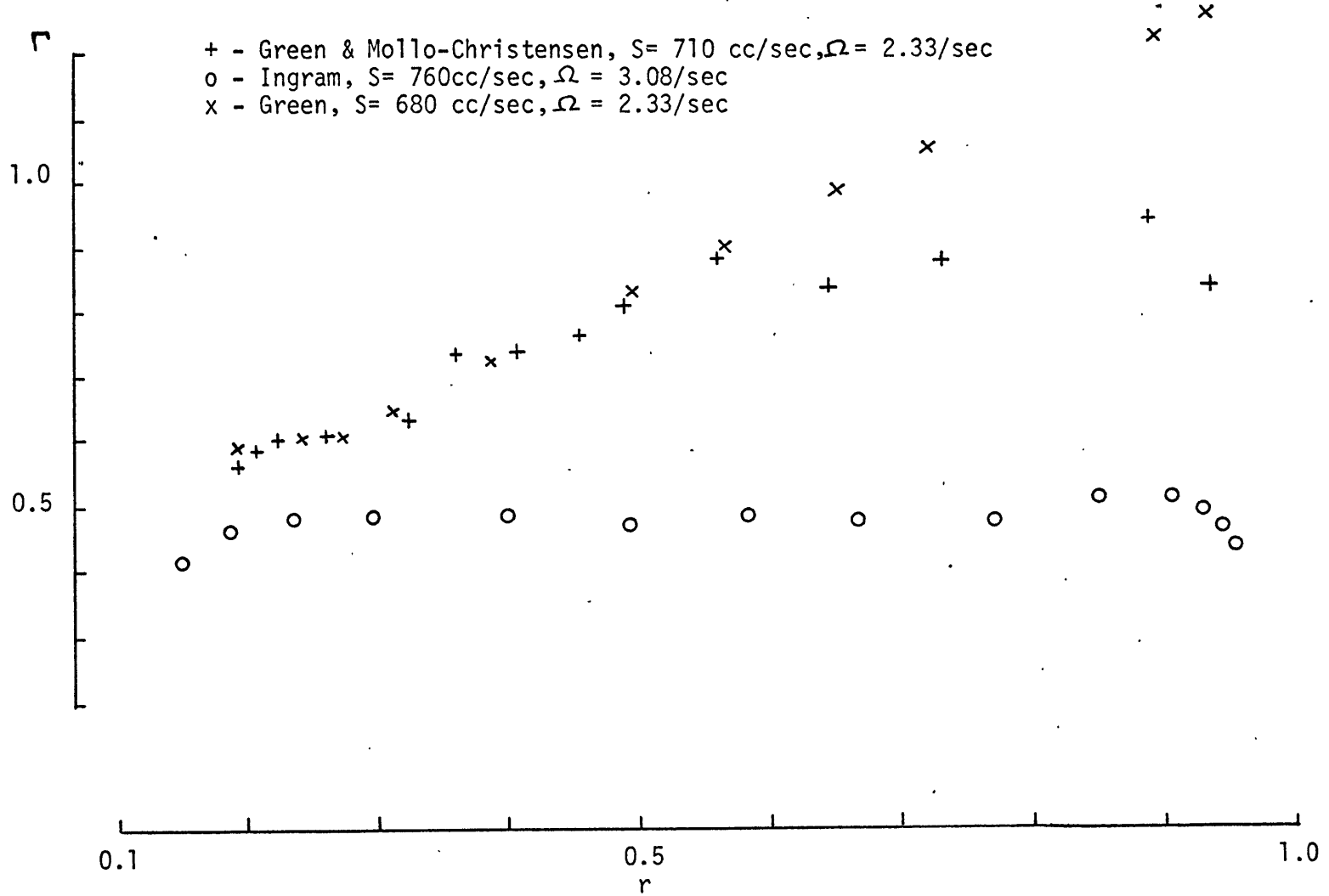
FIGURE 4.12 - COMPARISON OF CIRCULATION PROFILES

The figure shows a scatter plot with axis labels Γ (vertical) and r (horizontal), with the following legend:

+ - Green & Mollo-Christensen, S= 710 cc/sec, Ω = 2.33/sec
o - Ingram, S= 760cc/sec, Ω = 3.08/sec
x - Green, S= 680 cc/sec, Ω = 2.33/sec

Vertical axis values: 1.0, 0.5
Horizontal axis values: 0.1, 0.5, 1.0

most of their profiles were taken at low flux rates, Γ is found to vary widely. The "typical" values of non-dimensional circulation obtained by Green and Mollo-Christensen are comparable to both Tatro's and those shown presently. However, the unstable circulation distribution, $\dfrac{d\Gamma}{dr} < 0$ (Chandrasekhar [1961]) encountered in many of Green and Mollo-Christensen's results is not observed in figures 4.2 - 4.11.

Caldwell and van Atta (1970) obtain two series of five profiles, one with an effective tank radius of 109 cm and the other with a 190.5 cm radius. The results obtained using the smaller tank were discarded because of an unstable circulation distribution spanning over half the tank. The authors claim that centrifugal instabilities caused the unwanted response. The larger tank produced stable profiles at all radii less than 40 cm from the tank's outer vertical screen. No mention is made of side-wall boundary layers. Adjacent to the sink, their profiles do not show the expected Stewartson layer response (Hide [1968]), even to within 0.5 cm of the vertical screen. However, the smoothness of the interior profiles is a marked improvement over Green and Mollo-Christensen's results (1970). Caldwell and van Atta's work shows the superiority of continuously monitoring probes over fixed sensors. Although there is confusion in the article as to which hotwire configuration was used, their result format implies use of an extended probe (see Section 3.2).

Using their larger tank, Caldwell and van Atta show graphs of dimensional circulation (2π times Γ') against actual radius. Since no flux values are provided, the non-dimensional parameter, Γ ,

is uncomputable for comparative purposes. However, their curves
are somewhat similar to those seen in fig. 4.2 - 4.11. At the higher
fluxes they find a positive slope of Γ' with R. In contrast to
Green (1968), $\frac{d\Gamma'}{dR}$ shows a steady increase from the lowest
flow rate. Although the overall structure of Caldwell and van Atta's
profiles is comparable to the present work, the detailed distri-
bution is dissimilar. Only in the radial range of 0.35 - 0.50
(non-dimensional) is the $\frac{d\Gamma}{dr}$ relationship on flux equivalent for
both studies. Caldwell and van Atta find no change of slope $\frac{d\Gamma}{dR}$
from the inner vertical screen to r = 0.50, whereas figures 4.2 -
4.11 show a definite area of constant circulation and a side wall
boundary layer in the range r = 0.13 - 0.35. Lack of suitable
screening may have led to the unexplained profiles encountered by
Caldwell and van Atta. Similarly, the large inertial boundary
layer (adjacent to the source) produced in both their small and
large tanks could result from insufficient care to eliminate jet
effects on the outer screen. Although, Caldwell and van Atta ignore
results from r = 0.80 to 1.00, the influence of instabilities in
this region can distort profiles at radially inward locations. Sig-
nificantly, the change in slope of $\frac{d\Gamma'}{dR}$ (at r = 0.55 in the large
tank) for both of their tanks occurs 60 - 70 cm from the outer
screen. Although the present tank is 61.8 cm in radius, a compari-
son of the profiles seen by Caldwell and van Atta in their 107 cm
tank (discarded by them for being too small) and figures 4.2 - 4.11
show no resemblance.

A notable characteristic of the present work is a flattening
of the circulation profile radially outward from the inner side wall

boundary layer to the $\frac{d\Gamma}{dr} > 0$ region. In the literature, only Faller's (1965) numerical work shows any indication of a slope change in this region. This correction, dependent on local Rossby number, was presented in terms of velocity:

$$V_{Faller} = V_I \left(1 - \frac{3\epsilon_L}{10} + \frac{233\,\epsilon_L^2}{600}\right) \qquad\qquad \text{(Eq.4.3)}$$

where $\epsilon_L = S/2\pi R^2 \Omega \delta$

The present circulation profiles do not correspond to this curve, although the value of ϵ_L obtained for the change of slope is comparable. Furthermore, the observed velocities are 25 to 30% lower than those predicted by Faller.

The detailed structure of sidewall boundary layers in a rotating source-sink annulus, as a function of Rossby number, has not been reported previously in the literature. Linear theory predicts the formation of Stewartson layers with thicknesses of order $E^{1/3}$ and $E^{1/4}$ (Greenspan, [1968]), adjacent to both the source and sink walls. For example, the non-dimensional zonal velocity correction resulting from the $E^{1/4}$ layer adjacent to the source has a radial dependence of exp $(+ \sqrt{2}\ E^{-1/4}\ (r-1)\ )$. In Table 4-1, the observed thickness of the sidewall boundary layers is shown. For comparative purposes, values of ϵ_{sys} (ϵ_L evaluated at $R=R_0$) and $E^{1/4}$ are also included. The thickness of each boundary layer was calculated using the position of a detected change in slope of $d\Gamma/dr$, as seen in Fig. 4.13. In this particular case, (Fig. 4.13) a second (thinner) boundary layer is also observed. However, this thinner boundary layer was not considered in detail because of insufficient data coverage. No evidence of the thinner boundary layer was found adjacent

\

TABLE 4-1

Observed Non-dimensional Thickness of Side-Wall Boundary Layers

FLUX (cc/sec)	ROT(rad/sec)	ϵ sys	$E^{1/4}$	Observed Thickness	
				Source	Sink
.766	7.10	.03	.09	.20	.07
1040	7.10	.04	.09	.21	.10
1314	7.10	.05	.09	.15	.09
1588	7.10	.07	.09	.19	.09
1862	7.10	.08	.09	.17	.11
2136	7.10	.09	.09	.17	.15
2273	7.10	.10	.09	.17	.17
766	5.02	.04	.10	.20	.10
1040	5.02	.05	.10	.14	.11
1314	5.02	.07	.10	.17	.12
1588	5.02	.08	.10	.15	.13
1862	5.02	.09	.10	.17	.15
2136	5.02	.11	.10	.19	.17
766	3.08	.05	.11	.12	.09
1040	3.08	.07	.11	.17	.12
1314	3.08	.09	.11	.18	.12
1588	3.08	.10	.11	.20	.11
1862	3.08	.12	.11	.15	.13
2136	3.08	.14	.11	.18	.14
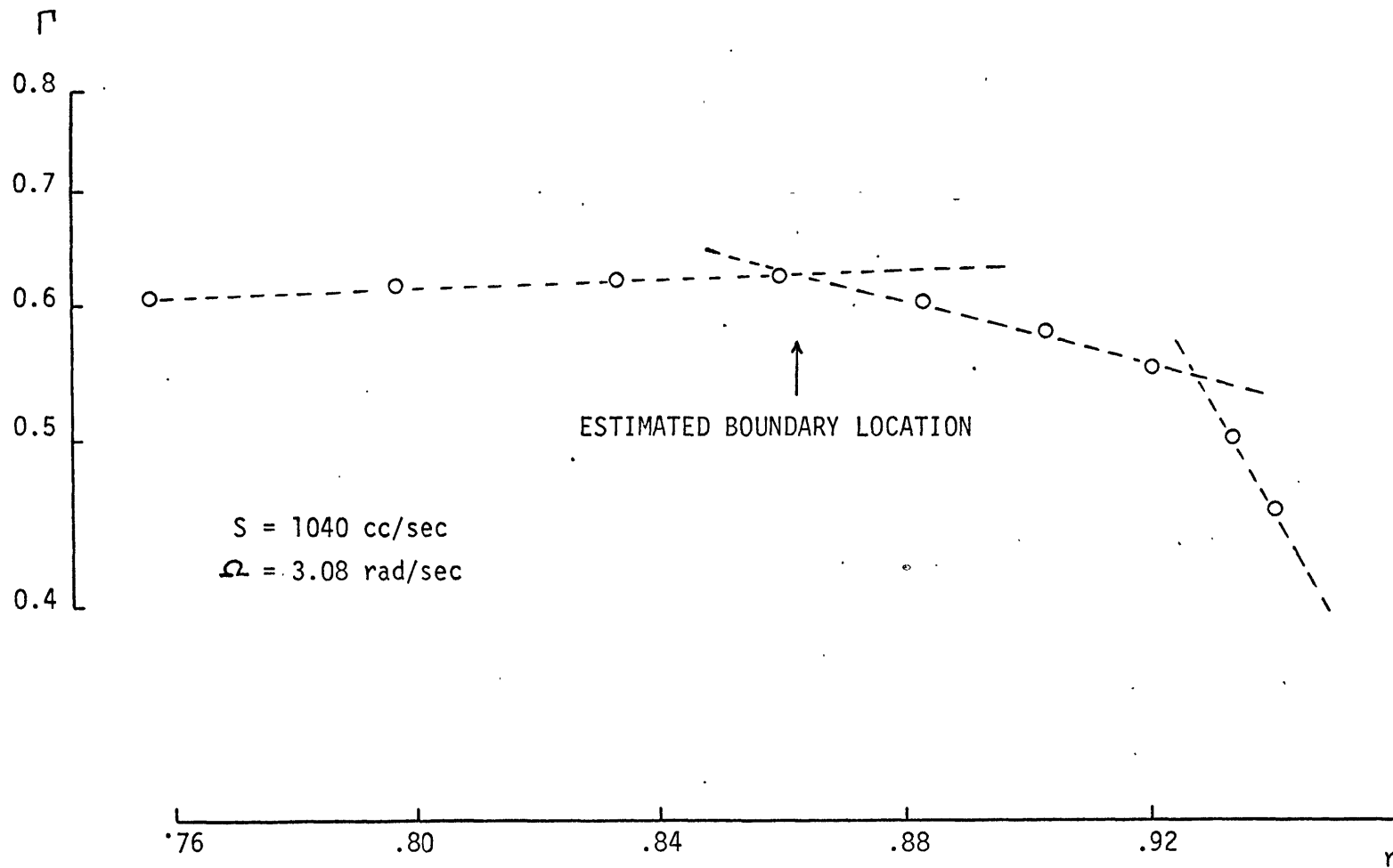
FIGURE 4.13 - TECHNIQUE OF LOCATING SIDEWALL BOUNDARY LAYER
(SEMI-LOGARITHMIC PLOT)

50.

to the sink. In contrast, the thicker sidewall boundary layers, shown

in Table 4-1, were observed in all of the circulation profiles, both ad-

jacent to the sink and the source. The characteristic slope ($d\,\ell n(v)/dr$)

of the thicker layer shown in Fig. 4.13 is -4 , which compares unfavorably

with the linearly predicted slope value of $-\sqrt{2}\,E^{-1/4}$ = -12 for the $E^{1/4}$

Stewartson layer, using Greenspan's non-dimensionalization.

From Table 4-1, the source sidewall layers are found to be signifi-

cantly thicker than those adjacent to the sink. A general tendency for

thicker boundary layers with increasing Rossby number is noted in the

sink region. However, no systematic dependence on system Rossby number

is found for the outer layer.

The sidewall boundary layers found by Caldwell and van Atta, using

their smaller tank, which under certain flow conditions, had a non-

dimensional thickness of 0.50, are not explained by the non-linear pre-

dictions of Hide (1968). However, Hide commented that "jet" effects often

play a dominant role in expanding the sidewall layers. This layer thick-

ening results from the fluid not being "spun-up" before injection from

the source to the interior. The unstable vorticity distribution produced

then generates large eddies at the outer radii. Caldwell and van Atta

mention observing similar large eddies in this region, but use the fact

as a rationale for building a larger tank. Jet effects are minimized

in the present work since the fluid passes through a large thickness of

polyurthane foam before entering the annulus. Green (1968), using a simi-

lar material, verified experimentally that the injected fluid was "spun-

up". This feature may explain the radically different profiles obtained

by Caldwell and van Atta both near the sink and the source. Since they

give no observations for the outer 35 cm of their larger tank, a definitive

comparison is not possible.

The circulation values (Fig. 4.2 - 4.11) were subject to the largest errors at the smaller radii. This was due mainly to the estimation of probe position as taken from the X-Y recorder. The region of increasing circulation was unquestionably present, and was shown to play a significant role in the wave dynamics (Chapter V). This feature may be a high Rossby number effect as mentioned by Greenspan (1968), but the dependency is a complex one.

Summarizing, the profiles of circulation demonstrate a greater amount of structure than predicted theoretically. The sidewall boundary layer adjacent to the sink is of order $E^{1/4}$ in thickness. In contrast, the thickness of the source sidewall layer is generally twice as wide. This difference is not explained quantitatively by Barcilon's (1970) work. However, both Barcilon and Hide (1968) claim that the source boundary layer is the only one subject to non-linear modification. In explaining the absence of a similar radial structure in the work of Green (1968), calibration techniques may be at fault. The assumed linear relation between $U^{1/2}$ and E^2, when calibrating (see Chapter III) at low speeds, is grossly in error. Obviously, the high flow speeds encountered near the sink do not allow a similar explanation for the absence of an inner sidewall layer in Caldwell and van Atta's work. Nevertheless, this distortion may be attributable to their inner screen. Since a vertically oriented probe cannot differentiate between radial and zonal velocities, a "jet effect" in the area of the sink would alter their observed circulation profile.

4.2   Vertical Structure of Velocity Adjacent to Horizontal Boundaries
4.2.1 Theoretical Predictions

Adjacent to any horizontal flat boundary in a homogeneous rotating fluid, an Ekman layer is formed. The characteristic thickness

of this velocity adjustment region is $(\frac{\nu}{\Omega})^{1/2}$ (Lewellen [1965]).

In the source-sink annulus, these Ekman layers are found on both the top and bottom walls. Their vertical structure is as follows (Greenspan [1968]):

$$\frac{u}{V_\infty} = e^{-z/\delta} \sin z/\delta \qquad \text{(equation 4.4)}$$

$$\frac{v}{V_\infty} = (1 - e^{-z/\delta} \cos z/\delta) \qquad \text{(equation 4.5)}$$

where u,v = radial and zonal components of velocity field

V_∞ = interior zonal flow (outside Ekman layer region)

z = vertical coordinate (measured positive inward from wall)

δ = Ekman layer thickness ($[\frac{\nu}{\Omega}]^{1/2}$)

A graphical representation of equations 4.4 and 4.5 yields a distribution of velocity with height as seen in fig. 4.14.

A slight departure from the theoretical profile has been predicted by Barcilon (1970), based on a non-linear modification. Figure 4.15 shows this influence as a function of the interior vorticity.
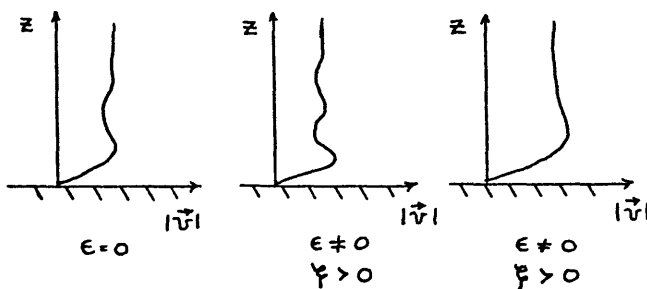
Fig. 4.15 Ekman layer changes as a function of ϵ and vertical vorticity. (Barcilon [1970])

The expansion procedure used by Barcilon is questionable since lower order terms dropped in the momentum equation are kept in the uniformity condition required for transition to the interior (A.Bennett, personal communication). By including these terms many "wiggles"
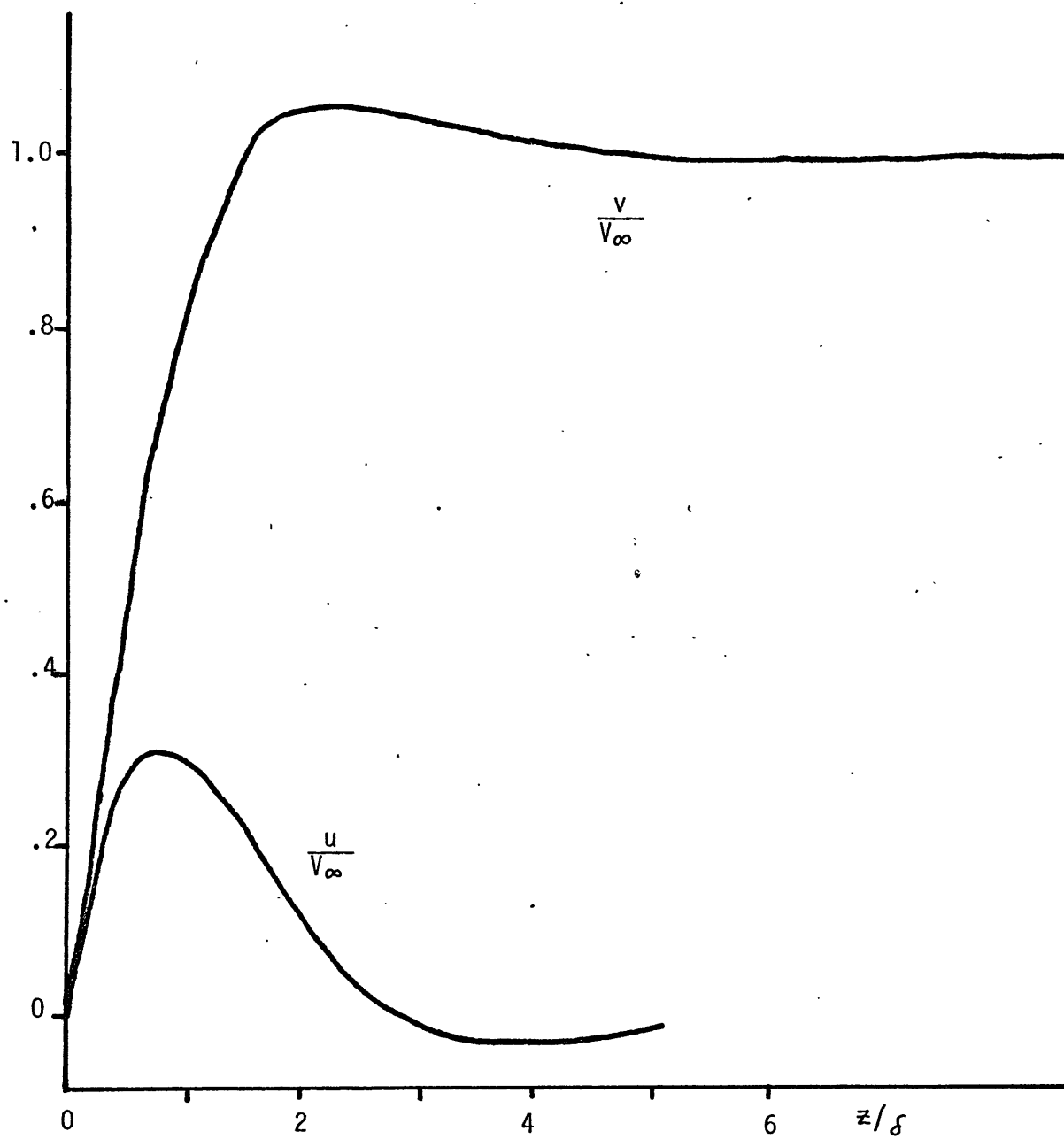
FIGURE 4.14

THEORETICAL STEADY EKMAN LAYER PROFILE

u: radial

v: azimuthal

V_∞ : azimuthal interior flow

of the type shown in figure 4.15 are expected. The constructive and destructive interference of these "wiggles" yields an Ekman layer profile which is different from Barcilon's prediction.

To date, no mention has been made in the literature of any alterations in the Ekman layer structure resulting from incident inertial waves.

4.2.2. Observed Vertical Structure

Incorporating the heat loss correction methods summarized in Chapter III, 26 azimuthal and 2 radial profiles were taken adjacent to the lower boundary. The sparseness of radial profiles is a result of the inherent technical problems (Appendix II). The two radial sets were obtained close to the sink, where the high interior velocity afforded better resolution. A number of similar observations, for lower interior speeds, were difficult to interpret. However, the position of the radial velocity maximum in this unreported work, varied little from the two profiles shown. Figure 4.16 shows two series of observed azimuthal velocities, and the theoretical Ekman layer curve (equation 4.5). Profile #23 shows a much higher degree of "wiggliness" than is general in most other results. This is attributable to the lower flow speeds attained at the outer radii and possibly to the higher system Rossby number (low rotation). Figures 4.17 and 4.18 show similar graphs of zonal velocity against non-dimensional height as well as the radial velocity distribution (compared to equation 4.4). These profiles are taken in two dynamically different regions. The former is within the side-wall boundary layer, while the latter is in the highest local

PROFILE 23

r= 0.76

S= 1314 cc/sec

Ω = 2.14 rad/sec

O = Theoretical prediction

• = Observed profile
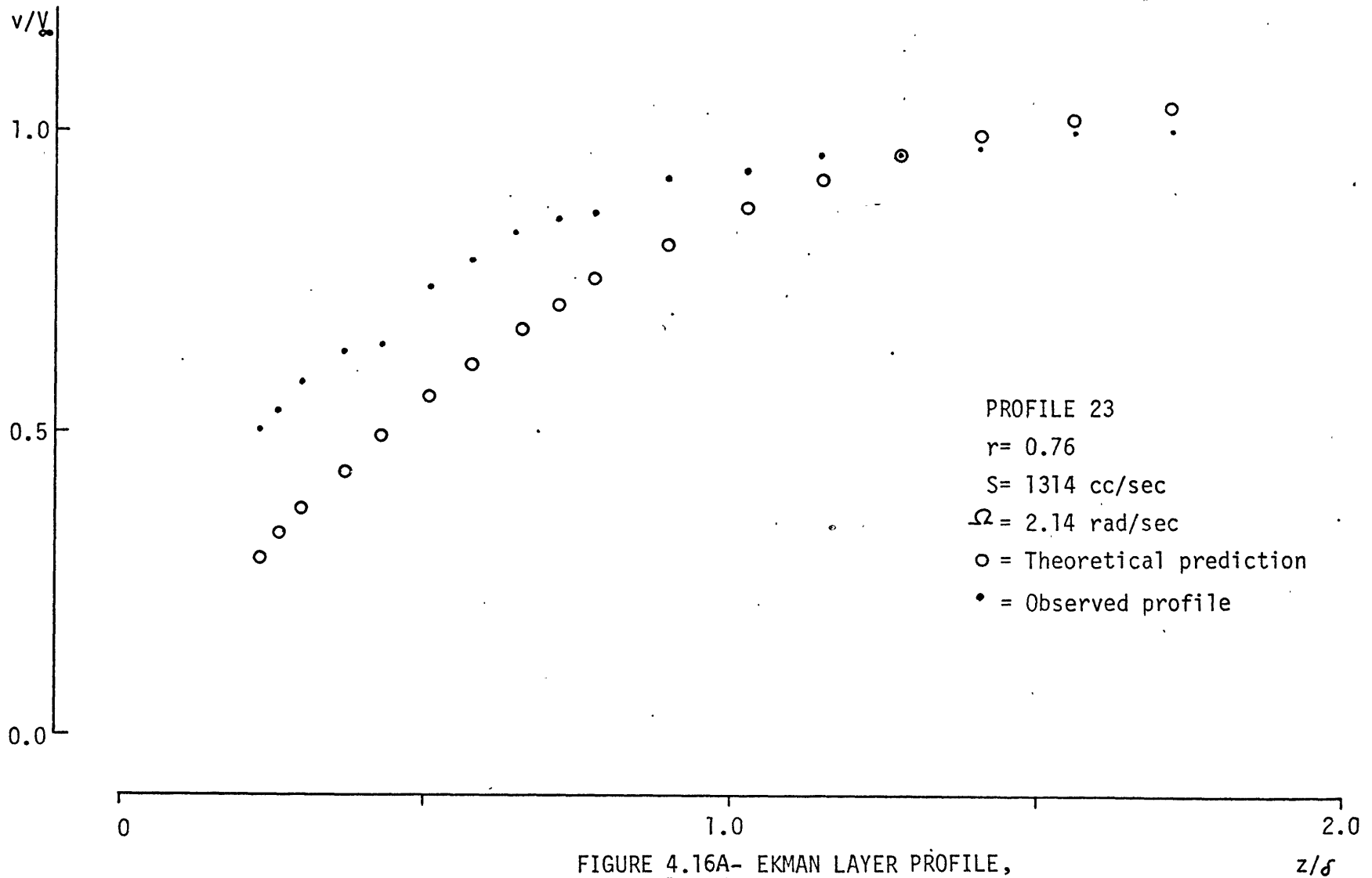
FIGURE 4.16A- EKMAN LAYER PROFILE,
R = 18.5", ZONAL VELOCITY

56.

PROFILE 25
r= 0.89
S= 1561 cc/sec
Ω= 6.53 rad/sec
O = Theoretical prediction
• = Observed profile
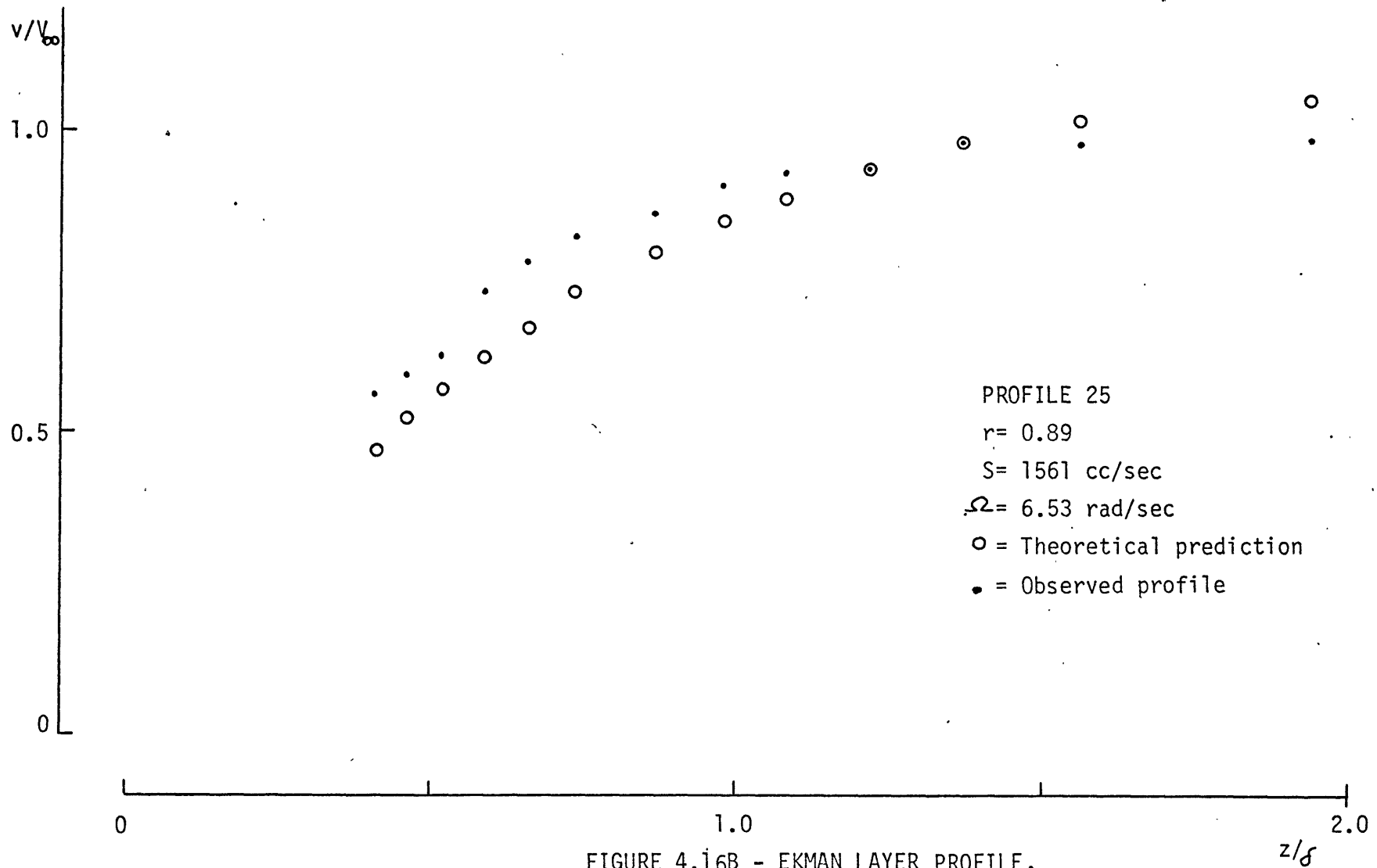
FIGURE 4.16B - EKMAN LAYER PROFILE,
R = 21.6", ZONAL VELOCITY
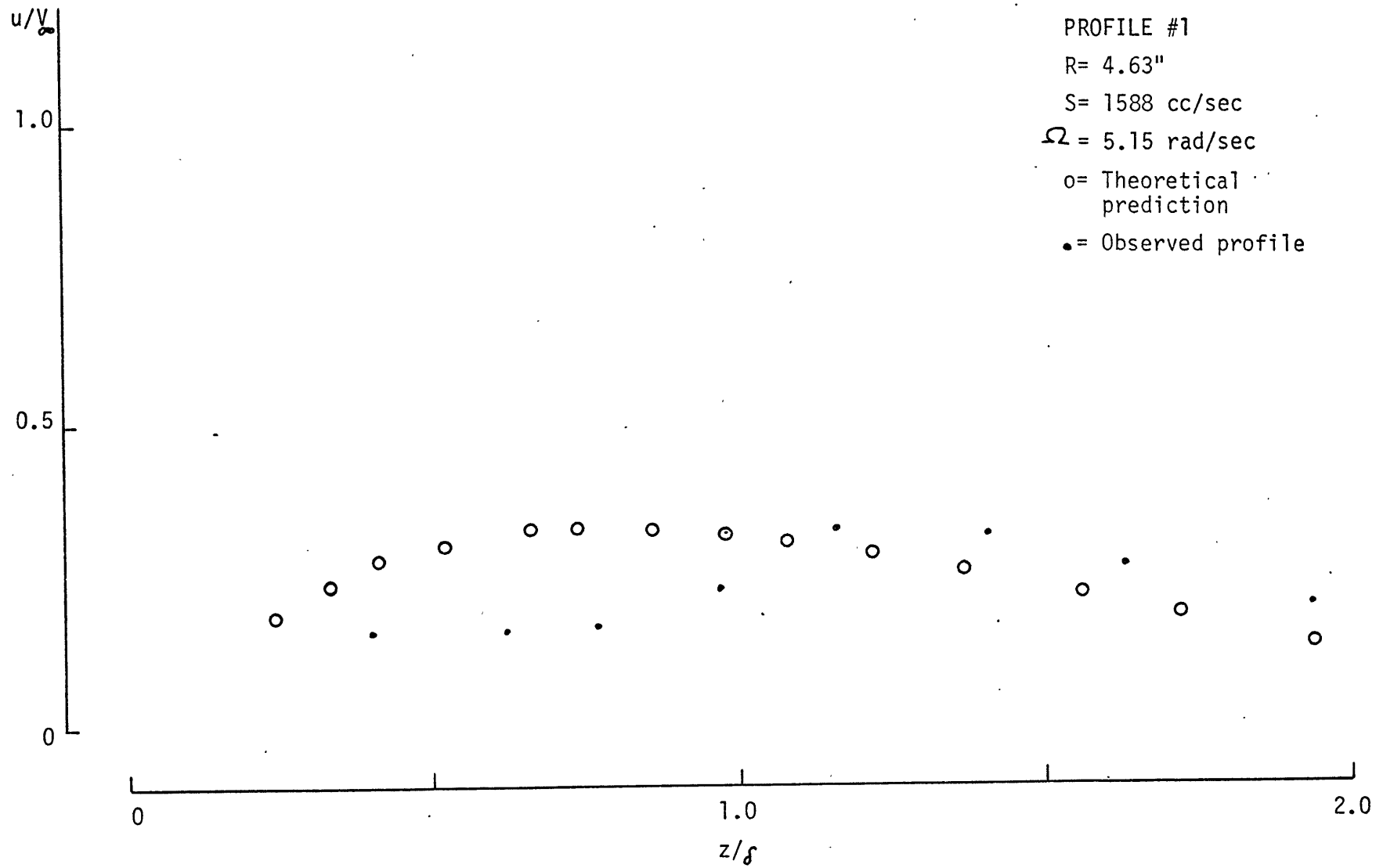
FIGURE 4.17A - EKMAN LAYER PROFILE, R =4.63", RADIAL VELOCITY
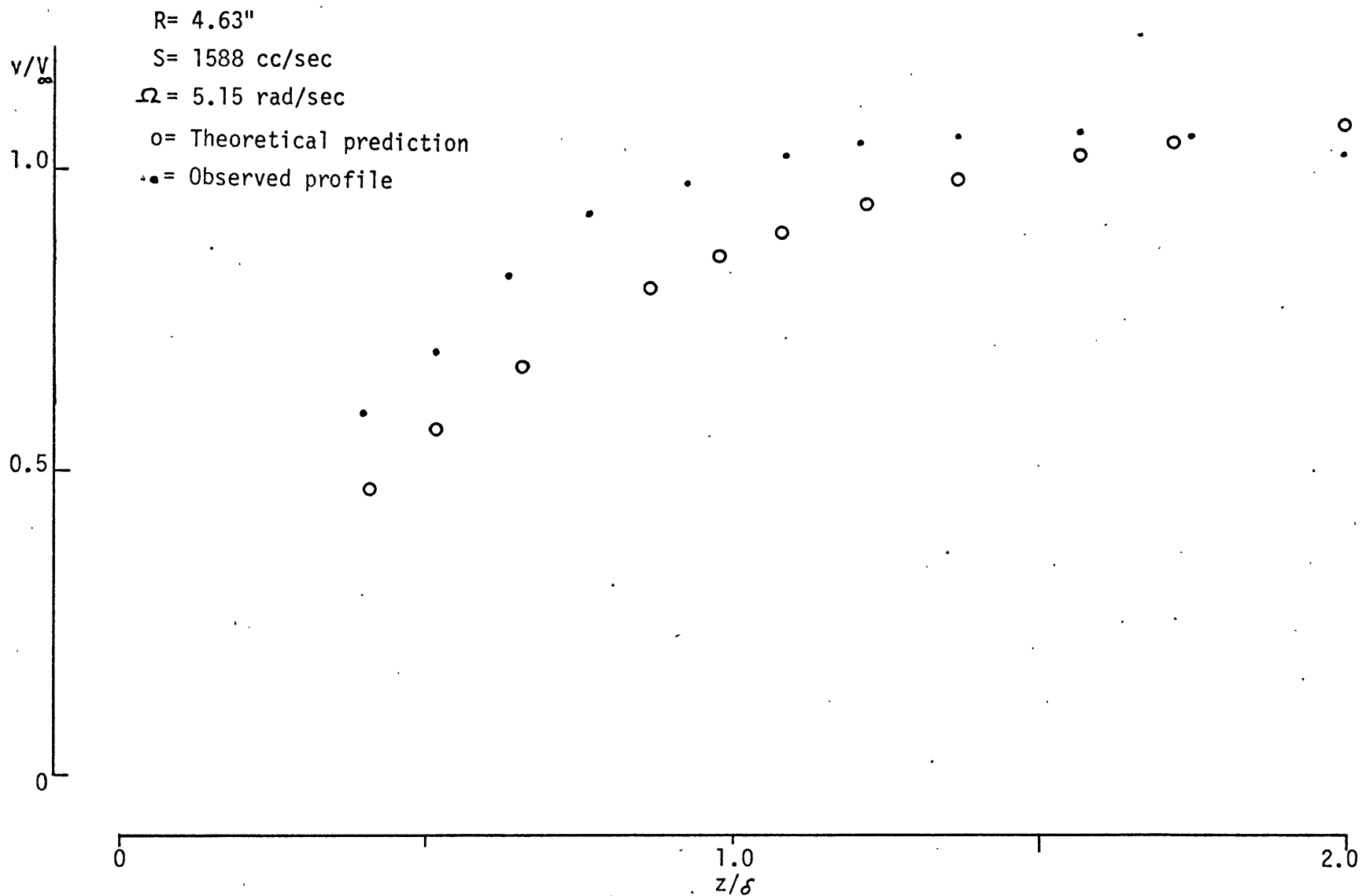
FIGURE 4.17B - EKMAN LAYER PROFILE, R= 4.63"
ZONAL VELOCITY
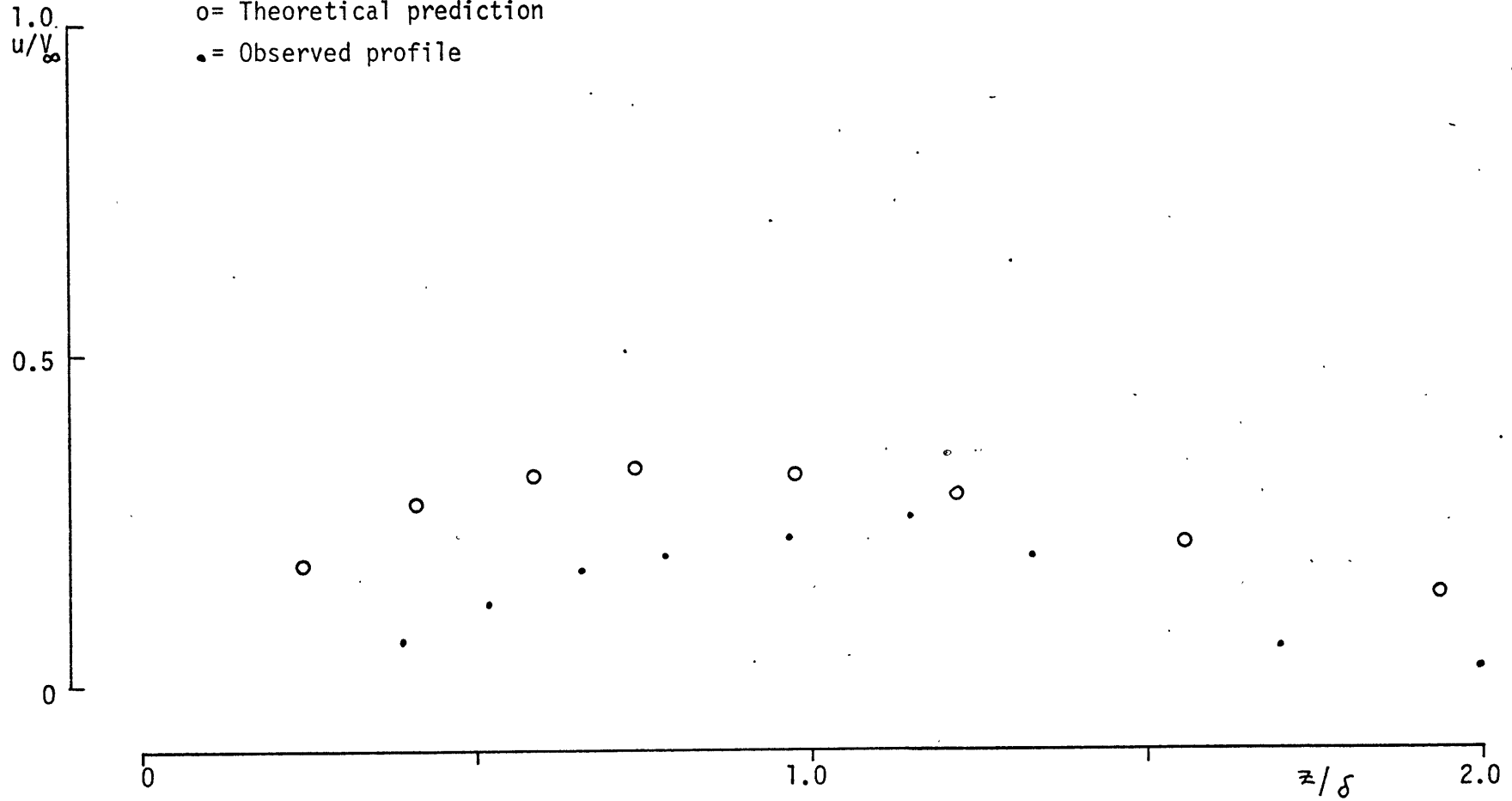
FIGURE 4.18A – EKMAN LAYER PROFILE, R= 6.00"
RADIAL VELOCITY
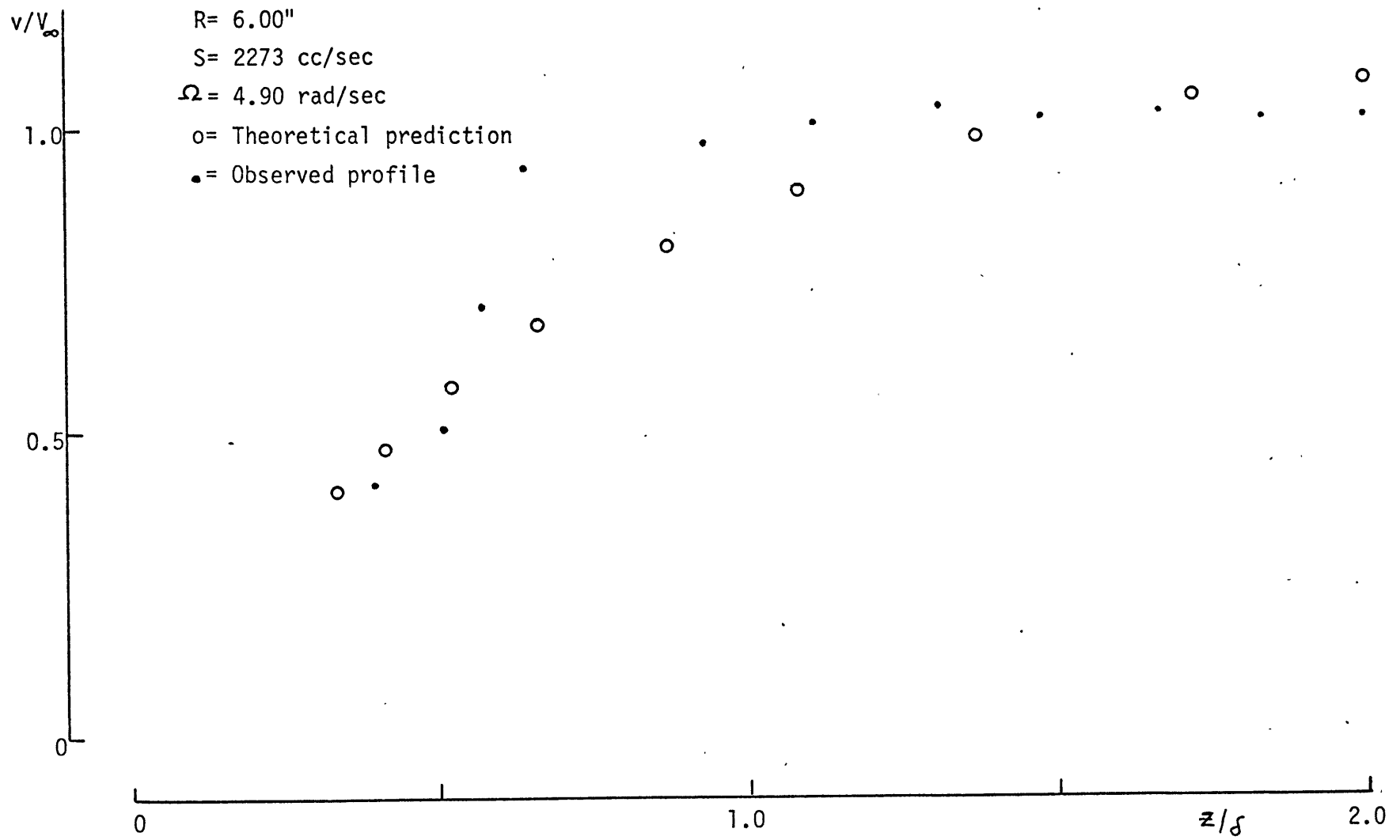
FIGURE 4.18B - EKMAN LAYER PROFILE, R= 6.00", ZONAL VELOCITY

Reynolds number region of the tank.

Table 4-2 shows a synoptic view of all the zonal Ekman layer velocity profiles obtained. This chart gives the ratio of measured Ekman layer thickness (δ_M) to the theoretical prediction (δ), as well as the actual and theoretically predicted Reynolds and Rossby numbers (assumes $\Gamma = 1.0$ in equation 4.2) Both sets of these parameters are included, since the wide diversity of measurement techniques in the literature leaves only the ideal Re and Ro numbers as invariant between different experimental setups. The measured Ekman layer thickness (δ_m) is the vertical distance at which the observed zonal velocity is 86% of the interior value (V_∞).

4.2.3 Discussion

The profiles confirm that the observed Ekman layers in the annulus closely match the prediction of equations 4.4 and 4.5. However, the measured boundary layer thickness is typically 15 - 20% smaller than the theoretical value. At the smaller radii, significantly thinner layers are observed. The modification predicted by Barcilon (1970) is not apparent, although, only a few of the profiles are in a parameter range suitable for comparison.

Tatro (1966) was the first experimenter to conduct Ekman layer studies in an annulus. He estimated the boundary layer thickness by observing the vertical position of the maximim radial velocity and multiplying this height by $4/\pi$. This technique can lead to erroneous thicknesses, as a result of heat losses near the wall. This influence is apparent on all of Tatro's Ekman layer profiles. It can explain his observation that the boundary layer thickness

TABLE 4-2

Comparison of Observed and Theoretical Ekman Layers

(Part 1)

PROFILE #	r	FLUX cc/sec	ROT rad/sec	δ_M/δ	MEASURED Re$_L$	ϵ_L	THEORETICAL Re$_L$	ϵ_L
1	0.19	1588	5.15	0.70	50.4	.52	139	2.05
2	0.25	2273	4.90	0.62	93.7	.68	153	1.79
3	0.28	903	5.28	0.89	26.6	.24	54	.54
4	0.28	1314	5.53	0.93	44.2	.40	79	.77
5	0.32	766	3.89	0.83	17.1	.21	42	.41
6	0.32	766	3.77	0.85	15.1	.19	42	.41
7	0.32	1561	3.77	0.81	36.2	.45	86	.84
8	0.41	766	5.02	0.77	12.3	.11	33	.21
9	0.41	1561	5.02	0.77	28.2	.26	68	.46
10	0.41	766	3.89	0.73	12.0	.13	33	.24
11	0.41	1561	3.89	0.74	26.7	.29	68	.51
12	0.41	766	6.28	0.76	11.5	.11	33	.19
13	0.41	1561	6.41	0.78	29.3	.23	68	.37
14	0.43	1040	7.47	0.77	21.0	.16	43	.24
15	0.43	1451	7.66	0.84	36.4	.17	60	.30
16	0.57	1382	5.28	0.91	18.3	.08	41	.20
17	0.57	2273	5.15	0.89	29.2	.13	67	.33
18	0.71	1451	5.40	1.06	16.3	.07	34	.13

TABLE 4-2.

(Part 2)

19	0.71	1999	5.53	0.89	20.0	.07	47	.18
20	0.76	1040	6.34	0.81	9.1	.04	24	.08
21	0.76	1561	6.41	0.86	16.4	.06	36	.11
22	0.76	1314	3.89	0.75	11.8	.07	30	.12
23	0.76	1314	2.14	0.76	13.4	.10	30	.17
24	0.76	2246	2.14	0.77	20.9	.16	51	.29
25	0.89	1561	6.53	0.87	9.1	.03	30	.08
26	0.89	1040	6.59	0.83	6.1	.02	20	.07

decreases with increasing flux. If one considers the heat loss to be invariant with the forced convection rate (see Appendix II), an increasing interior velocity would necessarily lower the observed location of the voltage maximum.

. Green and Mollo-Christensen (1970) show four velocity profiles in the boundary layer. They found no change in the measured Ekman layer thickness (1.7δ), with differing Reynolds and Rossby number combinations. Their work was limited by indefinite probe height location and a linearly extrapolated low velocity calibration (see Chapter III). Since Ekman boundary layer is of order 2mm in thickness, positional accuracy is a critical factor. Similarly to Tatro, none of their readings were corrected for wall losses.

Of the profiles shown in the literature, Caldwell and van Atta's (1970) provide the closest resemblance to theoretical predictions. In a Reynolds number range of 33 to 131, the authors found a negligible difference (less than 3.5%) in the observed Ekman layer height from δ. For a value of Re equal to 662, a slight decrease (10%) in height was noted (assuming a labeling error in their figure 7). Surprisingly, Caldwell and van Atta make no corrections for heat losses to the wall. In their article, they comment that no loss was apparent to within 0.02 cm of the boundary. As seen in Appendix III, studies using a similar plywood boundary for the tank wall, showed a sizeable loss at a height of 0.07 cm. This discrepancy is unexplained. Caldwell and van Atta plot only a single radial profile, because of the problems discussed previously. The authors do not discuss any problems associated with side-wise forced convection (see Appendix II). In agreement with Green

and Mollo-Christensen, they find no systematic change of Ekman layer thickness with radius.

The results of Table 4-2 show no consistent dependence on any of the system parameters. Similarly, Caldwell and van Atta were unable to relate their boundary layer thicknesses to the interior flow characteristics. For the higher Reynolds' number range, Caldwell and van Atta found the layer thickness to decrease (up 15% for Re_L = 662). Table 4-2 does not include any comparative values of Re_L.

Within the sink side-wall layer, a significant decrease of the Ekman layer thickness was noted. Of the two profiles taken, the higher Reynolds number flow produced the thinner boundary layer. In contrast, no changes were observed within the source side-wall layer. Caldwell and van Atta show no results under similar flow conditions. Although some of their observations are within the theoretically predicted sink side-wall layer region, no Ekman layer modification was detected. As mentioned in section 4.1, Caldwell and van Atta did not observe a side-wall boundary layer adjacent to their sink and their outer layer was distorted by eddy motions.

The differences observed between the results of Caldwell and van Atta and those of Table 4-2 can be explained to some extent by the interior flow field. All of Caldwell and van Atta's observations were taken for a radially increasing circulation distribution. In contrast, with the varied interior structure shown in figures 4.2-4.11 an alteration in the Ekman layer profiles is expected.

In analyzing the influence of non-linearities to the Ekman layer, profiles 10, 11, 23 and 24 are the most suitable. The results

show no important changes of boundary layer thickness and no increased "wiggliness" in the individual point profiles. In actuality, the higher Rossby number Ekman layers, generally exhibit a greater degree of uniformity than the rest.

4.3   Summary of Mean Conditions

The experimental flow conditions match the theoretical predictions of Lewellen (1965) and Greenspan (1968) more closely than previously reported in the literature (Green [1968], Green and Mollo-Christensen [1970], and Caldwell and van Atta [1970]).

The most striking feature of the interior circulation profiles was the positive vorticity region apparent in the higher Rossby number observations. As predicted by linear theory, the circulation was virtually independent of radius for small Rossby number. In all experiments, sidewall boundary layers were observed adjacent to the source and sink. The source boundary layer was found to be significantly thicker than the predicted Stewartson $E^{1/4}$ - layer. On the horizontal walls, Ekman layers are observed under all flow conditions. Their thickness is of order 15% thinner than the theoretical prediction.

Since the circulation is typically 60-70% of that predicted theoretically, the Re# and Ro# are greatly overestimated if an ideal profile is employed in their calculation. Notably, within the sink sidewall layer, the local Reynolds' number may be less than critical (see Chapter 2), while the opposite is true at a slightly greater radius. By assuming the existence of a theoretical Ekman layer thickness, errors (over-estimation) of 30-35% are possible within the

sink side-wall layer.   The usual technique of observing Ekman layer

instability has been to place a probe at one of the innermost radii,

and increase the local Re# (Tatro [1966], Green [1968]) to the

critical value.   Using this technique, the radius of the observed

"critical" Reynolds number for instability onset may be under-es-

timated.   Most authors do not give the actual radius of observed

instabilities, but mention that it is "close to the sink".   To

obtain accurate onset criteria, one must profile both the interior

and Ekman layer flow to ascertain the maximum Reynolds' number position

for each configuration.   Increasing the flux at a random fixed position

adjacent to the sink is a misleading method for observing instabilities.

CHAPTER V

Wave and Instability Phenomena

We now turn our attention to time dependent flows. As has been observed by previous workers, instabilities may occur in the Ekman layer for certain parameter ranges. These may be centrifugal instabilities and other linear or non-linear instabilities. An oscillation or wave phenomenon observed at a certain location does not necessarily imply that the flow is unstable at that particular place. Oscillatory disturbances may influence the flow at a distance by excitation of inertial waves or by propagating waves in the Ekman layers.

In order to obtain indications of where oscillatory disturbances originate and how they are distributed, a wave amplitude survey was made under varying flow conditions.(Section [5.1]).

Next, spectra of fluctuations were measured in a number of locations and for several values of flux and rotation rates. Section (5.2) describes a hysteresis in the dependence of spectra on flux. We then proceed to a discussion of a low Reynolds number instability observed previously by Arons, Ingersall and Green and analyzed by Stern. (Section 5.3). The remaining sections include a discussion of inertial waves and of Ekman layer instability.

5.1 General Oscillatory Activity

To give a picture of the distribution in intensity of oscillations the difference between the maximum and minimum zonal velocities was calculated for each mean flow measurement (fixed probes). This value was then divided by the steady velocity at the same location, and a "wave intensity percentage" was obtained. The results were subject to some estimation error (typically 5-10% for the lowest percentage shown), as they

were optically read from an oscilloscope.

5.1.1 Wave Intensity in the Interior and Side-Wall Regions

Table 5-1 shows the wave intensity percentage for four different flow conditions as a function of radial position (r) for $z=12cm$. From this chart, the region of greatest wave activity was found within the radial limits of r= 0.29 and 0.45. Also observed was a smaller local maximum at larger radii (r greater than 0.81). Only at the lowest flux values were the two peaks comparable in amplitude. Upon re-examining figures 4.2 - 4.11, one finds that the regions of high wave activity were those of $\frac{dr}{dr} = 0$ or $\frac{dr}{dr} < 0$. Furthermore, the inner maximum of wave intensity was located in the area of largest local Reynolds numbers in the tank, as discussed in Section 4.3. This is also the region of the most unstable Ekman layers. At the outer maximum, no large eddies, of the type indicated by Caldwell and van Atta (1970), were observed. The increasing wave intensities at larger radii were partially due to the smaller mean velocities encountered within the source sidewall boundary layer.

5.1.2 Variation of Wave Amplitude with Height in the Ekman Layer

In a similar fashion to the preceding section, wave intensity was recorded simultaneously with measurements of the mean zonal velocity profiles in the Ekman layer. This technique allowed a comparison of the interior and boundary layer oscillatory activity. To facilitate this analysis, the wave intensity percentage evaluated at an "interior" position (most distant observation from the horizontal tank wall) was subtracted from the values calculated at each of the smaller heights. These residual differences showed significant

TABLE 5 - 1

Interior Wave Activity

Wave Percentage (Peak-to-Peak)

ROT(rad/sec):	3.14	5.02	6.28	6.28
FLUX(cc/sec):	1176	1724	765	2272
r	%	%	%	%
.21	2.9	4.2	2.8	5.3
.25	2.8	2.8	2.8	5.4
.29	4.5	4.2	3.7	5.6
.33	3.0	5.6	1.8	8.5
.37	2.8	10.0	2.8	12.8
.40	3.9	9.1	3.0	11.9
.45	2.1	7.2	3.0	10.7
.50	2.6	5.4	2.6	9.0
.54	2.0	7.0	2.6	9.0
.58	2.7	6.2	2.6	9.0
.61	2.6	3.6	2.6	7.3
.66	2.6	4.0	1.3	3.6
.71	2.6	4.0	2.4	3.6
.78	2.4	2.0	2.8	6.0
.81	3.4	4.5	5.8	6.8
.87	4.0	5.2	6.6	7.3

variation with height, and it was thus possible to isolate minima and maxima. Attempts to compare extremum positions to features of the velocity profile, such as critical points in the zonal velocity field, were unsuccessful.

Table 5-2 shows four series of "residual" wave activity (interior wave intensity subtracted) as a function of non-dimensional height. By isolating local minima and maxima from these distributions, and the remaining Ekman layers, an overall view of wave activity is obtained in Table 5-3. The relevant system parameters for each experiment are found in Table 4-2. An initial glance at Table 5-3 reveals a large amount of scatter in the location of extrema. However, by taking account of the mean interior flow conditions (see figs. 4.2-4.11), some similarity can be deduced for different Ekman profiles. The characteristics of the interior are arbitrarily separated into five groupings: two side-wall layers (A, E) a transition zone (B) and zones with absence (C) or presence (D) of positive interior vorticity. Although qualitative, this approach shows the influence of the mean interior flow field in determining the wave activity pattern in the Ekman layer.

As the method of observing wave amplitude is subject to some degree of uncertainty, one cannot infer any precise conclusions.

5.2 Wave Spectra

5.2.1 Introduction

Although the wave intensities gave an overall view of time dependent motion, a more detailed picture is required. To separate the characteristics of wave frequency components, frequency spectra were calculated. This allowed a description of the frequency components of wave motions at differing locations in the annulus.

TABLE 5 - 2

Residual Wave Intensity in the Ekman Layer

(Part 1)

PROFILE #1		PROFILE #19	
Height(z/δ)	Percentage	Height(z/δ)	Percentage
0.40	4.0	0.42	0.0
0.52	5.0	0.51	+1.0
0.64	5.0	0.63	+2.0
0.77	0.0	0.74	+2.0
0.93	-3.0	0.87	+3.0
1.09	0.0	1.02	+2.0
1.21	-1.0	1.21	0.0
1.37	-1.0	1.42	0.0
1.57	0.0	1.69	0.0
1.75	1.0	2.00	+1.0
2.02	0.0	2.38	0.0
2.25	0.0	2.79	0.0
		3.10	0.0

Error: ± 0.2   Error: ± 0.2

TABLE 5 - 2
(Part 2)

PROFILE #12			PROFILE #25	
0.40	5.0		0.41	-0.1
0.47	-1.0		0.46	-0.1
0.53	-1.8		0.52	-0.8
0.60	3.0		0.59	-0.7
0.66	0.0		0.66	-1.0
0.72	2.0		0.74	-2.2
0.80	0.5		0.87	-1.0
0.85	4.3		0.98	-0.1
0.93	2.6		1.08	-0.2
1.02	0.9		1.22	0.5
1.12	0.9		1.37	0.2
1.26	-0.8		1.56	-0.6
1.46	0.1		1.94	-0.4
1.74	1.1		2.15	0.0
2.04	2.0			
2.50	2.8			
2.94	2.8			
3.38	0.9			
3.82	0.9			
4.58	0.6			
5.63	0.0			

Error: $\pm$ 0.3

TABLE 5 - 3

Height of Maxima and Minima in Residual Wave Activity of the Ekman Layer

(Part 1)

PROFILE #	LOCAL MAX(z/δ)	LOCAL MIN(z/δ)	LOCAL MEAN IN- IOR FLOW CHARACTERISTICS
1	0.64	0.93, 1.30	A
2	0.64		A
3	0.64	0.92, 1.55	A
4	0.88	1.44, 1.75	B
5	0.49, 0.85	0.58, 1.08	C
6	0.48, 1.01	0.59	C
7	0.48, 0.70	0.59, 1.48	C
8	0.57		B
9	0.51, 0.93	0.70	D
10	0.50, 0.93	0.66	D
11	0.57, 0.84	0.65	D
12	0.60, 0.85, 0.40	0.66, 1.26, 0.53	C
13	0.55	0.64	D
14	0.55, 0.72	0.66	D
15	0.77, 1.25	0.66	D
16	0.93, 2.09	0.50	D
17	0.49, 1.20	0.76	D
18	0.61, 1.29	0.75	C
19	0.87	1.42	C

TABLE 5 - 3

(Part 2)

20	0.62	0.70	C
21	0.53, 0.83	0.62	B
22	0.57	0.49	B
23	0.66, 1.03	0.51	B
24	0.40, 1.35		B
25	0.59, 1.22	0.52, 0.74	E
26	0.50, 0.73	0.58	E

KEY: A: Sink Side-Wall Boundary Layer.

                 B: Transition Region between A/C and D/E

                 C: Zero Vorticity Region

                 D: Positive Vorticity Region

                 E: Source Side-Wall Boundary Layer

The local Reynolds number, as defined by Tatro (1966), Faller (1965) and others, is included with each spectra in order to delineate any change that may have been attributed to previously predicted instability mechanisms. The experiments were planned so as to include a wide range of both Reynolds and Rossby numbers. These non-dimensional parameters were calculated assuming an interior potential vortex and thus derivable from system constants. They are as follows:

$$Re_L = \frac{S \delta}{2\pi R \nu \delta} = \frac{S}{2\pi R \nu} \qquad \text{(equation 5.1)}$$

$$\epsilon_L = \frac{S}{2\pi R^2 \Omega \delta} = \frac{S}{2\pi R^2 \nu^{1/2} \Omega^{1/2}} \qquad \text{(equation 5.2)}$$

where Re_L = local Reynolds number

ϵ_L = local Rossby number (Ro_L)

S = volume flux in cc/sec.

and the other variables as previously defined. The rationale for using this derivation was the inability to measure the local boundary layer thickness and circulation profile for each of the spectra. An analysis of the actual velocity (non-dimensional) values (e.g., figures 4.2-4.11) showed that using the ideal profile for calculating the zonal speed was subject to a substantial error. The theoretical relations employed in equation 5.1 provided a means of cancelling the Ekman depth dependence. However, in equation 5.2, this was not true. By assuming the theoretical Ekman layer thickness, overestimates of up to 30% in δ were possible (see section 4.2), but generally, 15% was typical.

The inertial frequency limit, 2Ω (Greenspan [1970]) was used to non-dimensionalize the wave frequencies. Frequencies above this limit were observed only in the region close to the sink. A typical spectral output showed the relative energy as a function of wave frequency in hertz. The energy scale was generally in arbitraty units (au), unless otherwise specified. Analysis using the auto-correlation computer was performed in the A.C. mode, and thus liable to a low frequency cutoff, from D.C. to 0.016 Hz (0.032 Hz double channel). As the typical rotational frequency was 1 Hz, this limitation was not crucial. Operating on the D.C. mode often lead to an excessive amplitude for zero frequency and a poor signal-noise ratio at higher frequencies.

All data were recorded on the eight-track magnetic tape recorder. Simultaneously, a short record of each signal was displayed on a 4-channel pen recorder.

5.2.2 Spectra Distortion and Hysteresis

The initial experiments (not shown here) produced a number of spurious spectra. This was attributed to the mean flow field being in a state of transition. By letting the fluid "spin up" and more crucially, allowing the rotation rate to stabilize, this shortcoming was alleviated. To avoid any gradual shift in the tank's angular velocity, delays much longer than the spin up time were required.

As mentioned in Appendix II, it was possible for large external disturbances to alter the mean and transient flows. Thus a distorted spectra resulted, when insufficient care was taken to avoid extraneous exterior forcing. This influence was significant only for

observations at the smaller radii. More specifically, the distur-
bances were apparent only in the region of constant circulation,
radially adjacent to the sink side-wall layer. The perturbations
were amplified in the high Rossby number zero vorticity flow field,
which existed adjacent to the sink sidewall layer.

The spectra were found to depend on the time history of the flux,
in the sense that a hysteresis effect was observed. Although un-
reported by previous workers, this phenomenon may have distorted
their instability onset criteria. The hysteresis feature was noted
during a series of transient flux experiments. Simply stated, on
increasing the flux, a large amplitude wave appeared at a particular
Reynolds number, and the wave did not disappear until the Reynolds
number was far smaller than the onset value. In the spectra of
figure 5.1 this feature is readily observed. The arrows (not
$2\,\Omega$) indicate whether the flux was reached by either an increase
or a decrease from the prior setting. A quick appraisal shows that
after the influence of a higher flux, the wave pattern is altered
so as not to return to its previous state. Comparing spectra at
a flux of 1451 and 1588 cc/sec. for ascending and descending changes,
portrays this difference. Furthermore, the dominant wave ampli-
tude was greater for fluxes lower than the original 1451 cc/sec. This
implies that by imposing a higher flux rate, changes were effected
in the flow conditions to such an extent, that on returning to an iden-
tical flux the dynamics have been altered. A simple analogy of this
feature from mechanics would be the static and dynamic friction which
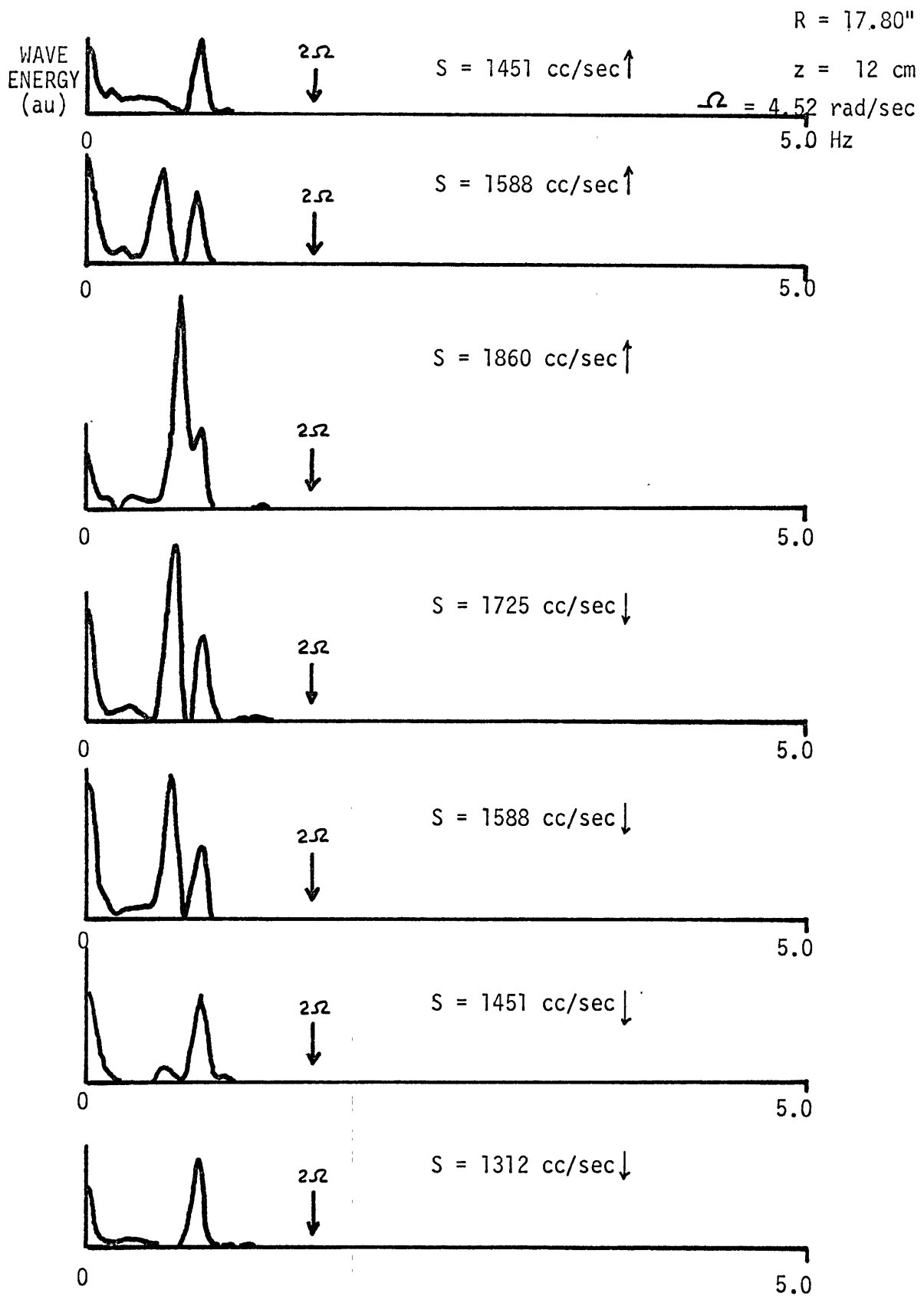differ for identical forcing, dependent on whether the object is

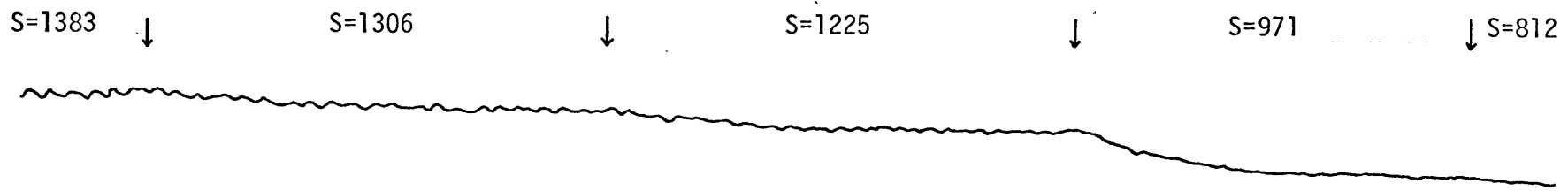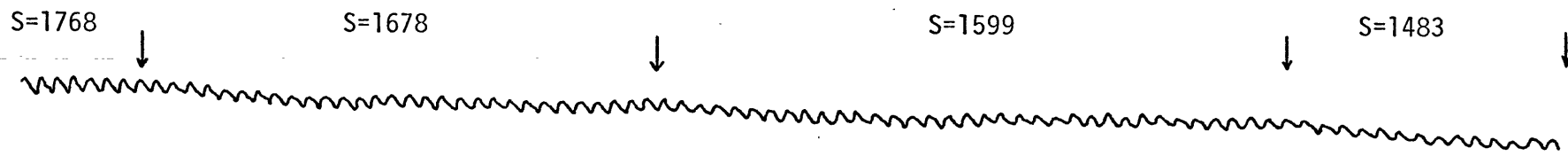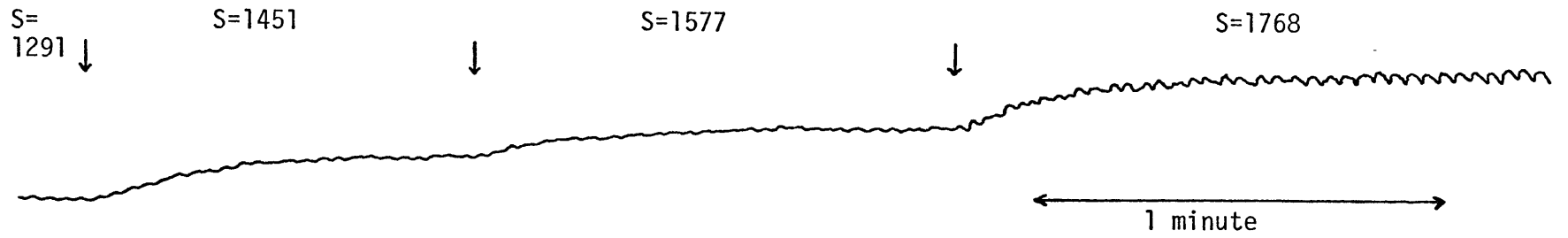FIGURE 5.1 - HYSTERESIS EFFECTS   Scale = 5cps

stopped or moving. Similarly, Coles (1965) in a Couette flow study found that the transition to turbulence occurred at a higher Rossby number than that at which it would disappear when conditions were reversed. Since a finite amplitude disturbance can exist and be unstable in a flow Reynolds number less than the initial value for production of infinitesimal disturbances, the present hysteresis results are explainable.

To obtain a more general view of this feature, the onset and demise of a certain wave was studied as a function of flux. Figure 5.2 shows the actual voltage response from the anemometer (with low amplification to give a wide mean flow range for differing volume flux). In this record, the wave onset occurred between 1577 and 1768 cc/sec., whereas on lowering the flux, a significant wave was observed to a value of 1225 cc/sec. These graphs clearly display the role played by hysteresis. Later, it will be shown how the observed frequency of some inertial waves changes with flux, but the hysteresis effect will nevertheless be apparent. The rotation rate in figure 5.2 was constant at 2.64 rad/sec. (which gave a somewhat higher Rossby number than typical in most of the present work). Since this feature is a non-linear effect, we expect it to be more apparent at the lower rotation rates.

The permanence of the hysteresis results was established by observing the configuration over an extended interval of time.

5.3   The "Body-Boundary" Modes

As mentioned in Chapter II, Stern (1960) had predicted the existence of an axisymmetric instability dependent both on local Reynolds

S=1291 ↓ S=1451 ↓ S=1577 ↓ S=1768

◄————— 1 minute —————►

S=1768 ↓ S=1678 ↓ S=1599 ↓ S=1483 ↓

S=1383 ↓ S=1306 ↓ S=1225 ↓ S=971 ↓ S=812

Ω = 2.64 rad/sec

r = 0.73

FIGURE 5.2

HOT WIRE VOLTAGE OUTPUT SHOWING HYSTERESIS EFFECTS

All Fluxes (S) in cc/sec.

number and system Taylor number (reciprocal Ekman number). Both
Arons, Ingersoll and Green (1961) and Stern (experimentally) found
waves, with appropriate wave-lengths, satisfying the above constraints.
Using a source-sink annulus, Hide (1968) also found ring-like sta-
tionary disturbances under certain conditions (even with slightly
non-uniform depth). In explaining the wave's appearance, small
differential temperature gradients (10^{-2}) have been suspected of pro-
ducing the observed structure. The reason why such temperature
influences should be band limited is not discussed by any of the
authors. In the present work, waves with some of these character-
istics were routinely observed. The typical Taylor numbers were
far greater than the critical value predicted by Stern. In comparing,
it must be remembered that his theoretical work was directed to
finding a lower limit for onset, rather than the observed values
inherent for the higher modes. Examples of the detected waves are
seen in figures 5.1 and 5.2 In these examples, the probe was located
at a radius of 17.8 inches ($r = .73$).

Initially, the spectra work focused on the inertial waves gen-
erated by class A and B (higher Re#) Ekman layer instabilities. Gen-
erally, with an increasing local velocity, one anticipates a Doppler-
shift (due to advection) of the observed inertial wave frequency,
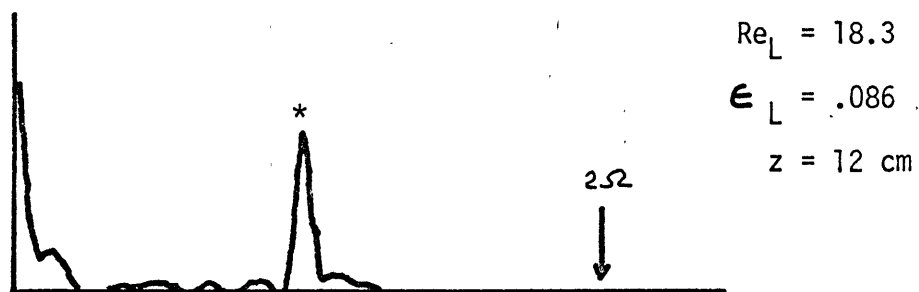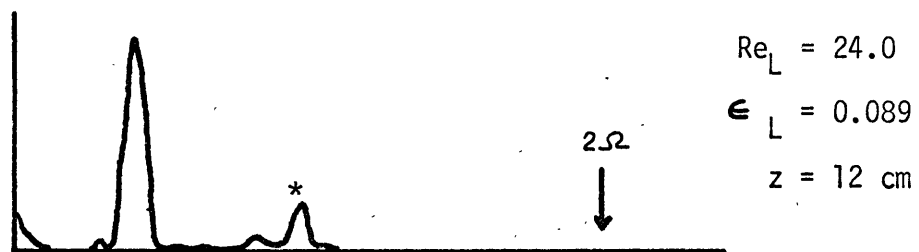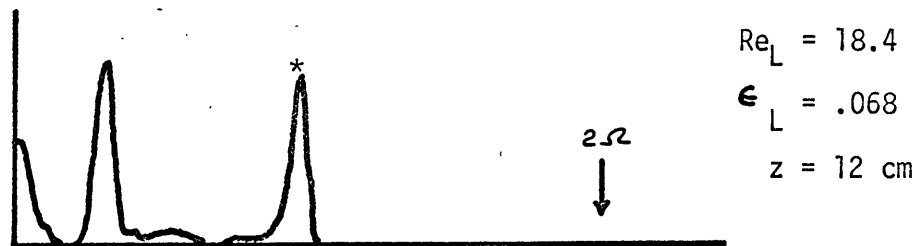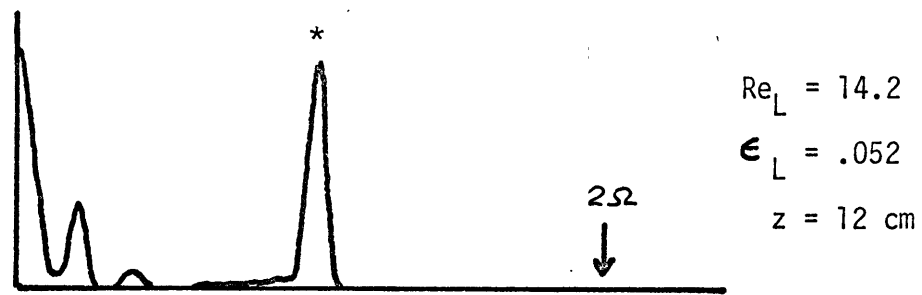as follows (Greenspan [1968]):

$$\sigma_{obs} = \sigma_o + \epsilon_{sys} \vec{U} \cdot \vec{k}$$ (equation 5.3)

where σ_{obs} = observed wave frequency (non-dimens)

σ_o = unadvected wave frequency (n.d.)

$\vec{U}$ = advection velocity (n.d.)

ϵ_{sys} = system Rossby number $\left(= \dfrac{S}{2\pi\, Ro^2\, \Omega\, \delta} \right)$

and $\vec{k}$ = wave number vector (n.d)

Although the dominant wave in figure 5.1 (at lower fluxes) suffers an amplitude change, no frequency shift for increasing values of $\vec{U}$ is observed. If the wave structure was axisymmetric (i.e., $\vec{U}\cdot\vec{k}$ =0), for a basically zonal interior flow, no Doppler effects would be observed.

A careful analysis of spectra at the larger radii (small Re#) showed similar axisymmetric waves, all of which had a non-dimensional frequency (with respect to 2Ω) of 0.52 $\pm$ .01. This value was independent of Rossby number. However, the amplitude of these disturbances was found to depend critically on the local Reynolds number. While an approximate upper Re# limit was established, it was not possible to determine a lower one, because the vacuum system monitor was not operable at the required smaller fluxes. Figure 5.3 shows a number of spectra, for different parameter ranges, in which these low Re# waves were present, they are identified by asterisks.

For comparative purposes, a chart showing the previously reported work, present results, and the critical Taylor number found by Stern is shown in figure 5.4. From this diagram we can conclude that the occurrence of these waves does not depend critically on Taylor # (at least in higher Ta# range) and that the Reynolds numbers obtained presently are significantly larger than those of Arons. Although Arons' results were generally in a Re_L* $\left(= \dfrac{S}{\nu\pi\, Ro}\left[\dfrac{Ro}{r} - \dfrac{r}{Ro}\right] \right)$ range of 1.6 to 3.6, he .

$Re_L = 14.2$

$\epsilon_L = .052$

$z = 12$ cm

2Ω

$Re_L = 18.4$

$\epsilon_L = .068$

$z = 12$ cm

2Ω

$Re_L = 24.0$

$\epsilon_L = 0.089$

$z = 12$ cm

2Ω

$Re_L = 18.3$

$\epsilon_L = .086$

$z = 12$ cm

2Ω

* : Wave Observations

FIGURE 5.3

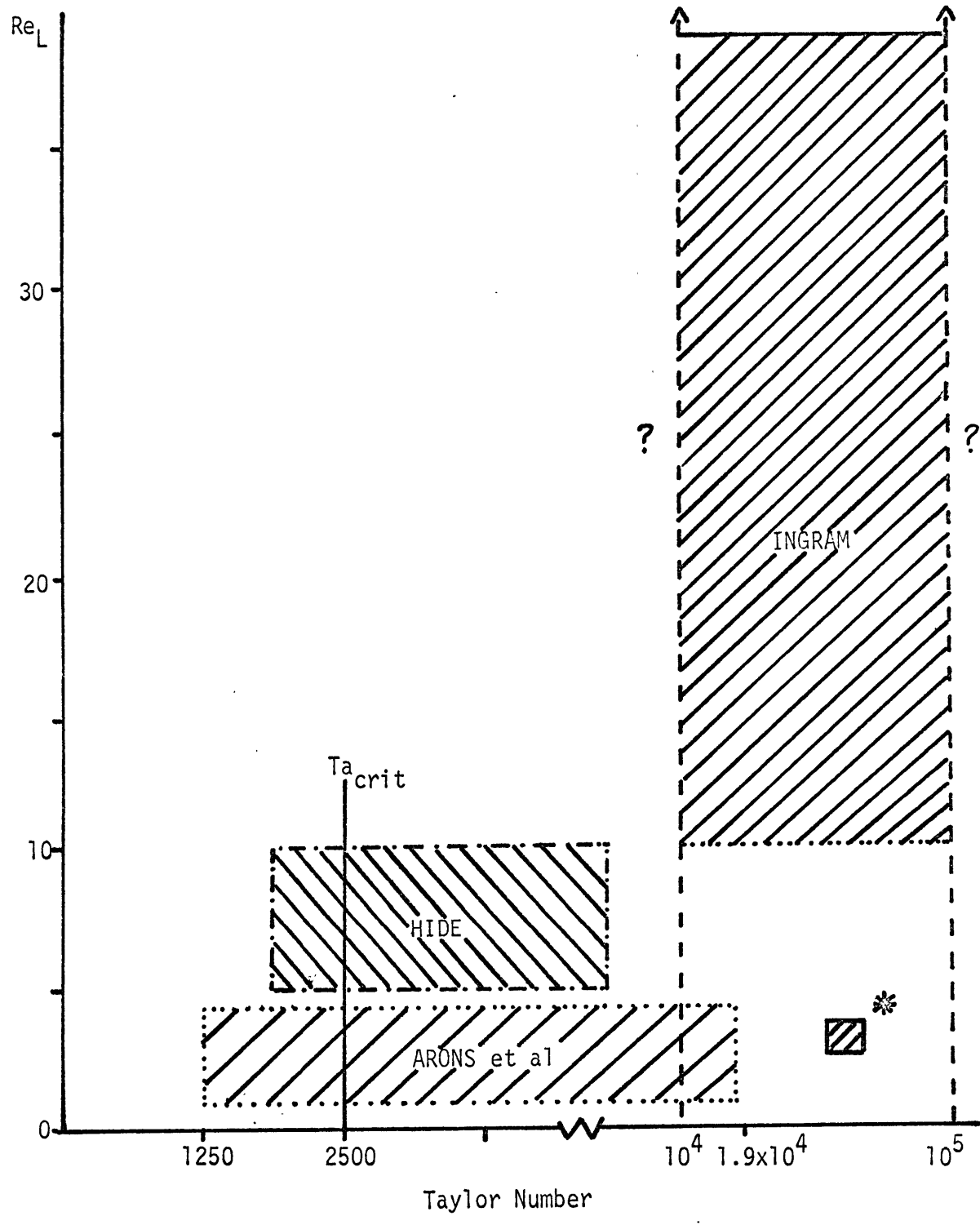SPECTRAL REPRESENTATION OF LOW REYNOLDS NUMBER WAVES

Figure 5-4. Observed Low Reynolds Number Waves.

mentions having observed an indication of waves up to a value of 10.
A slight difference in the comparisons can be attributed to the
method of the Re# computation, which are related as follows:

$$\frac{Re_L^*}{Re_L} = 2 \left(1 - \frac{R^2}{a^2} \right) \qquad \text{(equation 5.4)}$$

where Re_L^* = Arons et al (1960) local Re#

Re_L = local Re# as defined in eq. 5.1

R   = local radius (dimensional)

a   = outer tank radius.

It is important to note that the results quoted by Arons are all min-
imum Re# for the occurence of waves, and therefore do not preclude a
similar wave structure at higher values. Hide (1968), using a relation
identical to equation 5.1, found the waves in a Reynolds range of 5-10,
for Taylor numbers from 1700 to 6800. The starred data in figure 5.4
were observed with a reversed radial flux. This paralleled Aron's work
to some extent, since he used a centrally located funnel for fluid
injection. There was no sink to remove the water. All of the values
quoted in the present work are those of occurrence, rather than min-
ima. The question marks in figure 5.4 imply an arbitrary boundary,
as no experiments were performed past these limits.

The most interesting result of the present work is the existence
of an upper limit, past which these low Reynolds number waves decrease
to insignificant amplitudes. It is notable that no definite upper

Re# limit has been reported previously in the literature. This maximum value in Re# was found to be approximately 35.0. In contrast to recent Ekman layer instability work, the Reynolds # range of these waves is much lower than the "pure" boundary waves reported by Faller (1963) and others, where critical values of $Re\#_L$ = 50-100 are typical. It may be important to note that the low Reynolds number waves occurred only for small system Rossby numbers (less than 0.15).

Although the present wave observations were taken in the interior of the tank, the local Ekman layer characteristics under these conditions, are also of interest. Profile #18 in Table 4-2 is a suitable example. The observed boundary layer thickness of this profile was the only one recorded, that was larger than theoretical prediction. The wave intensity chart (Table 5-3) shows this Ekman layer profile to have the wave characteristics of a zero vorticity interior.

Since the interior vorticity structure played a definite role in the Ekman layer characteristics, it is expected to assume an equally important control over the Stern (low Reynolds number) waves. This influence was readily apparent in the wave observations. In fact, any significant departure from a zero vorticity interior (see fig. 4.2 - 4.11) inhibited the "Stern" wave production. This accounted for the failure to observe waves in some regions where the Re# - Ta# constraints were satisfied. The absence of waves adjacent to the source agrees with previously reported work.

To further investigate the ring-like structure of these waves, cross-correlations between probes at the same radius (but azimuthally separated) were taken. Without exception, the waves showed no phase lag between the two positions. Thus, by combining the av-

ailable results, "Stern" waves were found to be prevalent and of an entirely different nature than the inertial waves discussed by Green (1968), Tatro (1966) and others. Surprisingly, previous work with the higher Re# instabilities fails to report the existence of these "Stern" waves, although conditions were suitable in many cases. It would seem that their attention was focused solely on the inner radial positions.
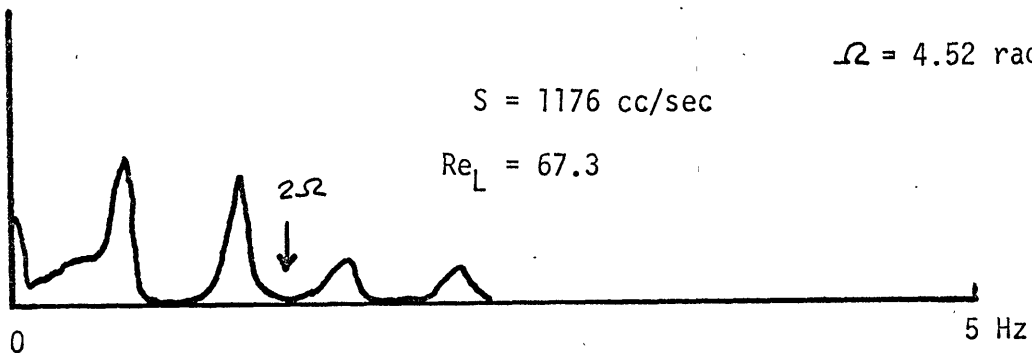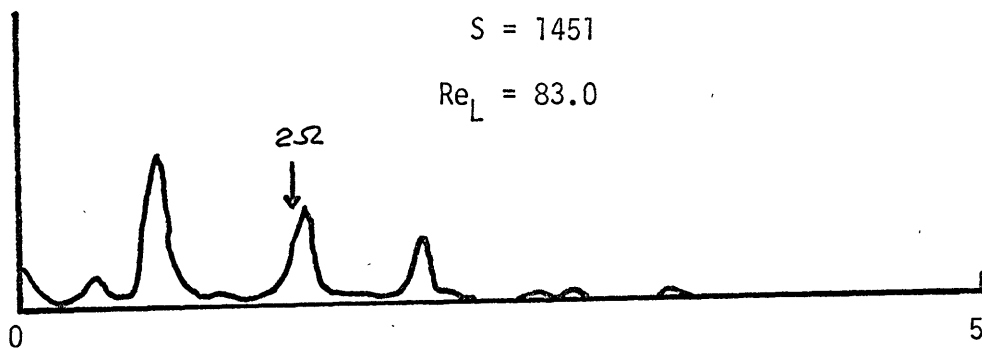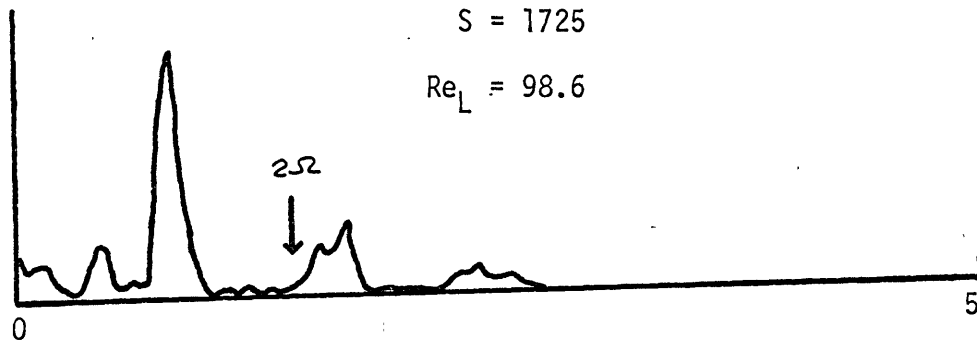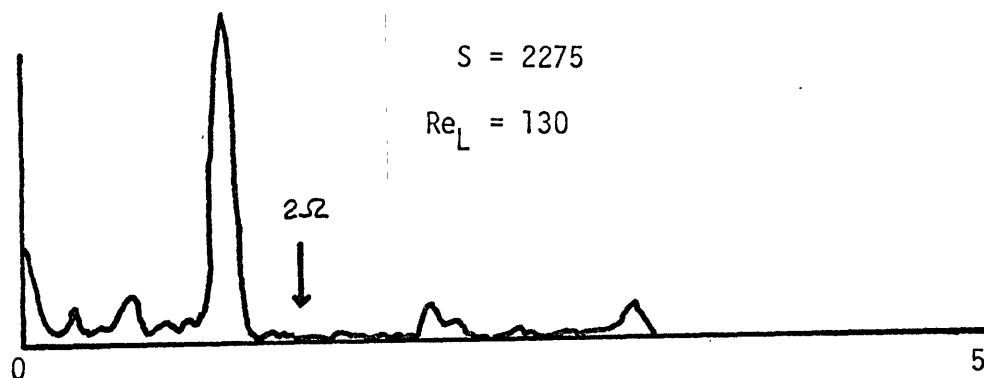
Additionally, Arons found (not detected in the present work) small zonal waves, which formed on the concentric rings, at the higher fluxes and lower viscosities (higher Re# range). However, he was unable to specify any onset criteria. The present results do differ from Arons' work substantially in one area, that is in time-dependence. Although previous authors mention the "slow" motion of these waves, a definite radial fluctuation is noted in the observed waves, with frequency 0.52 (non-dimensional). Both cross-correlation techniques and Doppler shift results authenticate the waves' ring-like structure. We are left with the conclusion, that the wave structure is almost identical to that previously reported, but not stationary. Since the probe executes a concentric path, stationary axi-symmetric waves would not be detected in any case.
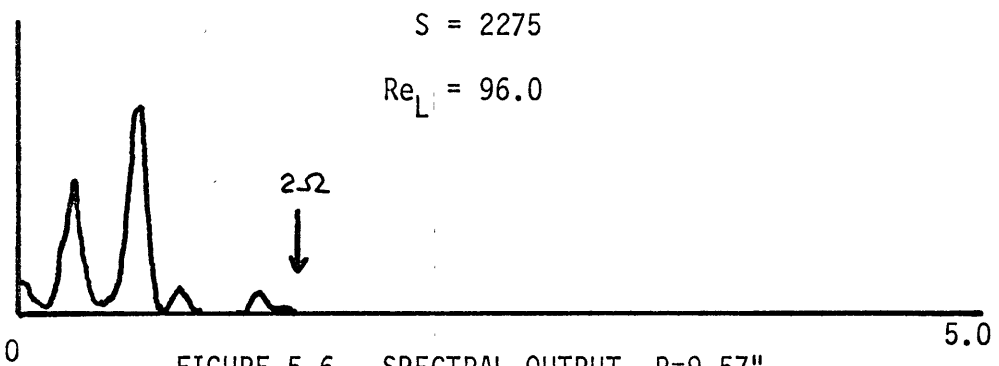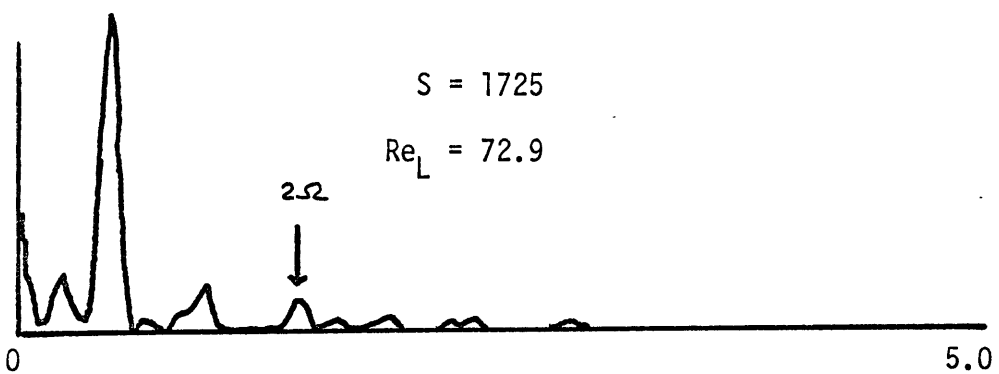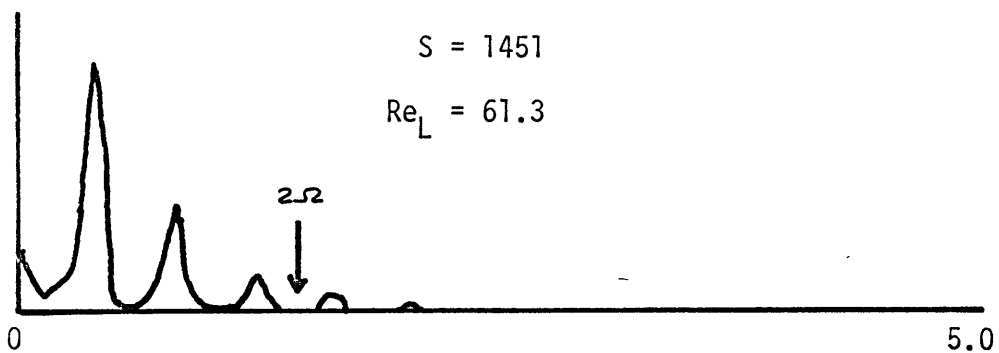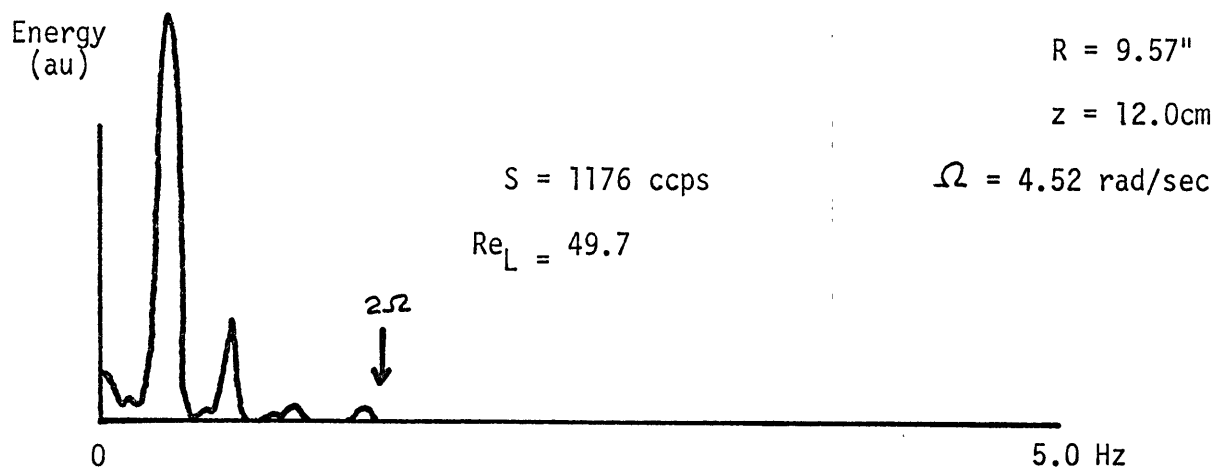
5.4 A Series of Representative Spectra of Velocity Fluctuations.

Looking at all the spectra, it was difficult to separate specific features. For this reason, a particular series recorded at a constant rotation of 4.52 rad/sec. with varying flux and position, were analyzed rigorously. According to Green (1968), we should expect the dominant wave peaks of these

spectra to be frequency invariant with radius, for conditions of constant flux and rotation. Implicit in this finding is that the inertial waves are axisymmetric, and thus unaffected by the differential Doppler shifting of the radially structured zonal flow. In a later work, Green and Mollo-Christensen (1970) found that the wave frequency increased linearly with system Rossby number, indicating non-axi-symmetric waves. From their results, such a response is verified, but as the parameter range was limited, only further work could test its generality. This was accomplished by varying the flux, to obtain a complete range of Reynolds and Rossby numbers. The observed pattern was similar to the findings of Green and Mollo-Christensen for the small ϵ_L ranges, but generally, a more complex (although regular) dependence was present.

Figures 5.5 - 5.10 show for individual radii, the influence of a flux increase on spectral characteristics, for constant rotation. These observations were recorded at the mid point (z = 12cm) of the tank interior. The inertial frequency limit (2Ω) is marked on all figures. As a means of comparison, figure 5.11 presents the same flow conditions as shown in diagram 5.7, but within the Ekman layer (at a height of 1.0mm). Summarizing the positional influence, figure 5.12 combines the individual spectra for varied radii in the case of constant flux. This allows a view of any radial variation of the dominant waves under otherwise uniform conditions. From these spectral results, the dominant wave peaks at R = 9.57" (r = 0.39) and 13.80" (r = 0.57) are seen to be essentially frequency invariant. Generalizing from all the observations, inertial waves whose frequency is independent of radial position were found

Energy
(au)

R = 7.07"

z = 12.0
cm

Ω = 4.52 rad/sec

S = 1176 cc/sec

Re_L = 67.3

2Ω

0   5 Hz

S = 1451

Re_L = 83.0

2Ω

0   5

S = 1725

Re_L = 98.6

2Ω

0   5

S = 2275

Re_L = 130

2Ω

0   5

FIGURE 5.5 - SPECTRAL OUTPUT, R=7.07"

Energy
(au)

S = 1176 ccps

Re_L = 49.7

R = 9.57"

z = 12.0cm

Ω = 4.52 rad/sec

2Ω

0   5.0 Hz

S = 1451

Re_L = 61.3

2Ω

0   5.0

S = 1725

Re_L = 72.9

2Ω

0   5.0

S = 2275

Re_L = 96.0

2Ω

0   5.0
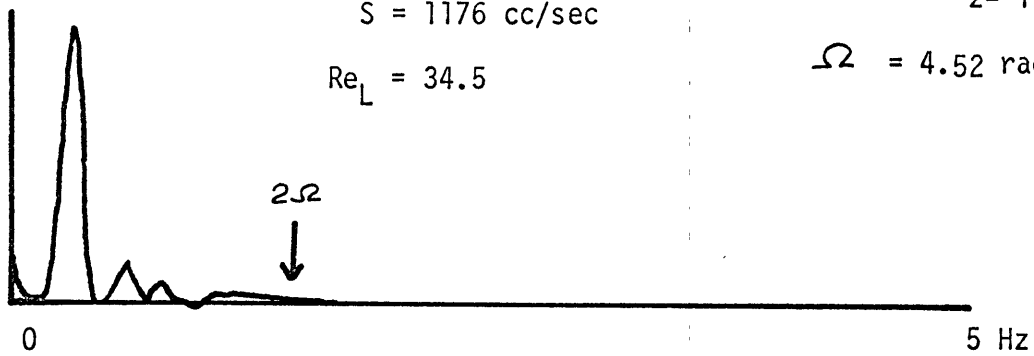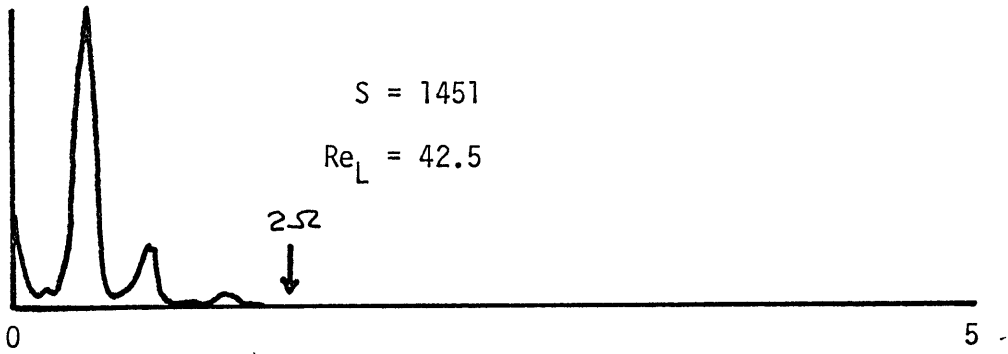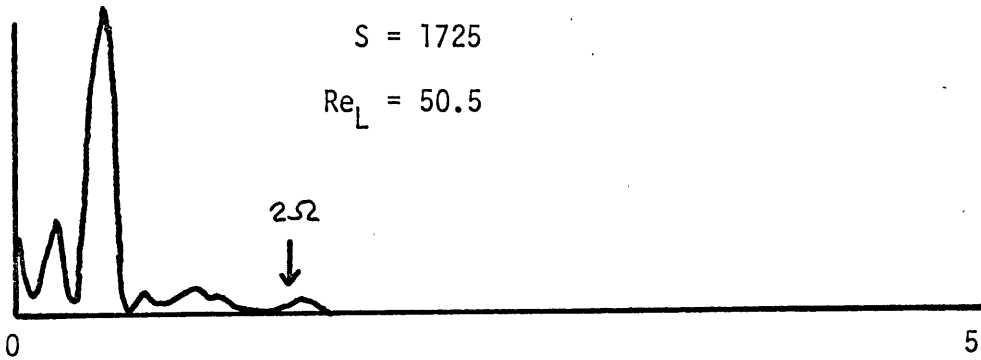
FIGURE 5.6   SPECTRAL OUTPUT, R=9.57"
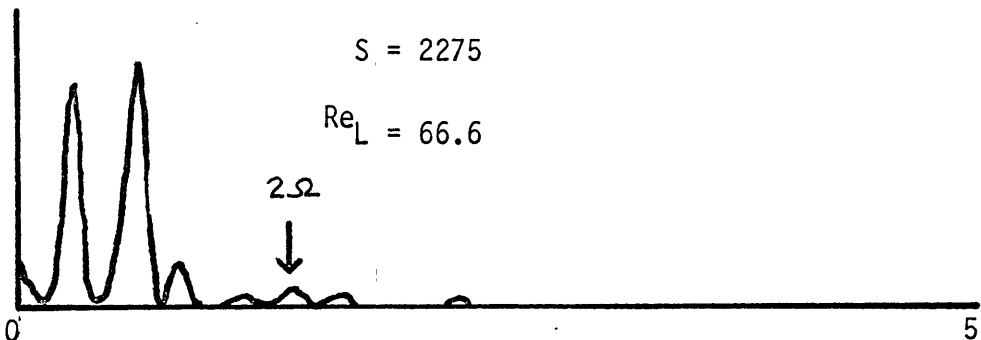
FIGURE 5.7   SPECTRAL OUTPUT, R=13.80"
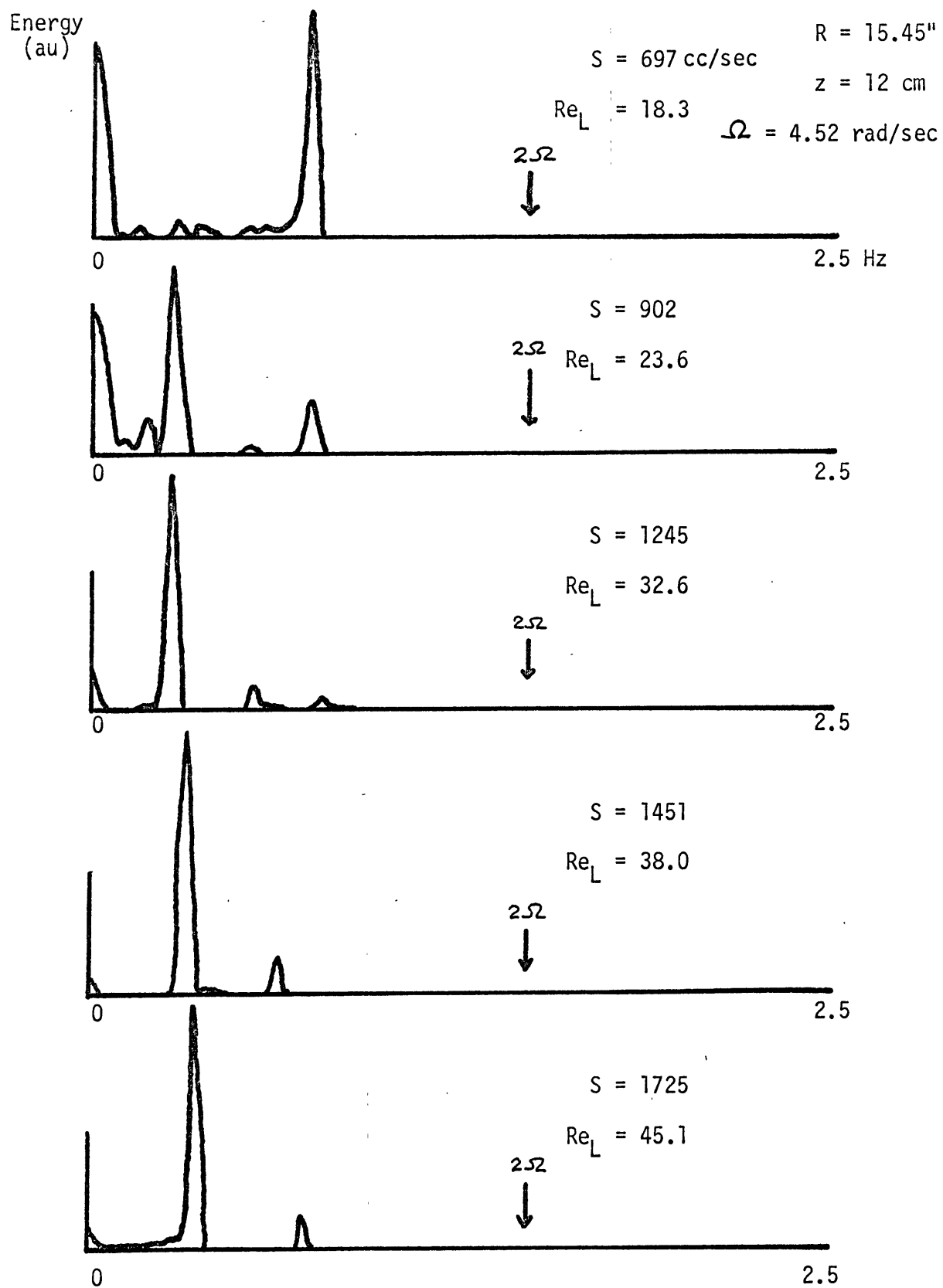
FIGURE 5.8   SPECTRAL OUTPUT, R = 15.45"
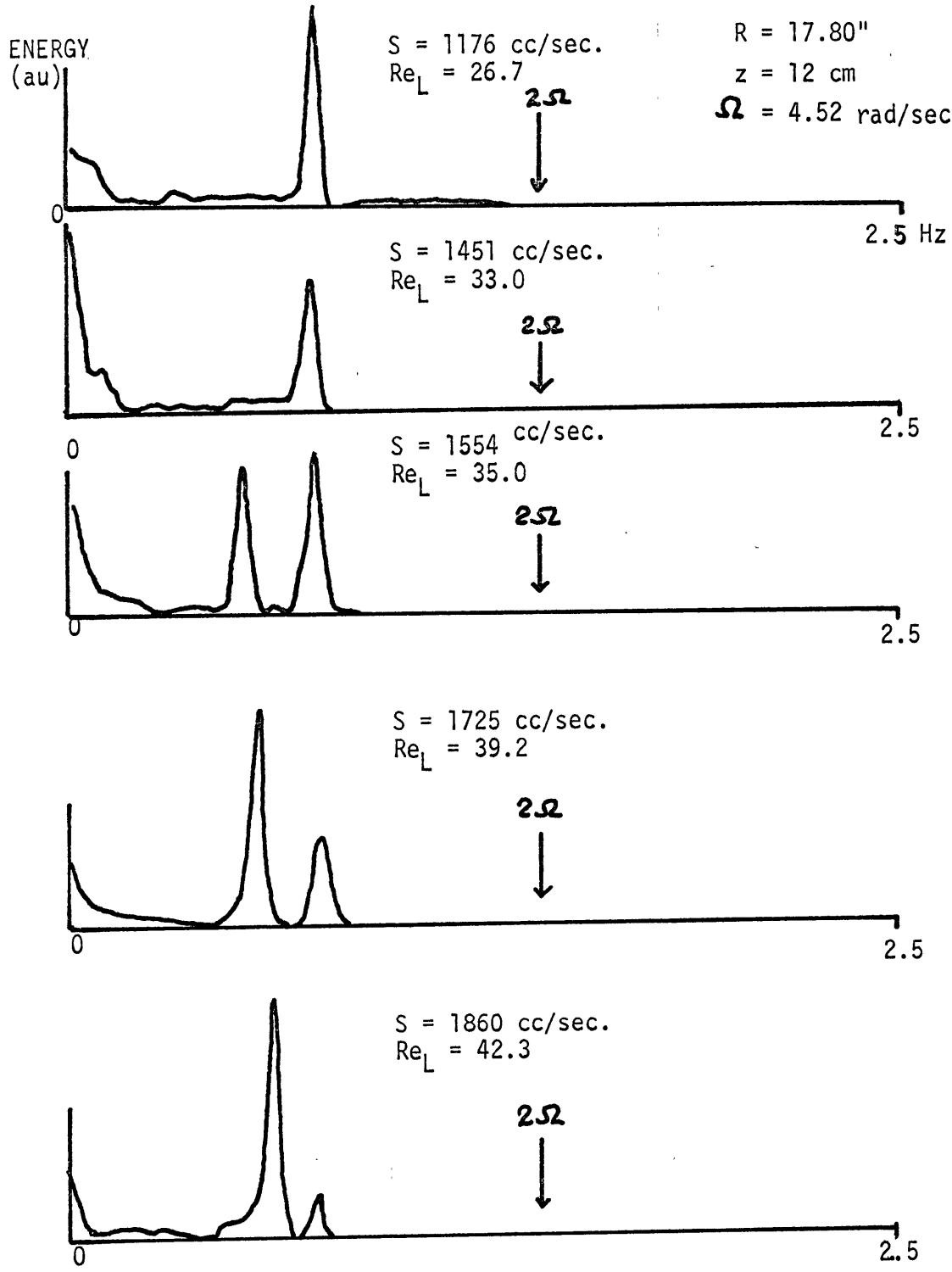
FIGURE 5.9 - SPECTRAL OUTPUT, R = 17.80"
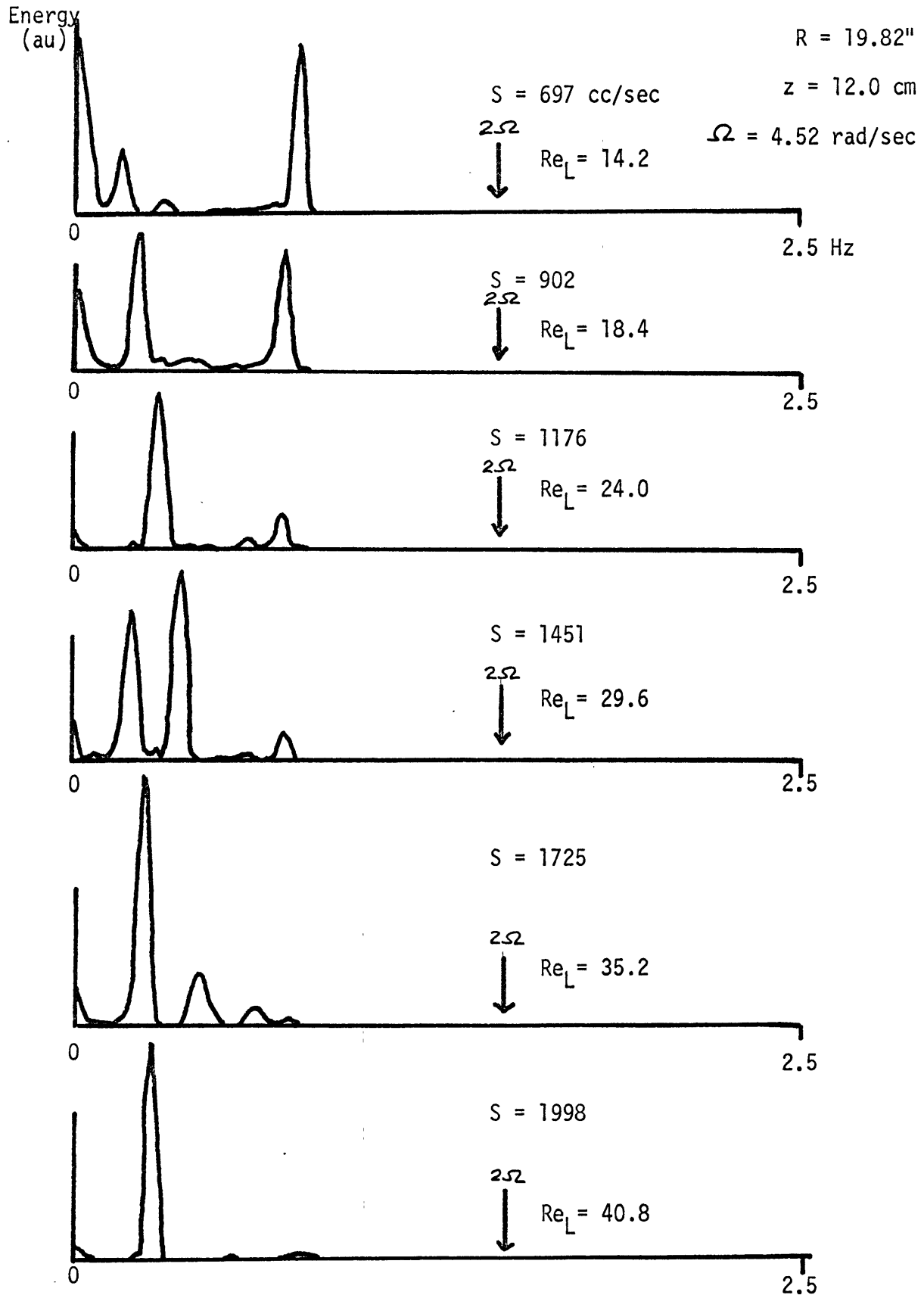
FIGURE 5.10 - SPECTRAL OUTPUT, R=19.82"

$\Omega = 4.52$ rad/sec
R= 13.80"
z= 0.10 cm

2Ω
S= 697 cc/sec
$Re_L = 20.4$

0   2.5 Hz

2Ω
S= 902 cc/sec
$Re_L = 26.5$

0   2.5

2Ω
S= 1176 cc/sec
$Re_L = 34.5$

0   2.5

2Ω
S= 1451 cc/sec
$Re_L = 42.5$

0   2.5

2Ω
S= 1725 cc/sec
$Re_L = 50.5$

0   2.5

2Ω
S= 1998 cc/sec
$Re_L = 58.6$

0   2.5
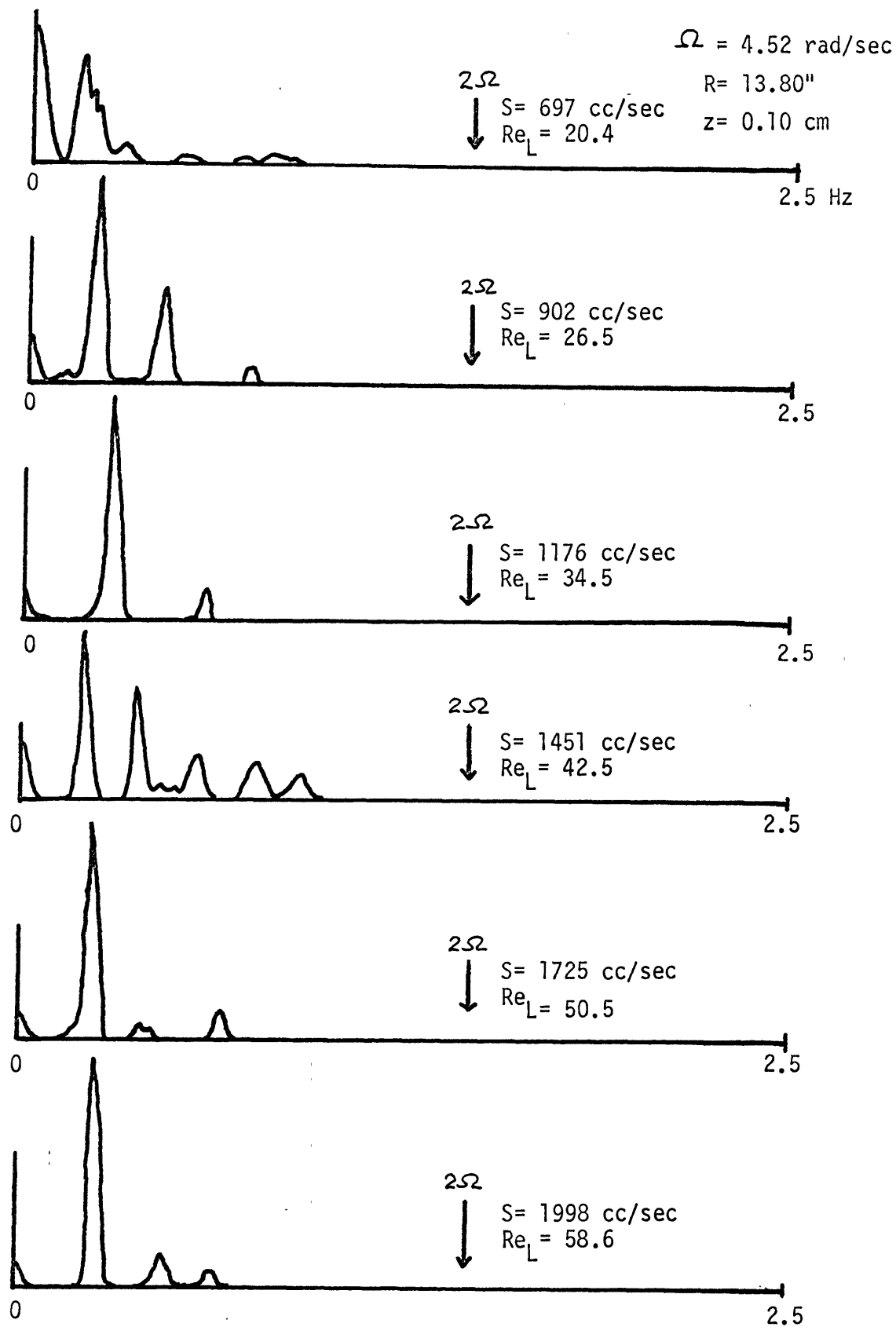
FIGURE 5.11 - SPECTRAL OUTPUT, R=13.80", z= 0.10 cm
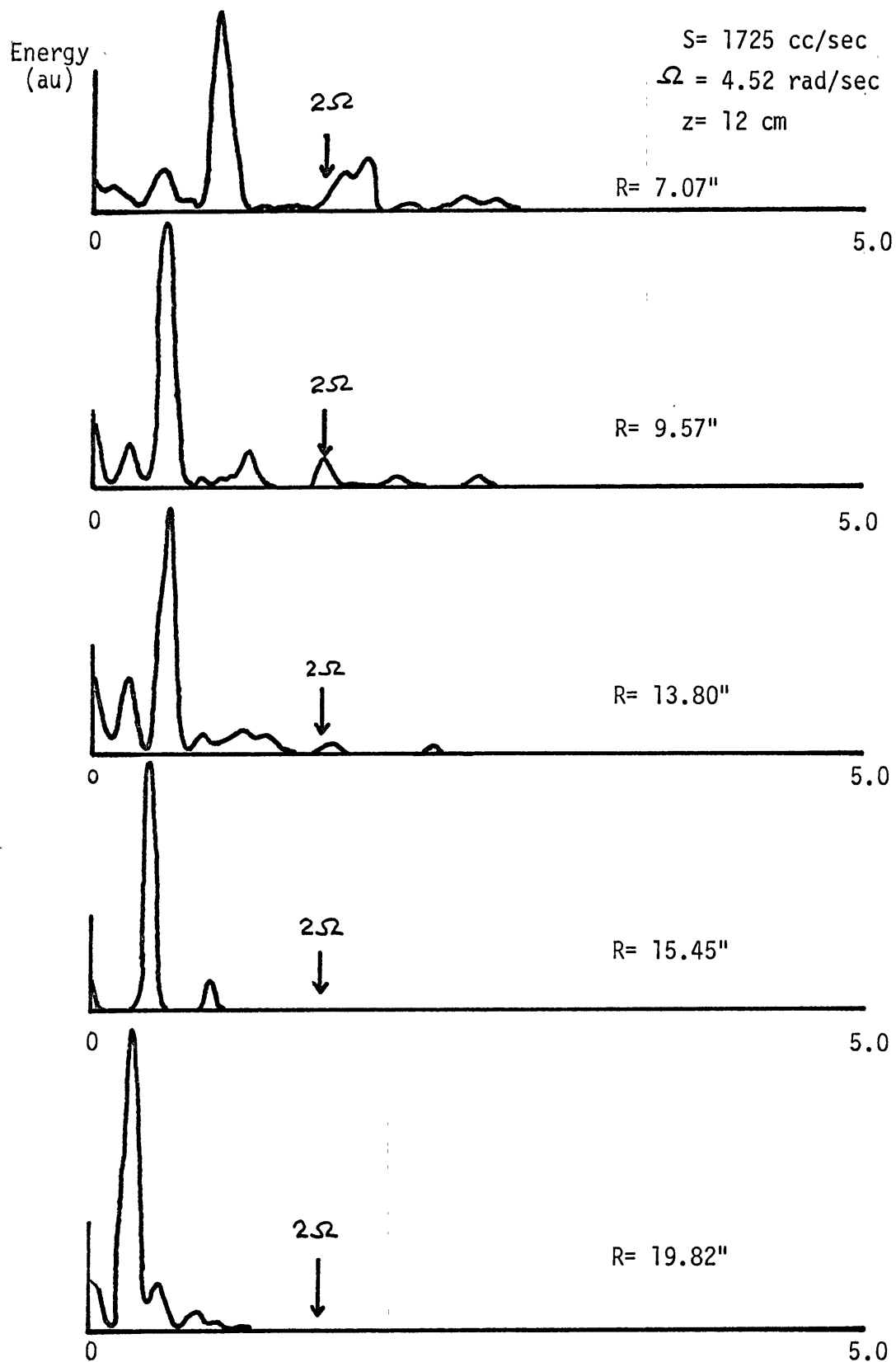
FIGURE 5.12 - SPECTRAL OUTPUT FOR CONSTANT FLUX, 1725 cc/sec.

99.

only in the mid-radial observations (e.g., r = 0.39, 0.57). This

range coincides with the region of increasing Γ (see figure 4.8).

The results also show, that for increasing flux, the frequency

of the dominant waves grew linearly with flux over a limited range at

the larger radii. In these cases, a lower frequency wave superceded

(in amplitude) the originally dominant one, at some specific flow

rate. This change can be very abrupt, with the transition of energy

to lower frequencies being accomplished over a narrow range of flux.

For example, in figure 5.10, the transition to a lower frequency occurs

between 1451 and 1725 cc/sec. In contrast, figure 5.7 shows that under

identical flow conditions (at a smaller radius) no such transition was

recorded, although the final two spectra do suggest an imminent change

above 2275 cc/sec.

The present results were compared with those of Green and

Mollo-Christensen, by plotting non-dimensional frequency (with respect

to 2Ω) against system Rossby number. The system Rossby number is

defined as follows:

$$\epsilon_{sys} = \frac{S}{2\pi R_0^2 \nu^{1/2} \Omega^{1/2}}$$
(equation 5.5)

where the parameters are as previously defined. The resulting graph

is shown in figure 5.13. Excluding the low Reynolds number waves (of

section 5.4) which are readily separable by their constant frequency and

lack of Rossby number dependence, the remaining points form a series

of lines. Additionally, some observations with constant radius, but

changing rotation, (not shown) demonstrate a similar multiple line

response. It can be discerned from the diagram how Green and Mollo-

Christensen with a limited number of points, may have found one line
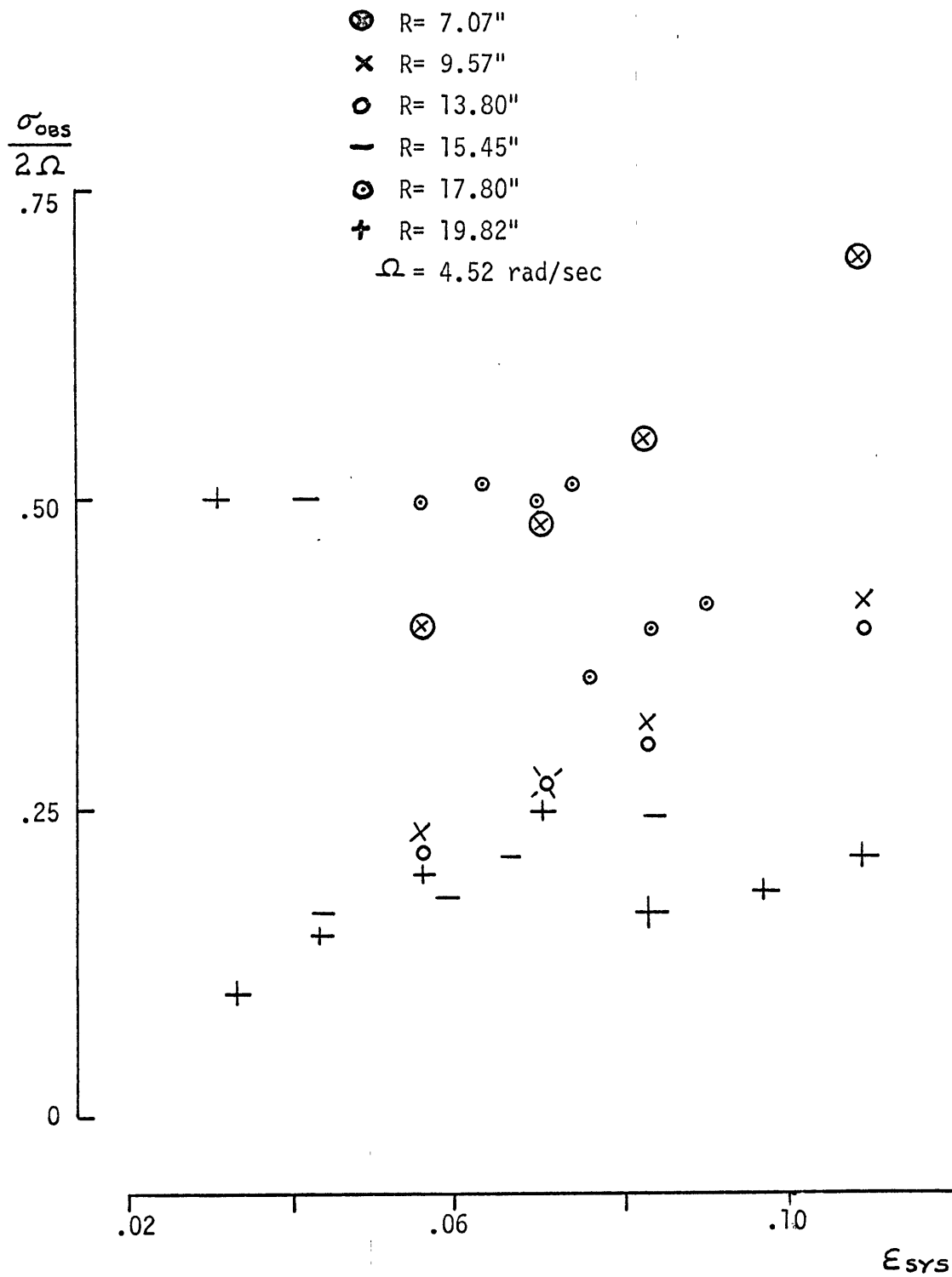
FIGURE 5.13 – COMBINED SPECTRAL RESULTS vs. SYSTEM

ROSSBY NUMBER

to satisfy their results. In general, the slopes obtained were nearly constant and the same order of magnitude (and sign) as their work (correction was made for different non-dimensionalization). It must be remembered, however, that Green and Mollo-Christensen utilized a single radius and a narrow flux range in plotting their graph.

An overall view affords the following comment: the observed waves can be axi-symmetric or non-axi-symmetric, the latter being the predominant by far. In the past, "Stern" waves may have been misinterpreted as axi-symmetric waves produced by the Class A instabilities. The observed frequency of both waves is invariant with radius. However, the low Reynolds number wave is a local phenomenon, dependent on suitable conditions in the interior and the Ekman layer, whereas an axi-symmetric inertial wave may be ubiquitous.

Although some systematic variation of $\sigma/2\Omega$ with ϵ is apparent in figure 5.13, it is difficult to explain the dynamics from this picture. A more systematic representation of the results was obtained by plotting the observed wave frequency versus the <u>local</u> Rossby number, ϵ_L, for contours of constant flux. In figure 5.14, the values graphed in fig. 5.13 were re-plotted with this change of abscissa. Also included in this diagram were the second largest amplitude peaks from each spectra. These points are designated by an enclosing circle. Even at first glance, the results separate into distinct groups, some of which are inertial waves whose frequency increases (not always linearly) with ϵ_L, and another set made up of the "Stern" waves, which are independent of ϵ_L (and not of present interest). Excepting the middle Rossby number range, the wave frequencies fall on two lines. By back-extrapolating these lines to zero Rossby number, the unadvected

inertial wave frequencies are obtained (.09 and .18 in this case).

This follows from equation 5.3. The branching of each line is only an artifact of calculating ϵ_L from the theoretical velocity profile. As we have seen in Chapter IV, the circulation profile showed greater distortions from theory for increasing fluxes. In actual fact, for the mid Rossby number range shown in figure 5.14, the zonal velocity was almost constant with radius for each of the higher fluxes. It can be readily seen how Green (1968) observed a wave, whose frequency did not change in the mid-radial positions, and erroneously concluded that it was axi-symmetric. Since the observed frequency of the two inertial waves detected in figure 5.14 was influenced by differential advection, we can assume that they were non-axi-symmetric in nature (selequation 5.3) By changing the rotation rate, for a constant flux and position, the additional points obtained coincide with the two lines of figure 5.14. In the small ϵ_L range we found the possibility of either the low or the high frequency wave being dominant in amplitude. The increasing amplitude of the second vertical mode affords the simplest explanation.

In an attempt to relate the pattern found (specifically the changes to lower frequency) in figure 5.14 to another system parameter, the observed frequency values were compared to Re_L. At the Re_L values of 56 and 125, which were obtained for onset of the types A and B Ekman layer instabilities (Tatro [1966]), no significant change of wave frequency was observed. This is expected, since the "local" Reynolds number (within the Ekman layer, under the probe) may not be the correct parameter to explain recorded inertial wave activity. Realizing that an unstable Ekman layer produces inertial waves having a positive radial component of group velocity (Green and Mollo-
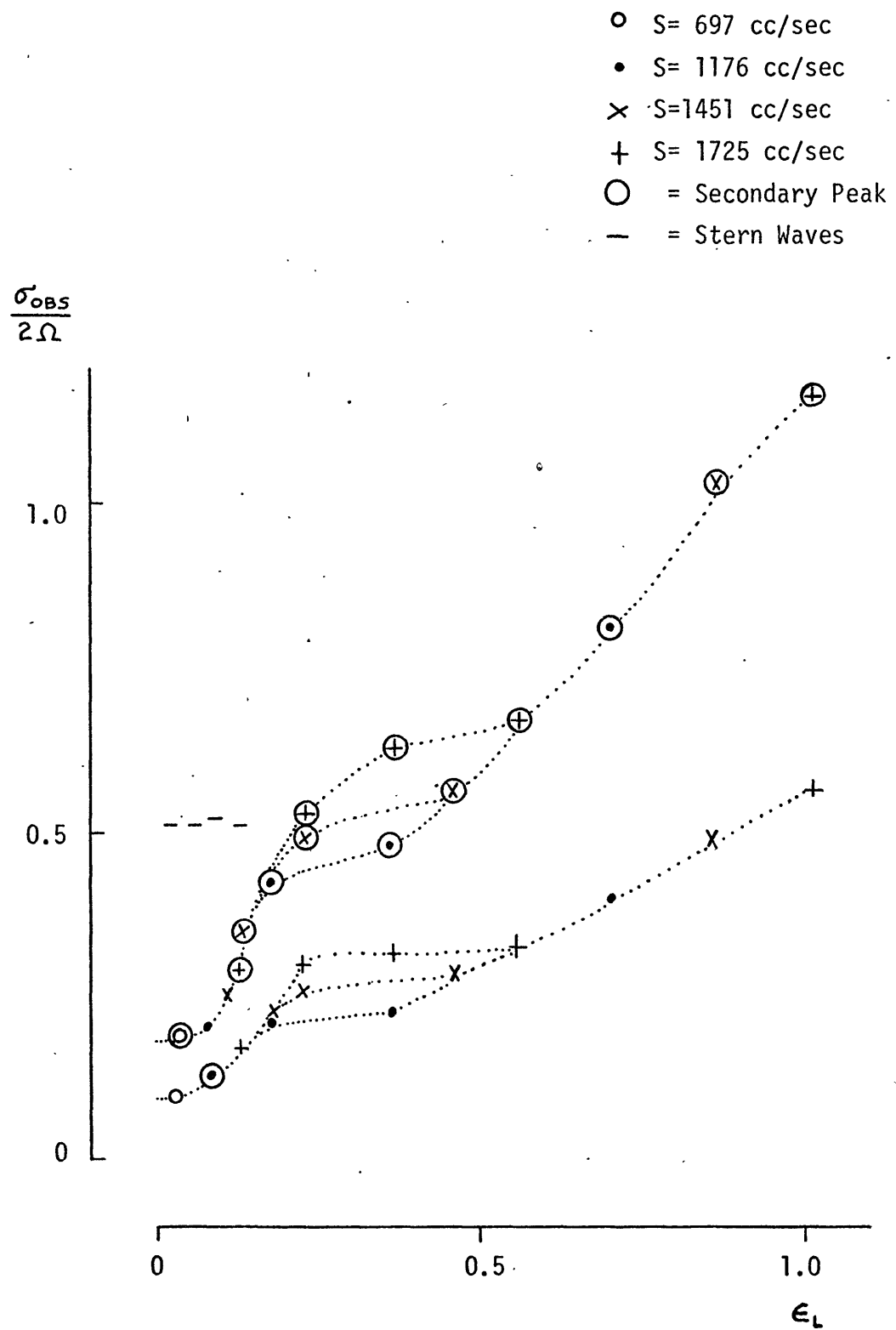
FIGURE 5.14 - OBSERVED FREQUENCY vs. $\in_L$

Christensen [1970]), the existence of instabilities at some smaller radii would seem sufficient to produce motion at an outer position.

By incorporating the results of Chapter IV and section 5.1, the optimum region for initial instability generation is found at the junction of the sink side-wall layer and the interior. From Table 4 - 1, a typical value of this junction is taken to be r = 0.25 (R = 6.1"). By calculating the local Reynolds number (Re_J) at this radius and plotting the wave frequencies against Re_J, figure 5.15 is obtained.

An analysis of figure 5.15 shows two transition Reynolds numbers. The first Re_J change took place at 52, when the low Reynolds number waves were superceded by inertial waves at r = 0.63 and 0.81. A similar transition at r = 0.73 did not occur until $Re_J \sim 92$. Significantly, a second transition, amongst the inertial waves at r = 0.81, occurred at approximately the same value of 92. In view of the assumptions used in computing Re_J, it would seem unwise to directly relate these transitions to the Ekman layer instabilities.

In summary, the wide diversity and similarity of interior spectra, as reported previously, can be explained by comparison with the local Rossby number. The observed inertial wave frequencies will differ for varying tank aspect ratios. Furthermore, care must be taken to differentiate between the local low Reynolds wave and inertial waves.

5.5   Wave Spectra Within the Ekman Layer and Related Interior
Motion

5.5.1 Reynolds Number Dependence of the Ekman Layer Spectra
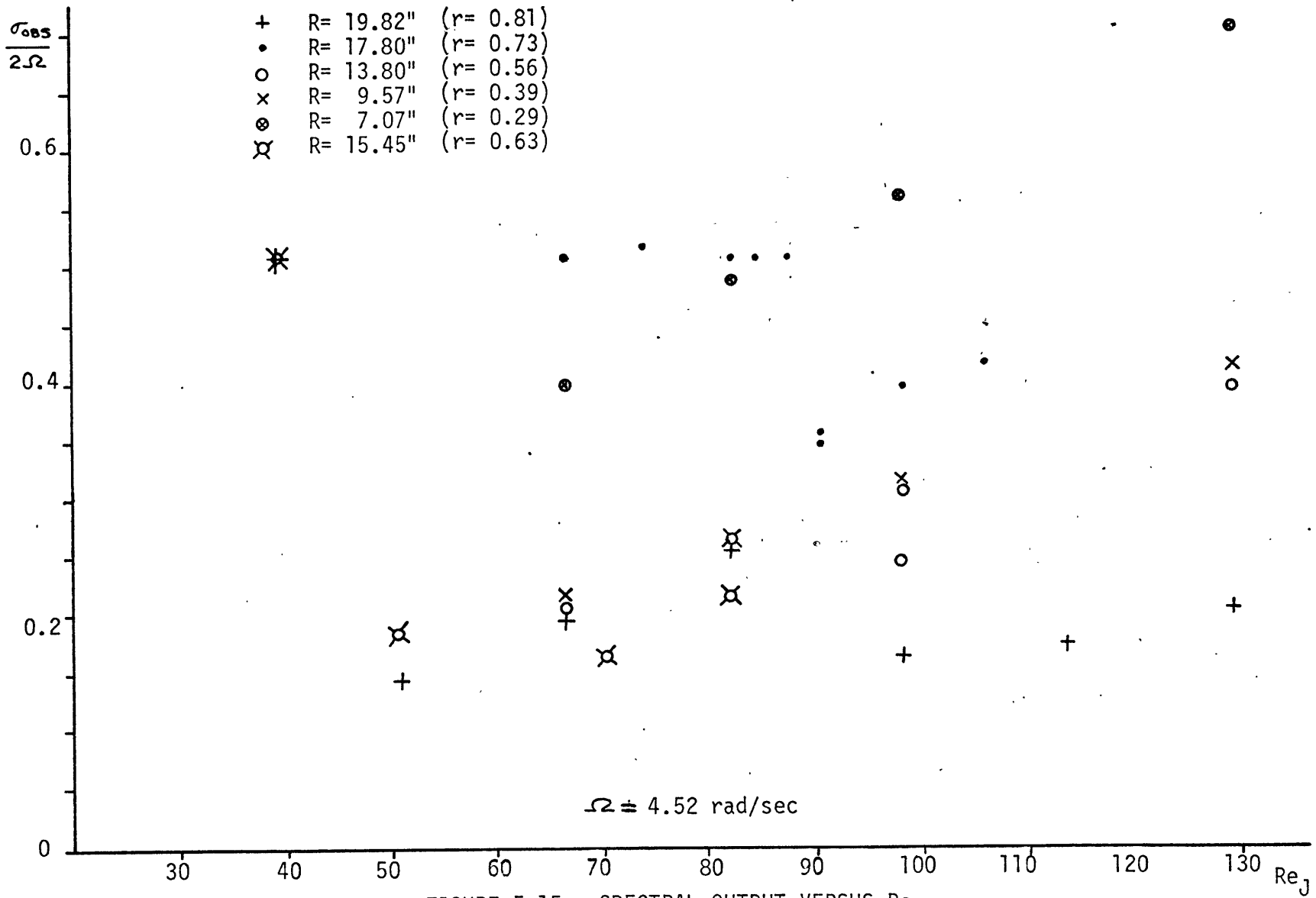
FIGURE 5.15 - SPECTRAL OUTPUT VERSUS Re_J

$$\frac{\sigma_{OBS}}{2\Omega}$$

+	R= 19.82"	(r= 0.81)
•	R= 17.80"	(r= 0.73)
○	R= 13.80"	(r= 0.56)
×	R= 9.57"	(r= 0.39)
⊗	R= 7.07"	(r= 0.29)
¤	R= 15.45"	(r= 0.63)

$\Omega \doteq 4.52$ rad/sec

The wave spectra observed in an Ekman layer have been found to depend crtically on the local Reynolds number. By observing these wave motions on an oscilloscope, Tatro (1966) noticed a significant change in structure for certain flow configurations. He attributed the alteration to the Class A and B Ekman layer instabilities, occurring at Re_L = 56 and 125. The Rossby number dependence of the critical Reynolds number was judged to be linear by Tatro, as follows:

$$Re_L^A = 56.3 + 58.4 \, \epsilon_L^A \qquad \text{(equation 5.6)}$$

$$Re_L^B = 124.5 + 3.66 \, \epsilon_L^B \qquad \text{(equation 5.7)}$$

where the superscript indicated the instability class.

Caldwell and van Atta (1970) reexamined the onset criteria established by Tatro. They found a corresponding Re_L for the Class A wave onset, but were unable to detect the presence of any Class B waves (higher Re#).

The present work includes a wide range of local Reynolds number, at four radial positions. By comparing spectra at different heights within the Ekman layer, a significant change in the relative size of wave amplitude was observed.

In the lower Reynolds number range, figure 5.16 shows eight spectra taken at R = 14.70" (r = .61), for three different heights. For the two lowest fluxes (and z = .06cm), the large spectral peaks correspond to the lowest Reynolds number "Stern" wave. As was apparent in the results of section 5.4, a lower frequency wave grew sufficiently in amplitude, for Re > 35, to become the dominant peak. The fre-
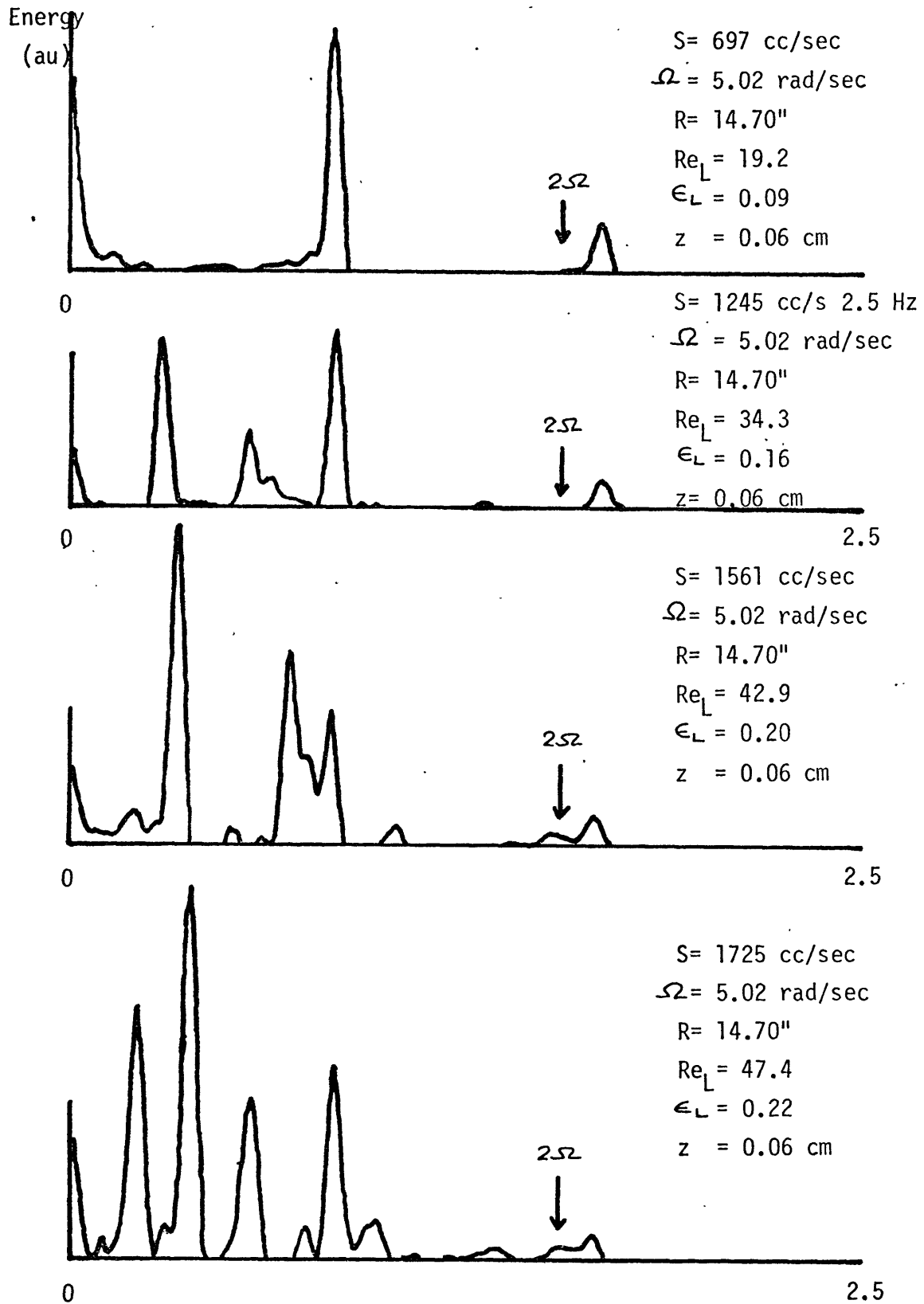
FIGURE 5.16A - LOW REYNOLDS NUMBER EKMAN LAYER SPECTRA.
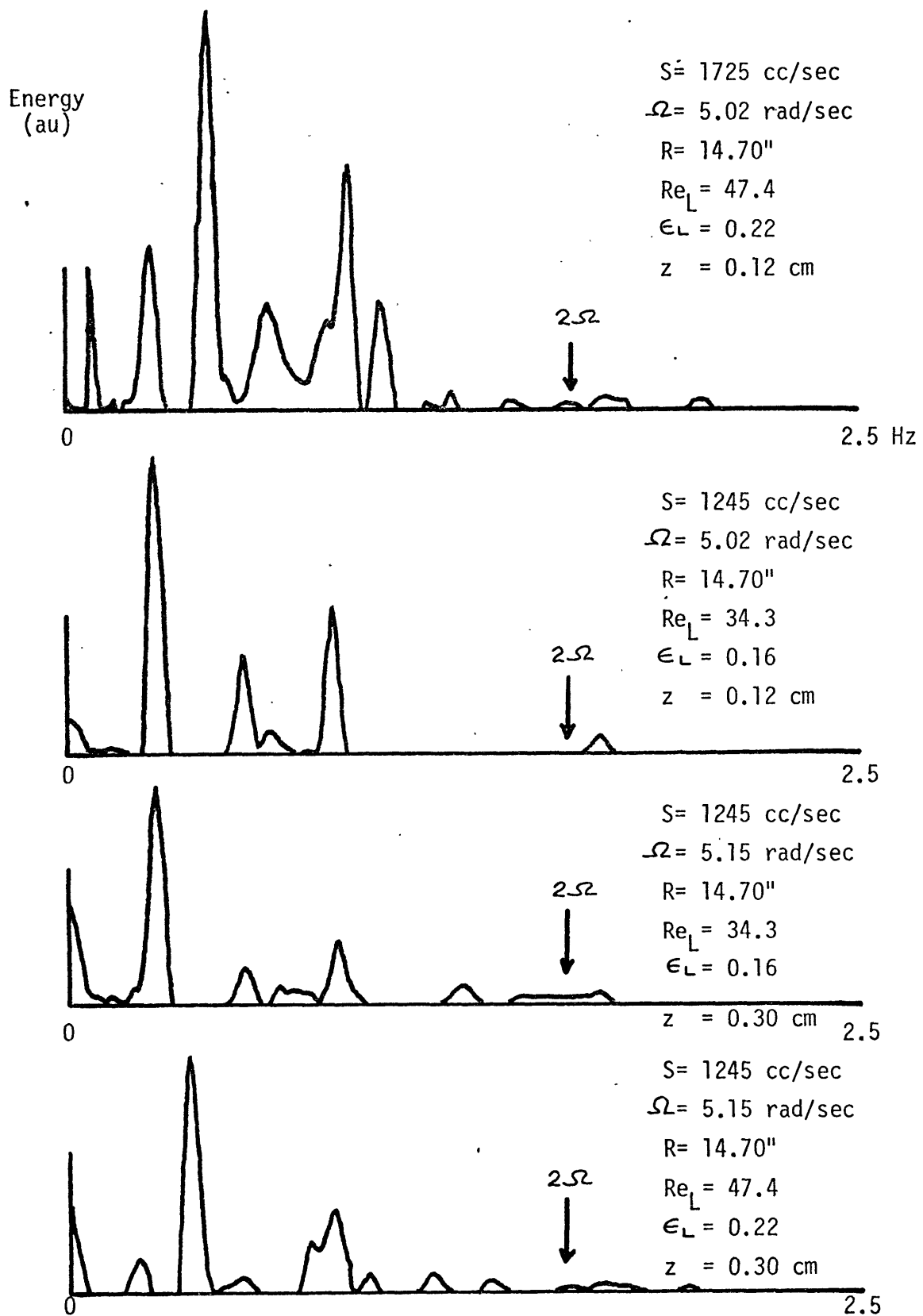
FIGURE 5.16B - LOW REYNOLDS NUMBER EKMAN LAYER SPECTRA.

quency of this wave increased with larger fluxes, as a result of
Doppler shifting. The most significant feature apparent in the spec-
tra is the continuous decrease of the "Stern" wave amplitude with
distance from the lower wall. A comparison of the results for a
flux of 1245 cc/sec., shows a rapid wave attenuation at $Z = 0.30$cm.
This finding agrees with the results of section 5.3. From this finding,
we assume that the interior vorticity structure inhibits the Stern wave
appearance. The height dependence of the other waves in the spectra
consists essentially of relative amplitude changes amongst the
secondary peaks.

The above results include no Re_L values within the critical ranges,
as defined by equations 5.6 and 5.7. This omission was intentional
in order to exhibit the typical wave motion found within a supposedly
"laminar" Ekman layer (see Greenspan [1968], figure 6.5a). For great-
er values of Re_L, the observed wave motion undergoes a rapid change,
as seen in figures 5.17 and 5.18. However, this transition differs
noticeably from the results of Tatro (1966). The contrasting wave
traces can be explained by his lower signal amplification and incom-
plete removal of the mean velocity component.

The spectra of the above wave traces (fig. 5.17) are found in
figure 5.19. The two large waves apparent in each spectrum changed
their relative amplitudes, so that the lower frequency wave was dom-
inant at the highest Re#. This transition, occurring for $Re_L > 62.7$,
is similar to the frequency shift mentioned in section 5.4. For
the same Reynolds number range, wave energy with frequencies above
2Ω was observed. For all higher Re# observations in the Ekman
layer, energy was found above this inertial frequency limit. Although

Re$_L$ = 51.6

1 sec

Re$_L$ = 62.7

Re$_L$ = 80.8

Re$_L$ = 116.2
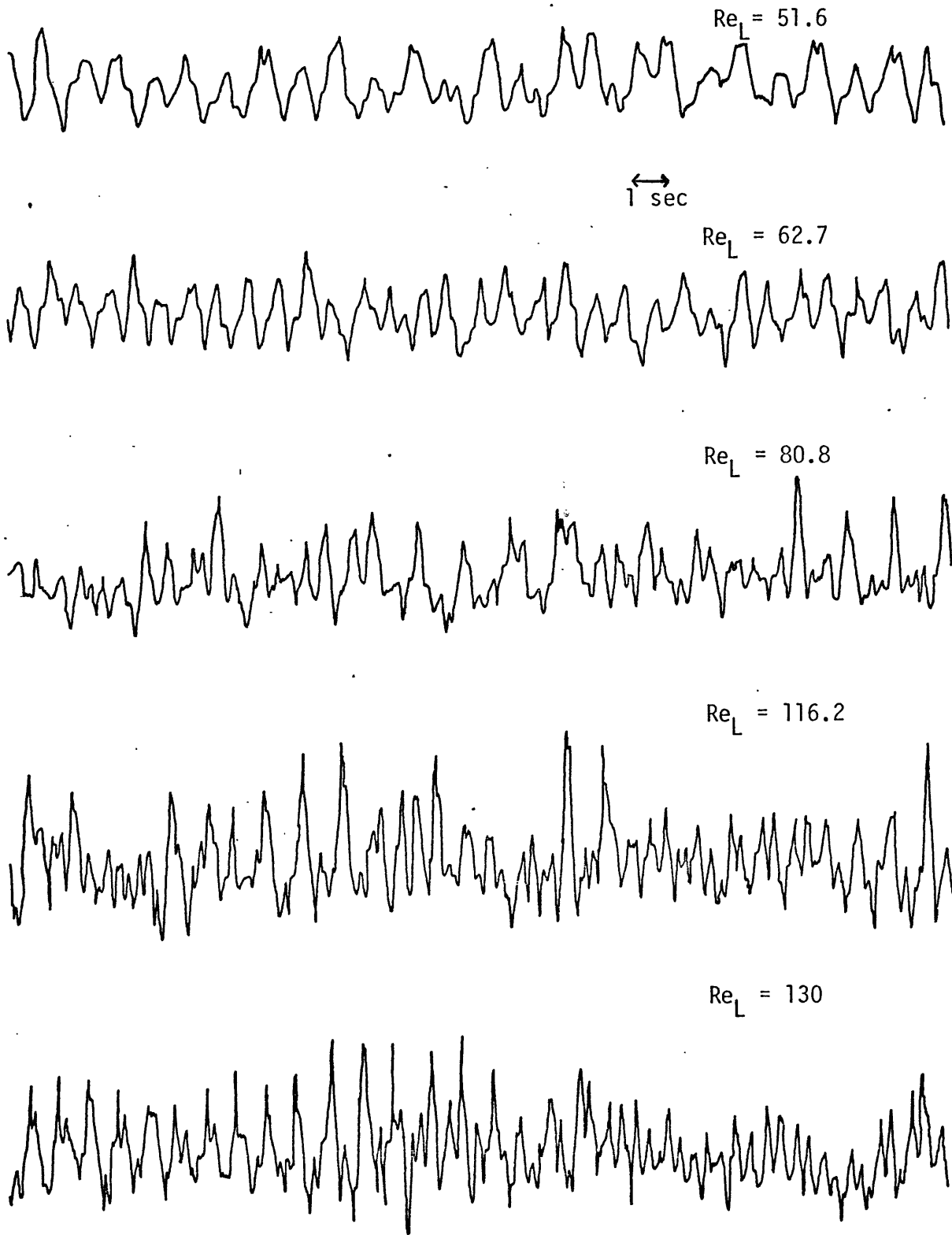
Re$_L$ = 130

FIGURE 5.17 - HOT WIRE VOLTAGE OUTPUT

1 sec

$Re_L = 80.8$

$Re_L = 116.2$
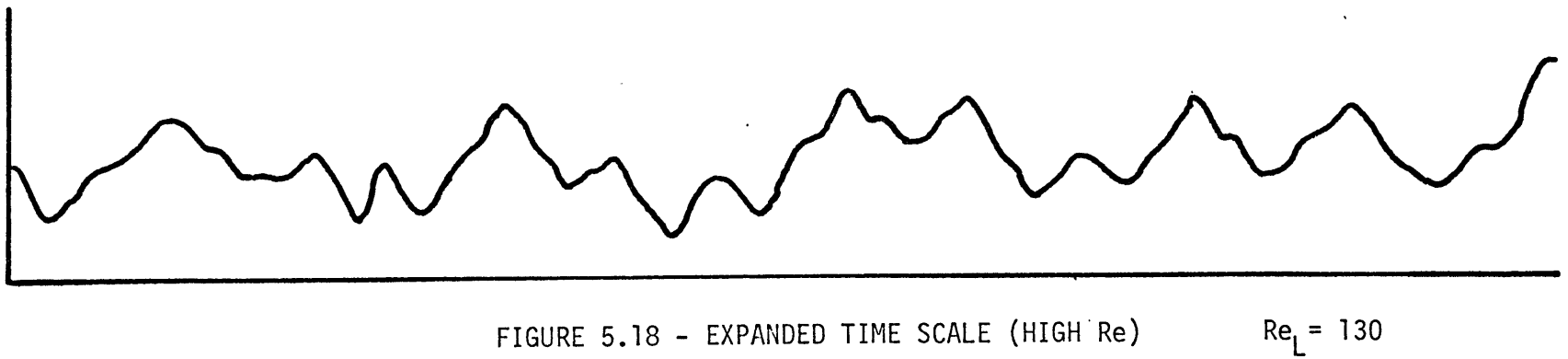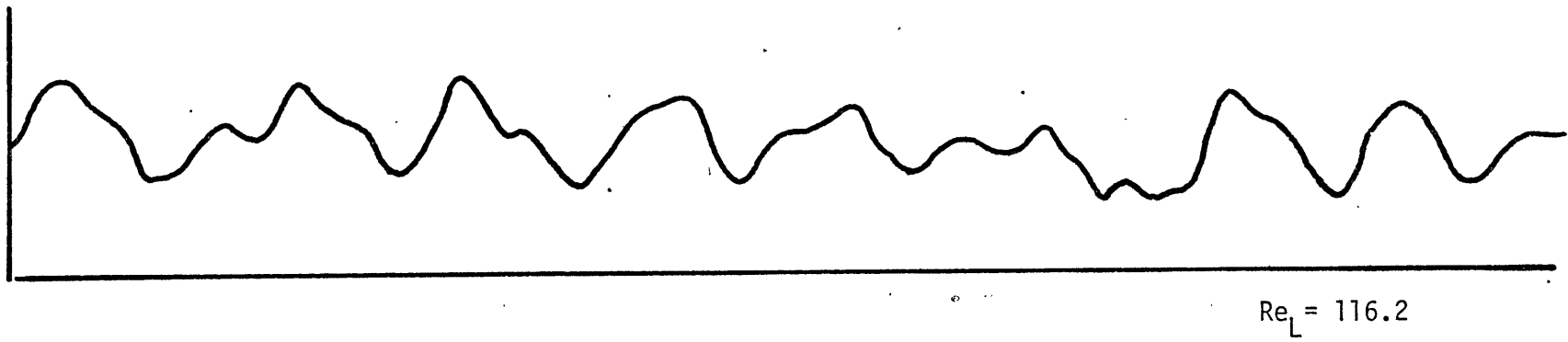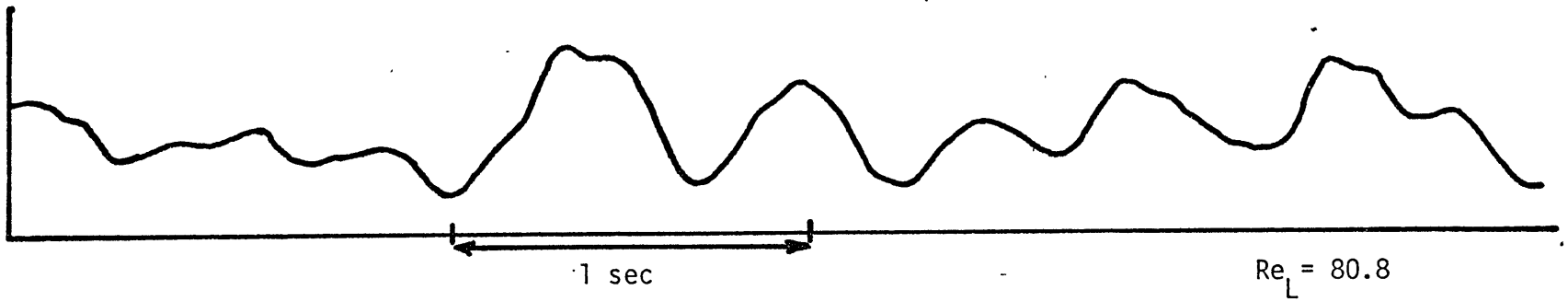
FIGURE 5.18 - EXPANDED TIME SCALE (HIGH Re) $Re_L = 130$
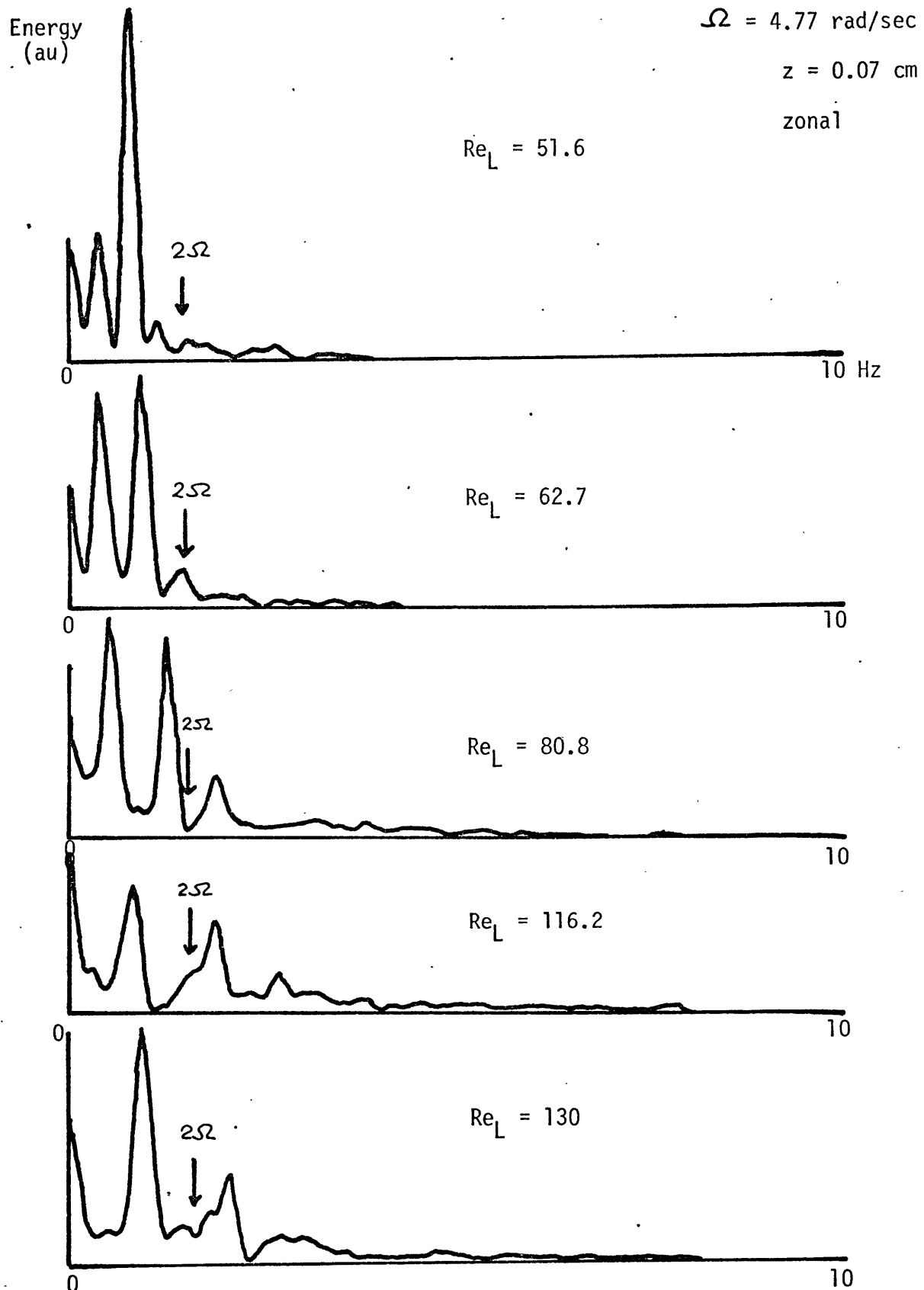
FIGURE 5.19 - EKMAN LAYER SPECTRA, R = 6.00"

the theoretically calculated Re# overestimates the actual value by approximately 40%, the motion observed at Re = 116.2 is certainly in an actual Reynolds range greater than 56.

Additional results taken for larger Re, are depicted in figure 5.20. In contrast to all previous spectra, two of the records were obtained with the hot wire aligned to give maximal response for radial directed flows. The most interesting feature of this series is a large peak (slightly above 4Ω in frequency) observed with the radial probe at $\mathbf{z}$ = 0.21cm. The remaining spectra show only a minor amplitude wave at this frequency.

A further series of observations was taken deep within the sink side-wall boundary layer, at a radius of 4.50" ($\mathbf{r}$ = 0.185). These spectra, shown in figures 5.21 and 5.22 include a theoretical Re# range of 80 to 360. Since the measured velocities and Ekman layer thicknesses are substantially smaller in the side wall layer, the ideal Re# overestimation is great (of order 60%). In the Re_L range of 80.8 to 233, the dominant peak is found to vary little from a frequency of 4Ω (independent of Re_L and ϵ_L). Above Re_L = 233, the frequencies change, but are still greater than 2Ω. These waves may correspond to those mentioned by Green and Mollo-Christensen, which had frequencies in the range of 2Ω to 4Ω (they show no spectral results). The sink side wall boundary layer was the only region in the tank to have no significant waves with frequencies below 2Ω.
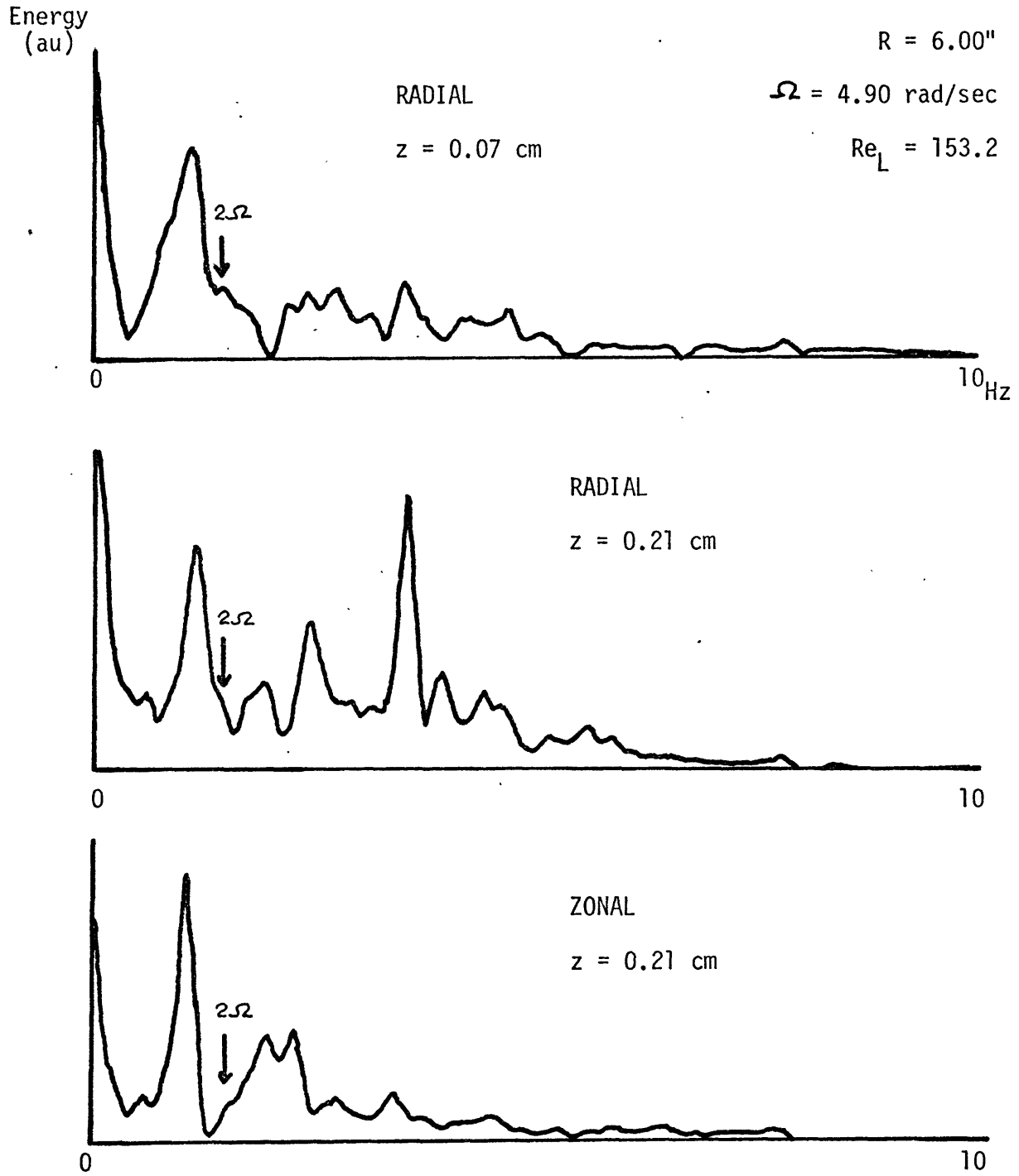
FIGURE 5.20

EKMAN LAYER SPECTRA, R = 6.00"
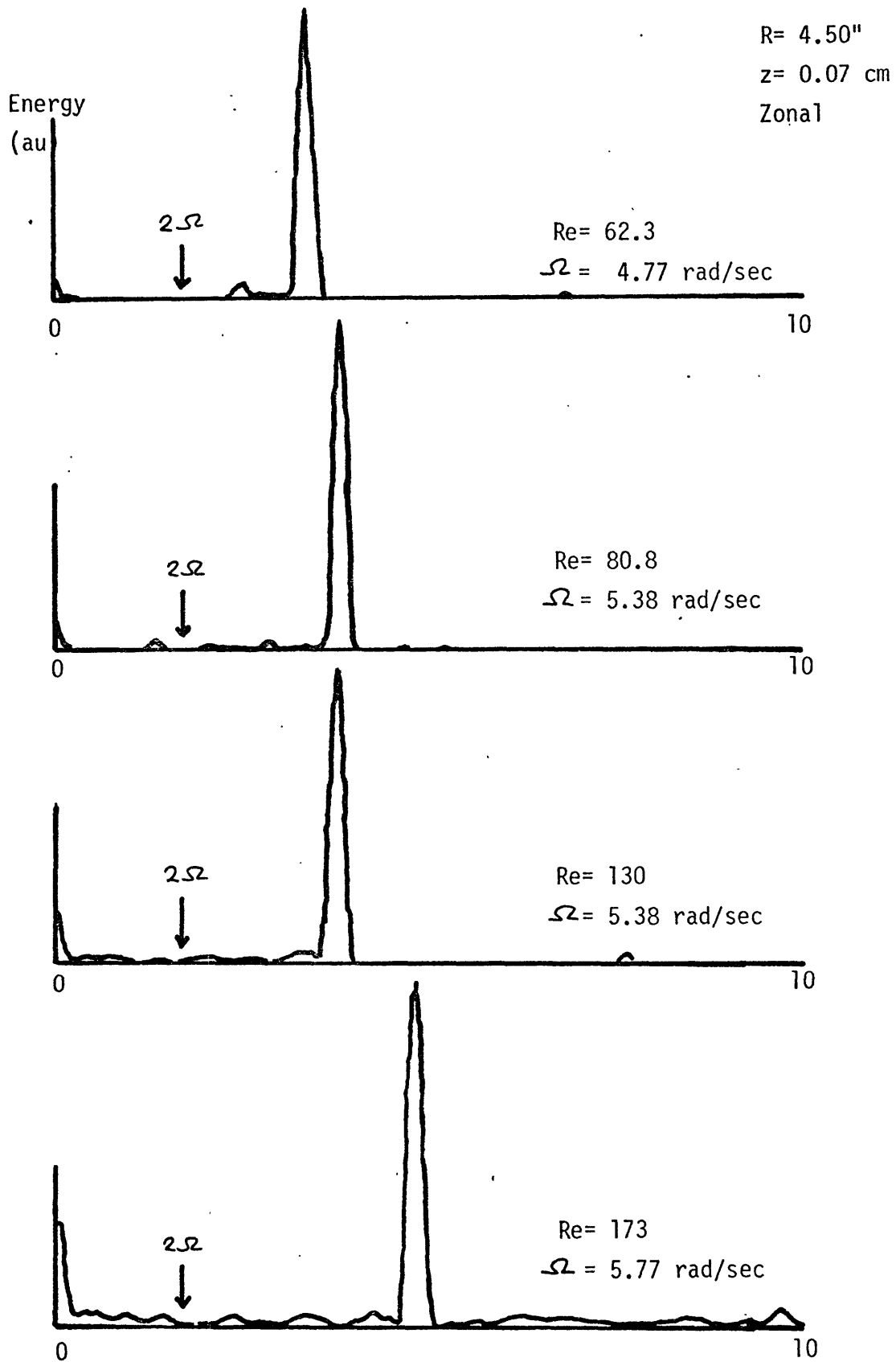
FIGURE 5.21 - EKMAN LAYER SPECTRA: R= 4.50"
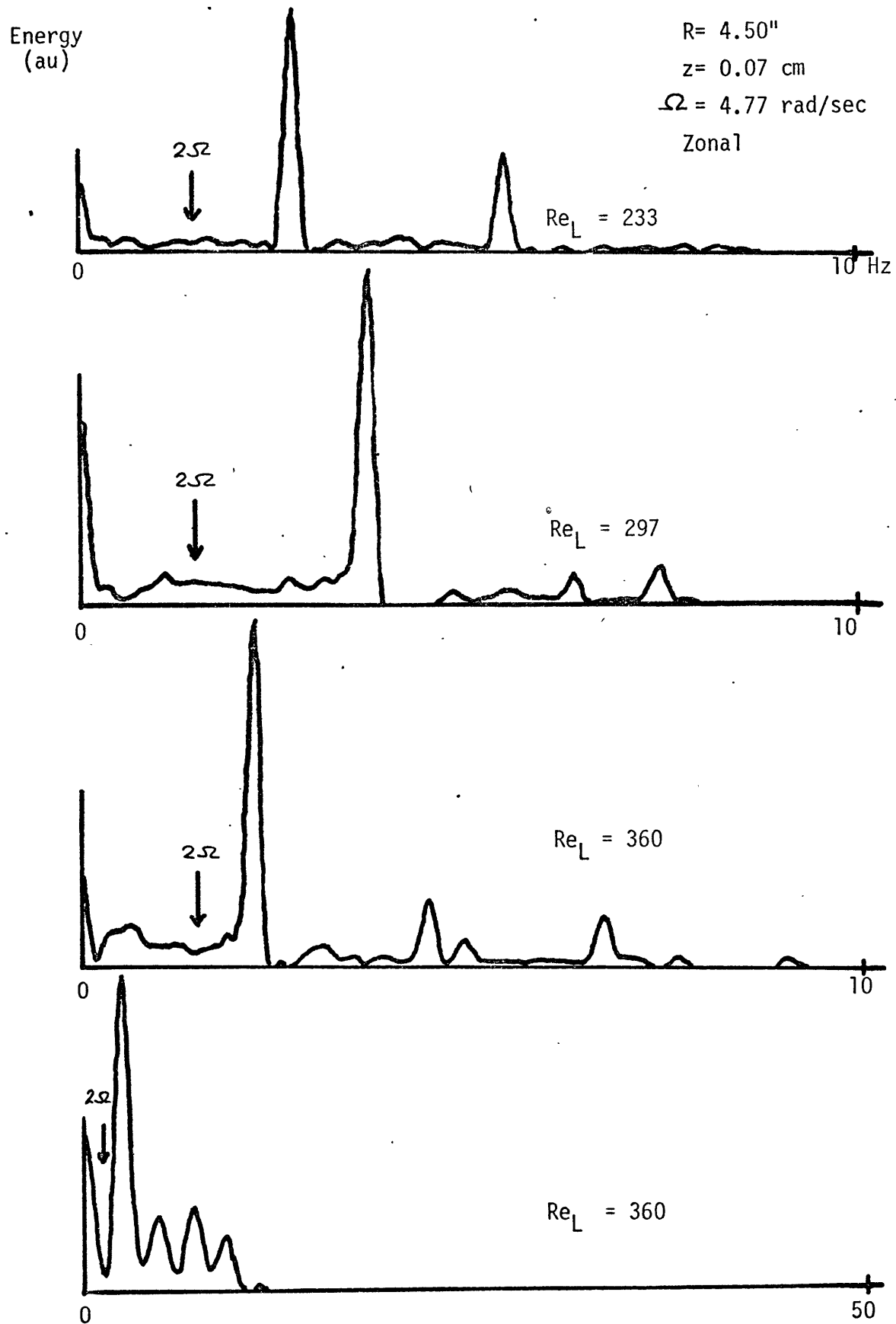
FIGURE 5.22 - EKMAN LAYER SPECTRA, R= 4.50"

We now turn to a short discussion of some previous Ekman
layer wave studies in source-sink annuli. The work of Tatro (1966),
and Caldwell and van Atta (1970) is found most relevant to the pre-
sent results. Their primary aim was to delineate the onset criteria
for the Class A and B Ekman layer instabilities. Figures 5.23 and
5.24 illustrate their results. Tatro separated his results into
two classes of instabilites by linear fitting techniques. On com-
paring the actual points shown in his diagram to those of Caldwell
and van Atta, a striking similarity is found for Re $\leqslant$ 130. In con-
trast to Tatro, Caldwell and van Atta used a least squares fit of
Faller and Kaylor's (1966) onset criteria. By extrapolating their
curves to zero Rossby number, the critical Reynolds number was ob-
tained. Both Tatro and Caldwell and van Atta find this number to
be slightly above 56. Furthermore, Caldwell and van Atta claim that
no class B waves were apparent in their results. As both figure
5.23 and 5.24 display a similar distribution of points about the
Re_{crit} = 125 line, it would seem their differences lie in definition
and not in the dynamics.

In the present work, profiles # 1, 2, 3, 4, 7, 9, 11, 13, 14,
15 and 17 (of Table 4 - 2) are found to exhibit characteristics of
the class A instability. The observed wave motion in these profiles
was substantially larger (by a factor of 3) than in all others. A
similar technique (wave amplitude) was used by Tatro and Caldwell
and van Atta to estimate onset of the instability. The amplitude
increase noted by Caldwell and van Atta is essentially the same as
found presently. However, the most interesting comparison can
be found among the local Reynolds numbers. From the theoretical
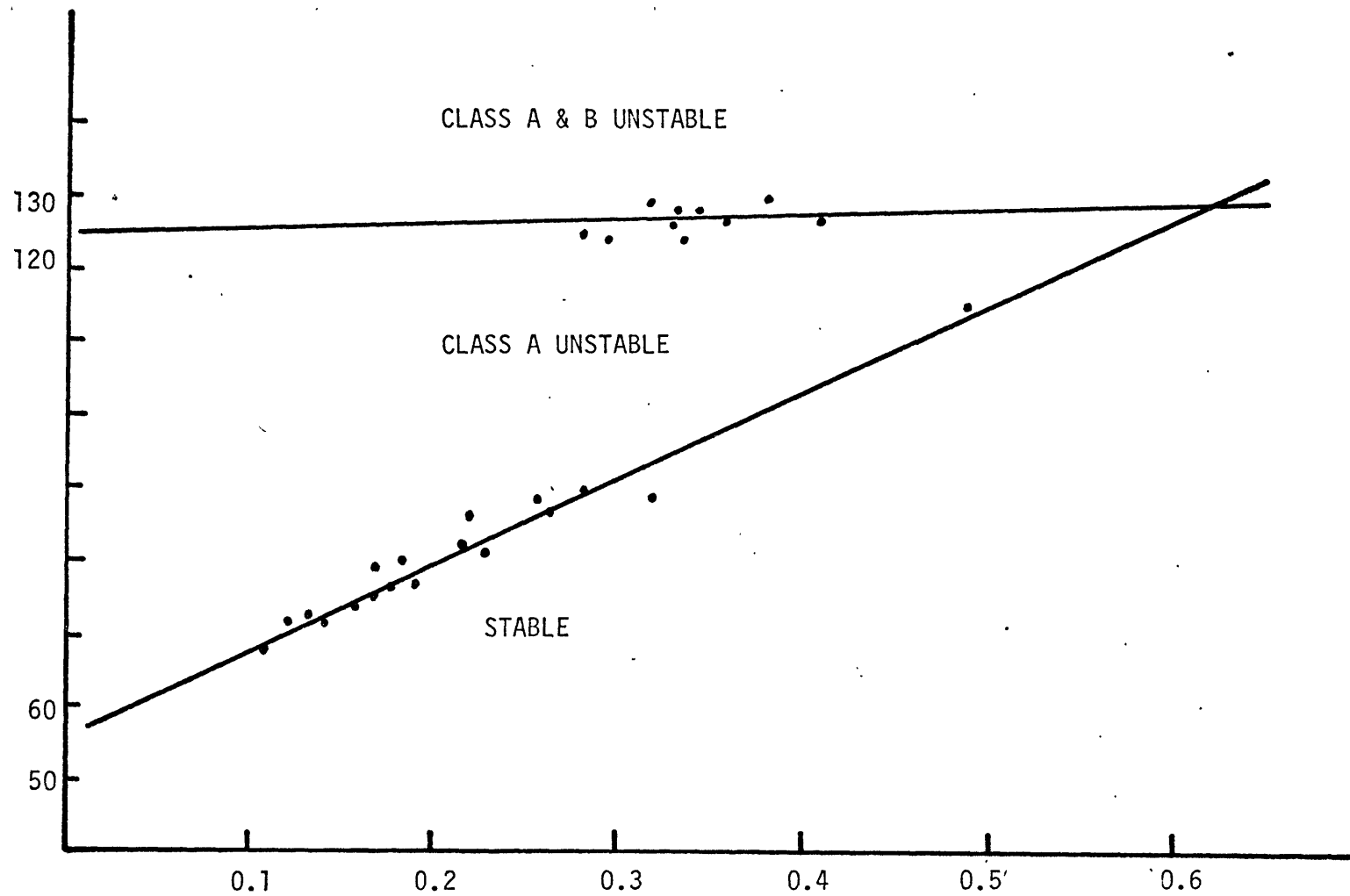
FIGURE 5.23 - CRITICAL REYNOLDS NUMBER VERSUS ROSSBY NUMBER FOR EKMAN LAYER INSTABILITIES (TATRO)
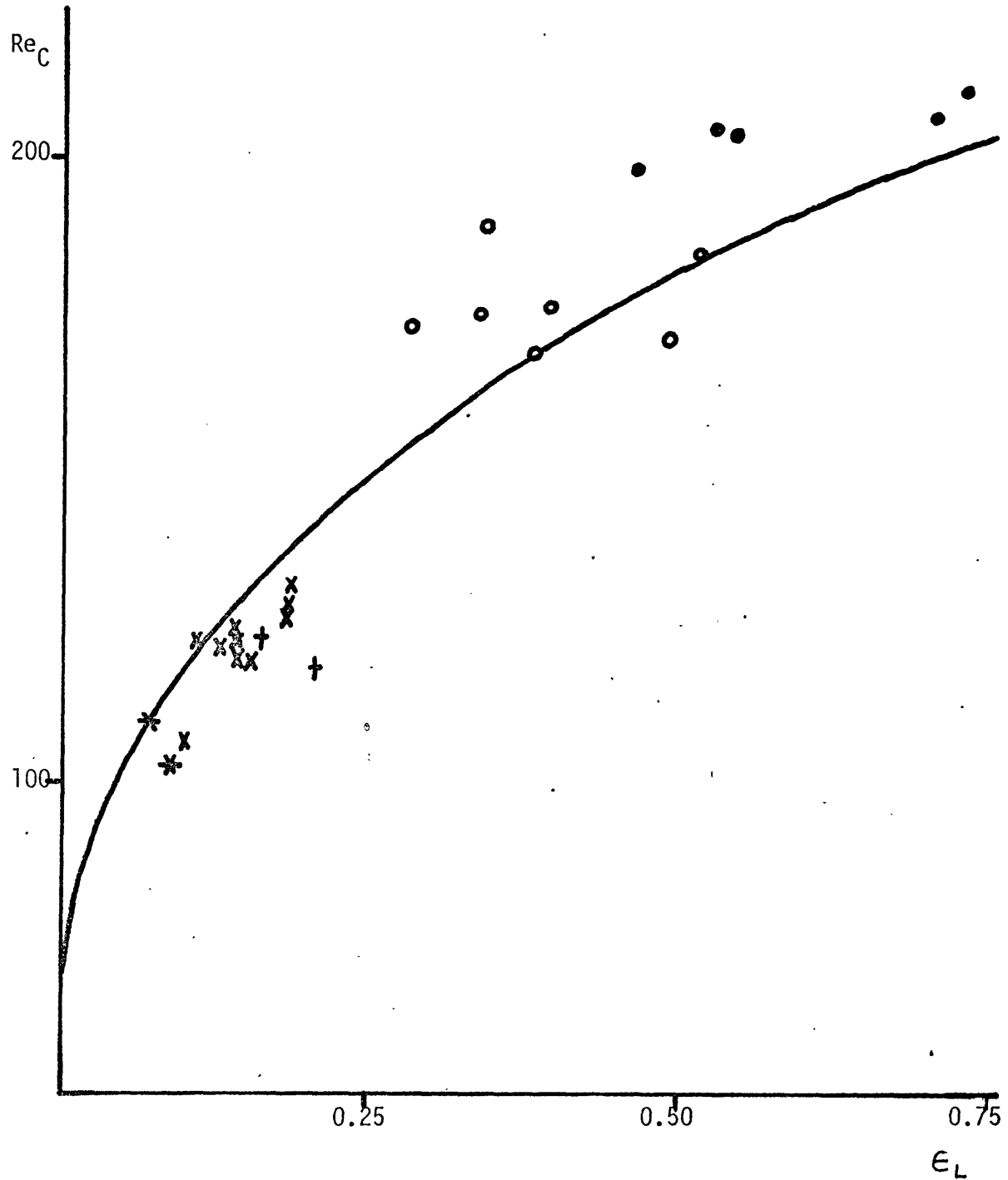
FIGURE 5.24

CRITICAL REYNOLDS NUMBER VERSUS ROSSBY NUMBER FOR EKMAN
LAYER INSTABILITIES (CALDWELL & VAN ATTA)

values shown in Table 4-2, we find Re_{crit} is of order 50. The

measured values were substantially lower (by one-half). Comparable

Re_{crit} values in the work of Tatro (1966) and Green (1968) were much

higher, resulting from their overestimation of the Ekman layer thick-

ness.

The spectra of velocity fluctuations for Ekman layer profile #2

(see Table 4-2) was shown in figure 5.20. In this figure, at Z = 0.21cm,

we assume the large amplitude high frequency peak corresponds to the

class A instability. In a similar fashion, the spectral results shown

in figure 5.21 are representative of Ekman profile #1.

Figure 5.25 shows a spectral representation of Ekman layer in-

stability onset observed by Caldwell and van Atta. A comparison of

these results with all of those obtained presently, reveals a marked

difference. The dominant wave frequency in figure 5.25 is approxi-

mately 10Ω. In contrast, figures 5.20 and 5.21 exhibit dominant

peak frequencies between 4 and 5Ω. Similarly, Caldwell and van Atta's

wave frequency is essentially invariant with increasing flux. The only

comparable wave dependency on flux is found in fig. 5.21 and 5.22.

Caldwell and van Atta also found an onset of turbulence in the

Ekman layer for Re > 148 (see figure 5.25). At this Reynolds number

their observed spectrum became quite broad. To test this response

in the present work, two spectra in a very high Reynolds range were

obtained, as shown in figure 5.26. Allowing for a small overesti-

mation in the Re value, the results were found to be definitely

within Caldwell and van Atta's turbulent range. However, the present

results displayed an orderly onset of turbulence, with all the harmonics

and sub-harmonics having grown to equal amplitude. This "slow"
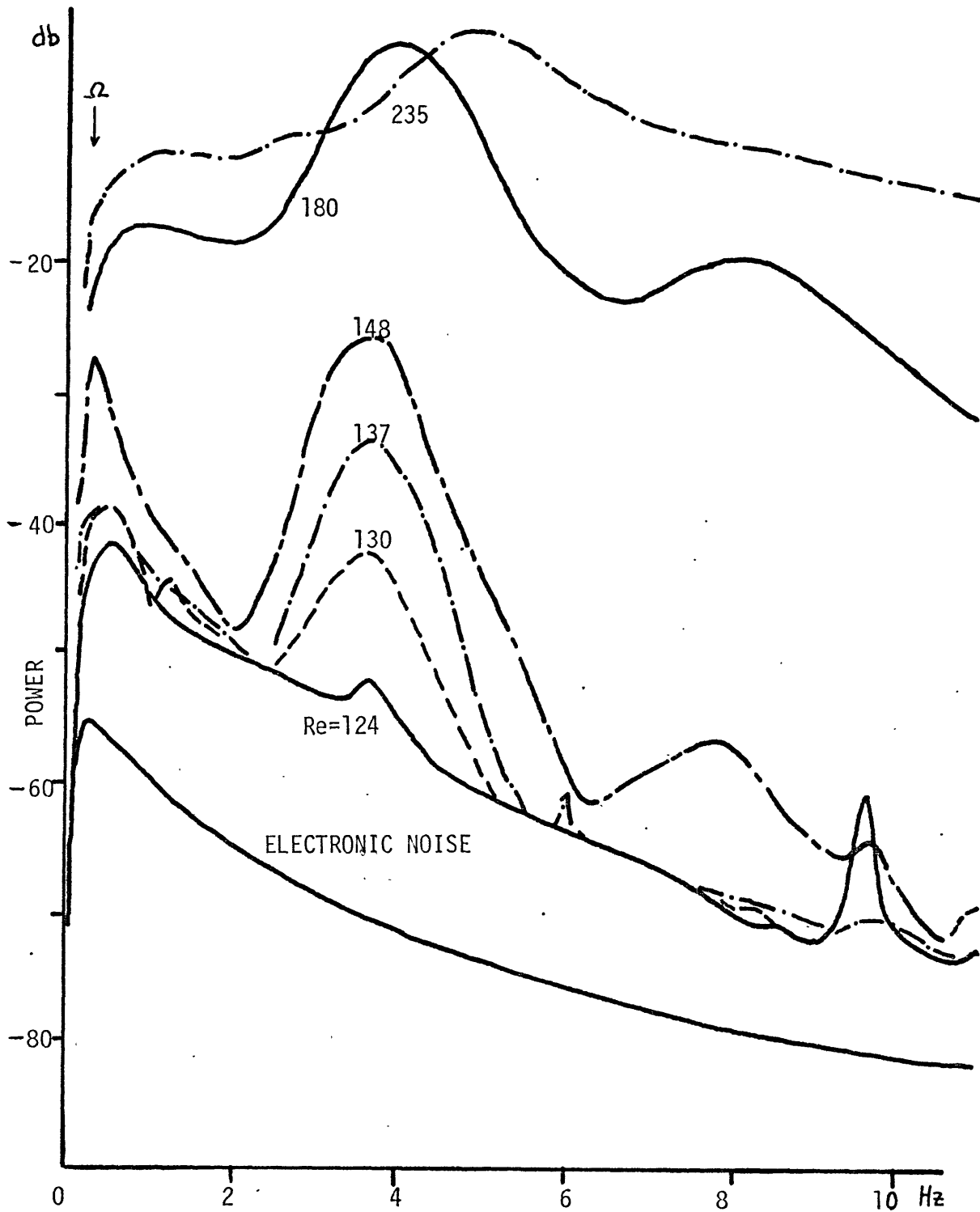
FIGURE 5.25 - EKMAN LAYER SPECTRA (CALDWELL AND VAN ATTA)

Energy
(au)

S= 3500 cc/sec

Ω= 3.39 rad/sec

R= 7.80"

Re_L = 182

ϵ_L = 1.97

z = 0.10 cm

2Ω

0   2.5 Hz

S= 3300 cc/sec

Ω= 3.52 rad/sec

R= 7.84"

Re_L = 170

z = 0.06 cm

ϵ_L = 1.80

2Ω

0   2.5
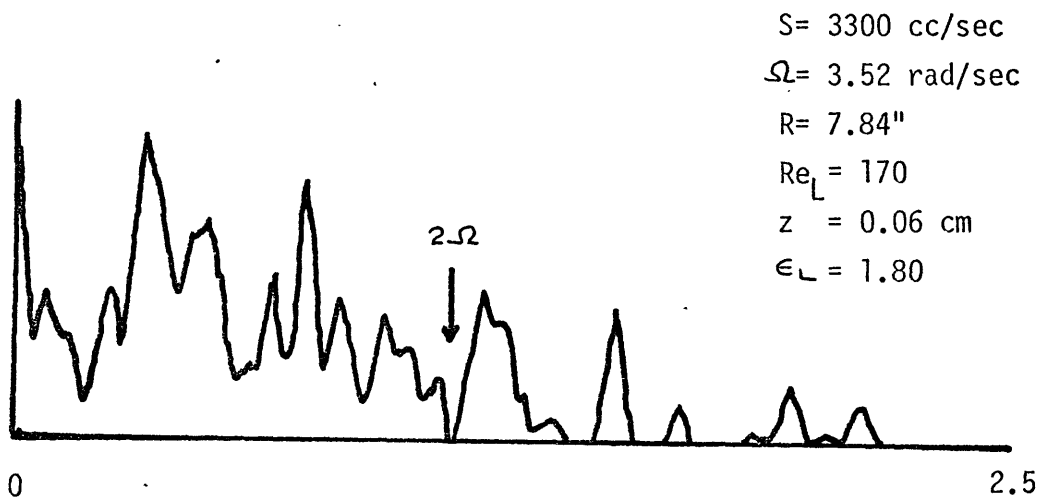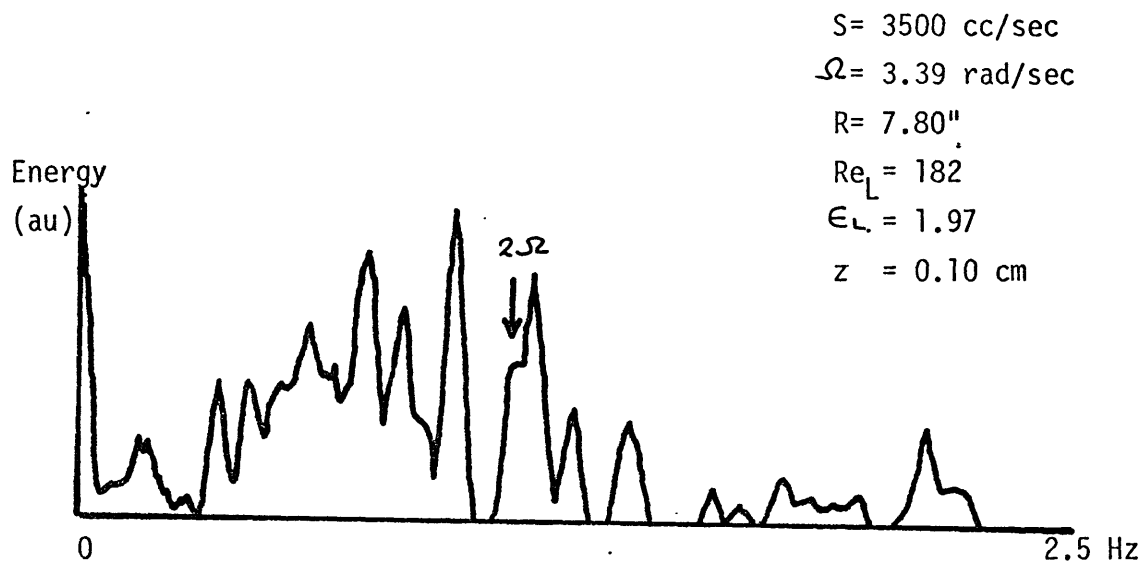
FIGURE 5.26 - EKMAN LAYER SPECTRA FOR HIGH REYNOLDS NUMBER FLOW

transition to turbulence may be related to developing non-linear modes
(Ffowcs Williams, Rosenblat and Stuart, [1969]). A relevant exam-
ple is found in the Taylor instability work of Coles (1965).

5.5.2 Comparison of Interior and Ekman Layer
Spectral Results.

According to Green and Mollo-Christensen (1970) similar spec-
tra (the actual spectra is not presented) should be expected within
an unstable Ekman layer as well as at an interior mid-tank position.
It is not clear in their discussion whether oscillations of frequency
greater than 2Ω were also predicted at the interior position. How-
ever, a comparison of figures 5.5 - 5.10 and 5.11 shows that at mid
radial positions, similar inertial wave frequencies were observed
in the interior and the adjacent Ekman layer. This frequency invar-
iance with radius in the interior, was explained in section 5.4, as
resulting from non constant circulation profiles. Also, the domi-
nant inertial wave in the interior was readily perceived within the
Ekman layer (see figures 5.7 and 5.11) at the same radius. As Green
and Mollo-Christensen located their sensors at r = .37 and .63
(inner probe within Ekman layer), results obtained at these positions
would be almost identical in dominant wave frequency (see section 5.4).

To further examine this dependency, another series, for larger
Re#, is shown in figure 5.27. The interior probe (r = 0.89) was lo-
cated within the outer Stewartson layer. The spectra exhibited few
peaks of similar frequency. For Re_L = 64.2, only one peak was clear-
ly transmitted to the outer radius. For the two higher Re# comparisons,

S= 1245 cc/sec
Ω= 3.52 rad/sec
R= 7.84"
Re_L= 64.2
ϵ_L = .68
z= 0.06 cm

S= 1245 cc/sec
Ω= 3.52 rad/sec
R= 21.57"
Re_L = 23.3
ϵ_L = 0.09
z = 12 cm

S= 1561 cc/sec
Ω = 3.52 rad/sec
R= 7.84"
Re_L = 80.5
ϵ_L = 0.85
z = 0.06 cm

S= 1561 cc/sec
Ω= 3.52 rad/sec
R= 21.57"
Re_L=29.2
ϵ_L = 0.11
z = 12 cm
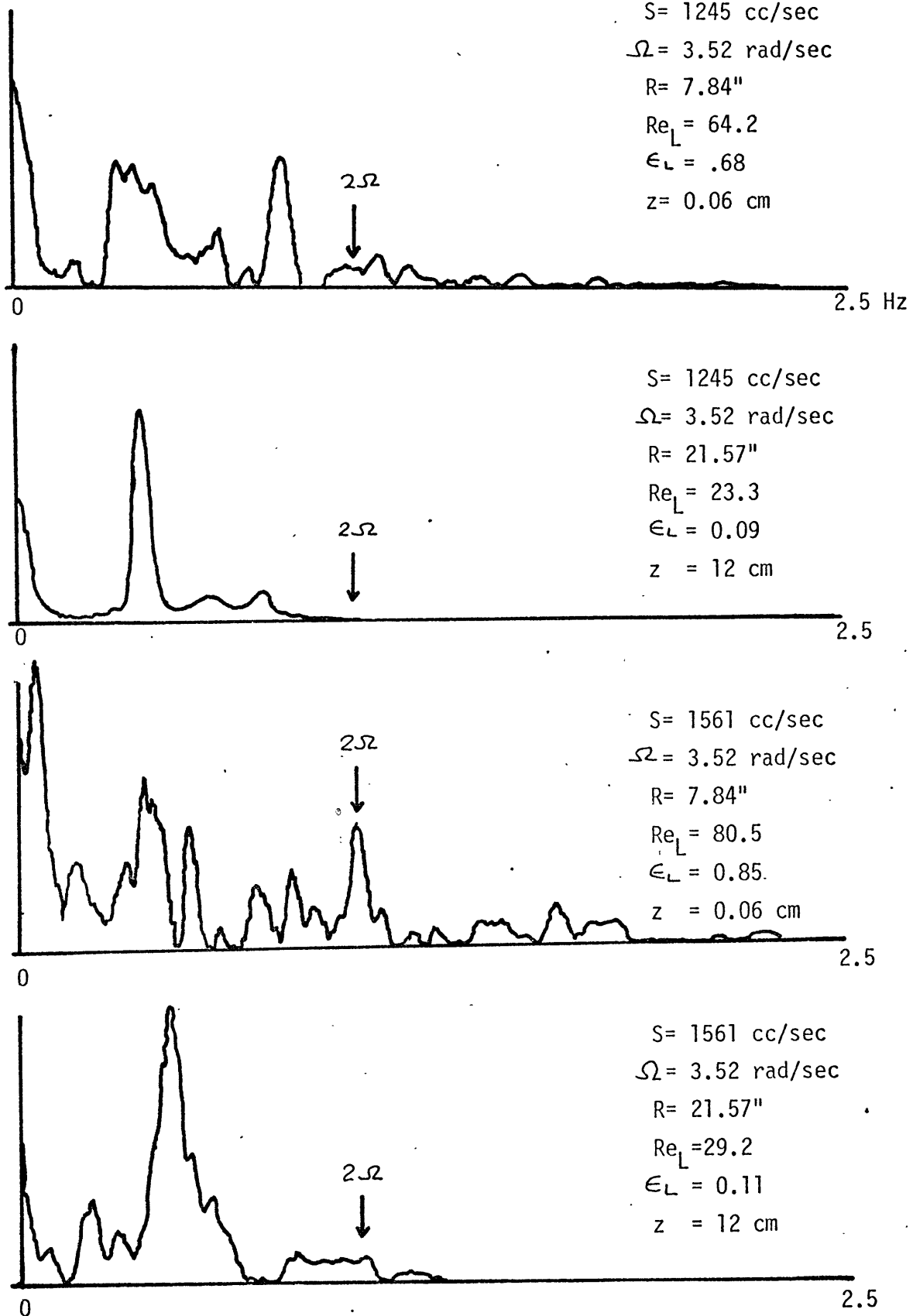
FIGURE 5.27A - INTERIOR AND EKMAN LAYER SPECTRAL COMPARISON

S= 1725 cc/sec

Ω= 3.52 rad/sec

R= 7.84"

Re_L = 88.9

ϵ_L = 0.94

z = 0.06 cm

2Ω

0

2.5 Hz

S= 1725 cc/sec

Ω = 3.52 rad/sec

R= 21.57"

Re_L= 32.3

ϵ_L = 0.12

z = 12 cm

2Ω

0

2.5
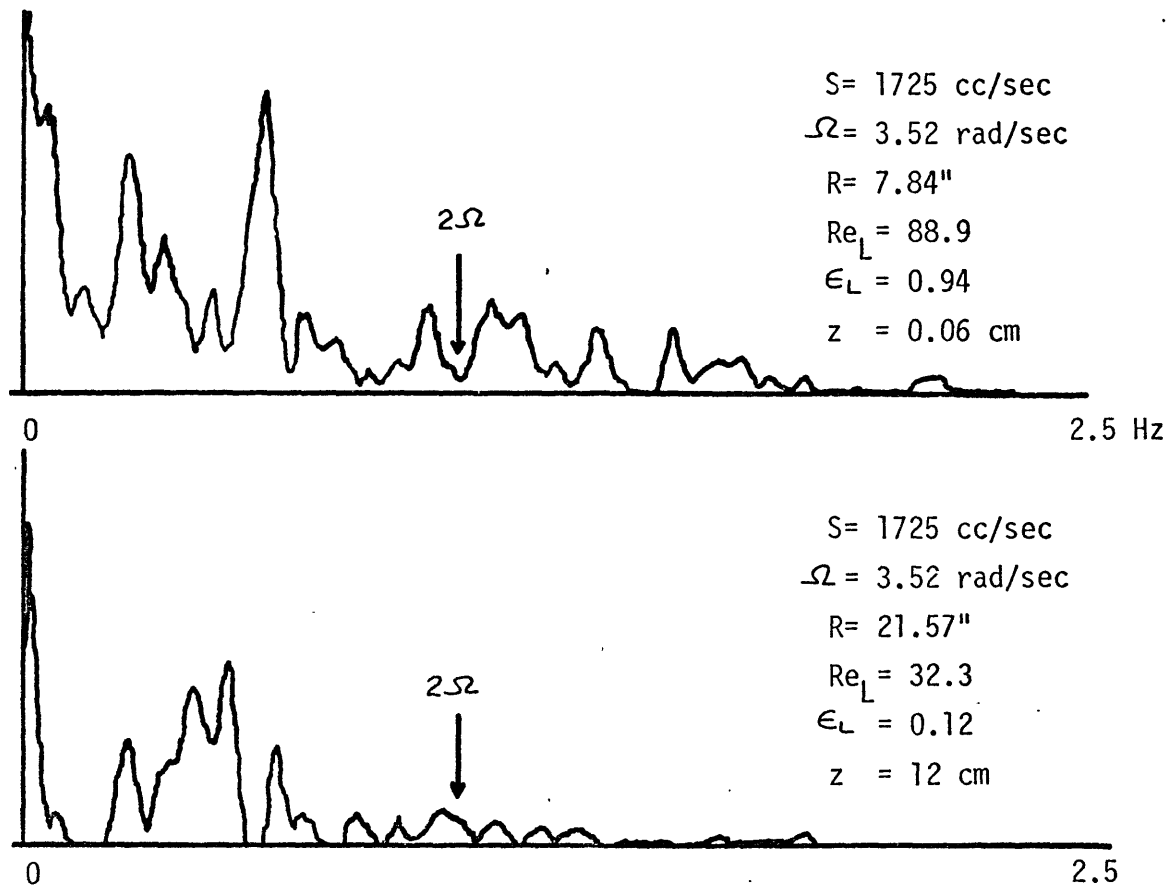
FIGURE 5.27B - INTERIOR AND EKMAN LAYER SPECTRAL COMPARISON

only two low frequency peaks were found at both locations. This is not surprising, since the radial distribution of similar frequencies in the first series was limited to $r <$ 0.65 (in general). It should be remarked, that the absolute amplitudes of the waves shown at R = 21.57" (Fig. 5.27) were much lower than their equivalents at R = 7.84". Only a much larger amplification brings the two wave sets to comparable size. Two additional comparisons (not shown) for S = 697 and 903 cc/sec., produced no wave activity at the outer location. This implies that the wave amplitude was less than .01% of the mean flow.

One can conclude from these comparisons, that the inertial waves generated by instabilities in the Ekman layer will be observed at most mid-tank locations (r = 0.35 - 0.65). Furthermore, the inertial wave activity above the Ekman layer is usually observable in the spectra (some peaks) taken deep within the boundary layer. Green and Mollo-Christensen's results were within the radial range mentioned above. It appears that they are observing the inertial wave activity of the interior, which may have been generated at some other radius.

5.6   Measurement of Azimuthal Wave Number by Cross Correlation

To obtain the azimuthal wave numbers for some of the non-axisymmetric waves, two probes were placed at the same radius, but separated zonally by a known angle. The cross correlation was measured as a function of the relative delay time between the signals recorded at the two positions. Thus the phase difference and therefore the azimuthal wave number could be determined. Additionally, the azimuthal wave structure in the Ekman layer and its relationship to the interior motions

were studied. For most interior correlations, the probes were 60° apart.
When using only two probes, a definite separation of progressive and re-
trogressive modes was not possible in all cases.

The auto-spectra results for one of the three cross correlation
measurements is shown in Fig. 5.28. The probe configuration had two
sensors at a similar height within the Ekman layer and an interior hot
wire located between them. The parenthesized spectra numbers show place-
ment for the second series. The third series (Fig. 5.29) used only two
probes, one of which was in the Ekman layer, while the other was placed
at varying heights in the interior. All other correlations (interior)
were taken with the probes separated by 60°. Table 5-4 is a chart of
cross correlation results with the pertinent experimental conditions
listed. The wave class designation divides progressive and retrogres-
sive, whenever possible. Two values are given when thechoice is uncertain.

In the Ekman layer, the dominant wave was found to be axi-symmetric
for both cases observed. The correlations between waves in the boundary
layer and the interior at R = 13.80" showed a constant time lag for the
three different heights. The "Stern" waves (cross correlations #14 and
#15), were found to be axi-symmetric in the interior. The final corre-
lations showed the non-axi-symmetric to be compatible in modal number.
The dominant waves had a retrogressive direction with m = 3, whereas,
the secondary peaks were either progressive m = 1 or retrogressive
m = 5 azimuthal waves.

By using an extended probe in conjunction with a fixed hot wire,
it was possible to estimate the radial wave length. Of the three runs
taken, the wave length varied from 4 to 6 cm, but on the average was 5cm.
The rotation rate was 4.52 rad/sec. and the fluxes varied from 1000 to
1500 cc/sec. (R = 12.0").

R= 10.52"

S= 1040 cm/sec

Ω= 6.28 rad/sec

2Ω

z= 0.08 cm

2Ω

z= 0.08 cm

2Ω

z= 12.3 cm

PROBE CONFIGURATION

25°   50°

171
(174)
zonal flow

172   173
(176)   (175)
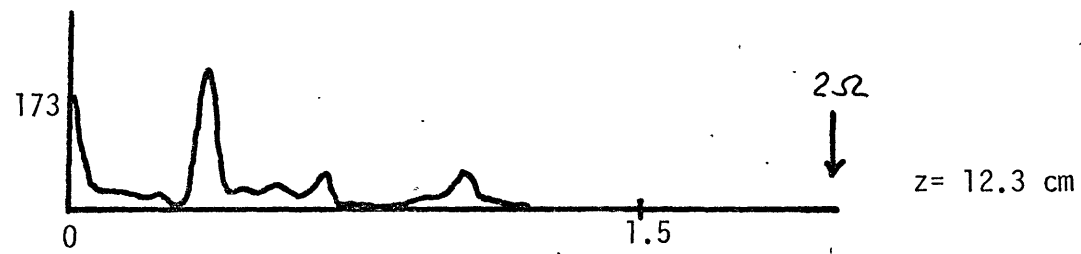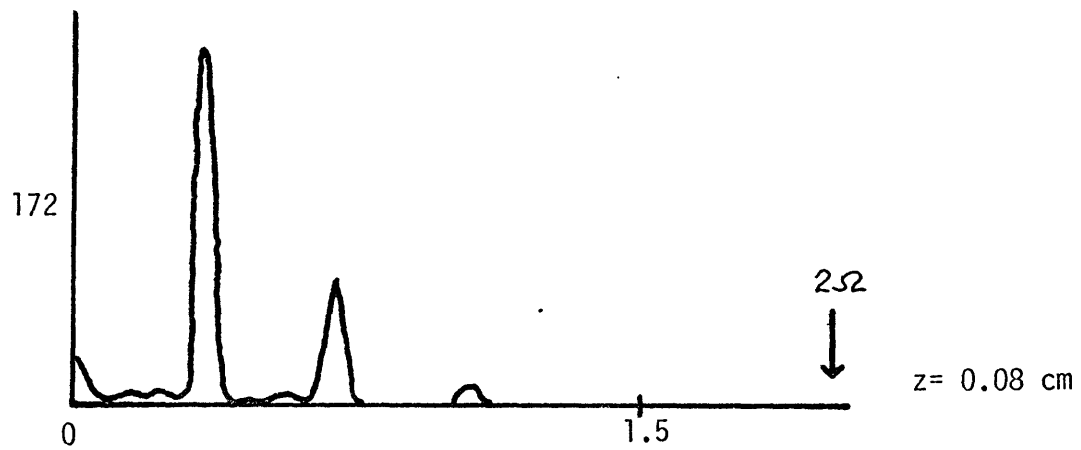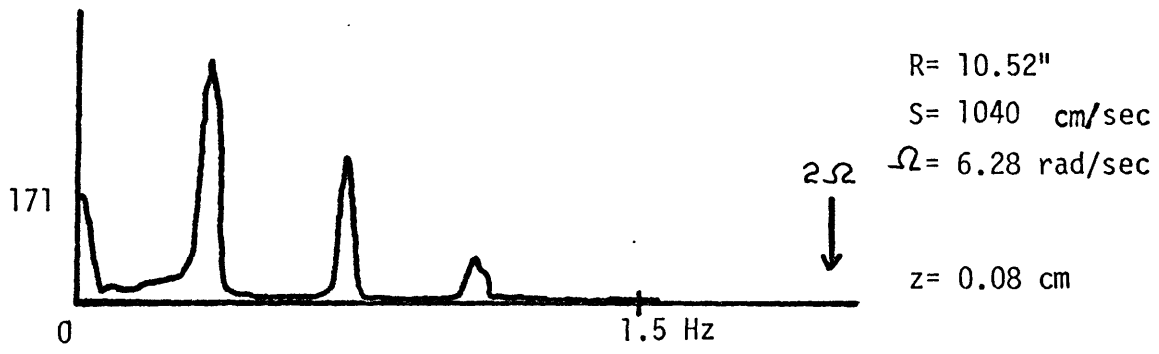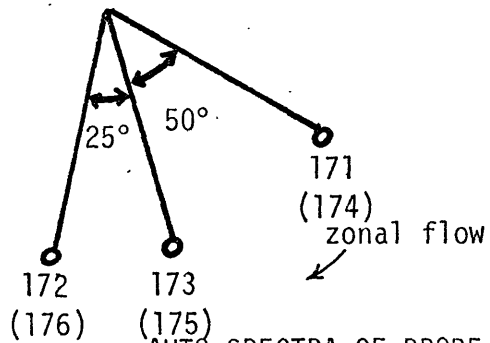
AUTO-SPECTRA OF PROBE OUTPUTS DURING

FIGURE 5.28 - CROSS CORRELATION MEASUREMENTS: EKMAN LAYER

Energy
(au)

R= 13.80"

S= 1312 cc/sec

Ω = 5.02 rad/sec

271

2Ω

z= 0.10 cm

1.5 Hz

274

2Ω

z= 4.oo cm

1.5

272

2Ω

z= 8.00 cm

1.5

275

2Ω

z= 12.00 cm

1.5

PROBE CONFIGURATION

60°

Zonal flow

272
274
275

271
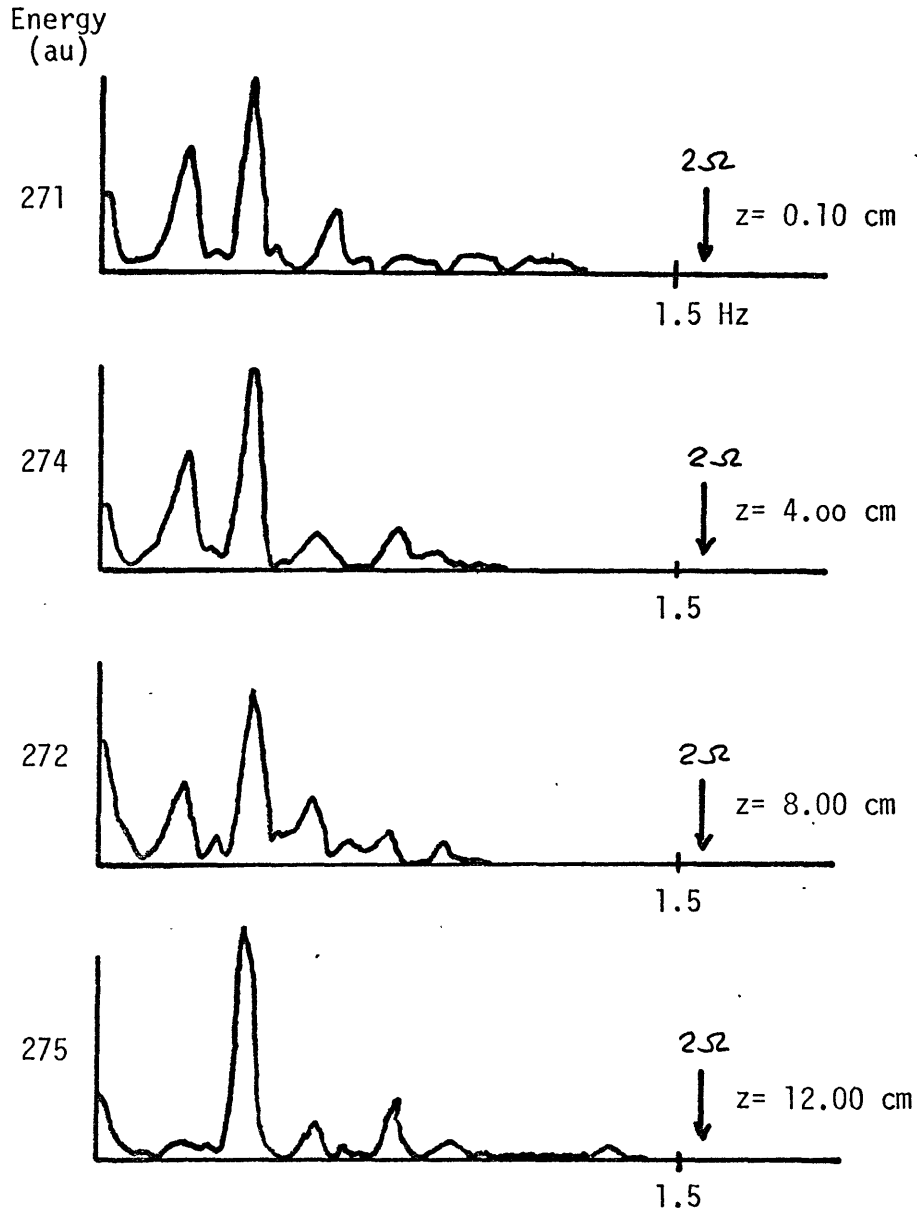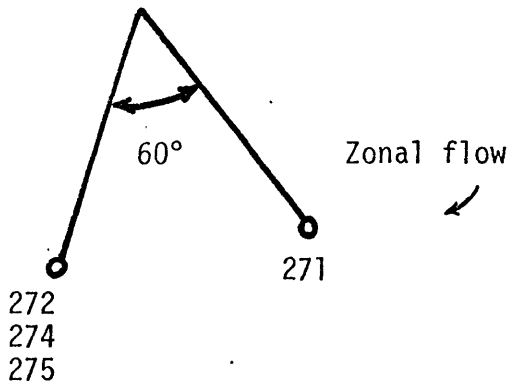
FIGURE 5.29

CROSS CORRELATION CONFIGURATION:

VERTICAL SEPARATION

TABLE 5 - 4

CROSS-CORRELATION RESULTS & AZIMUTHAL WAVE NUMBERS

#	FLUX(cc/sec)	ROT(r/s)	Radius(in.)	A		B		σ(cps)	$\Delta\tau$	m
				Spectra#	z(cm)	Spectra#	z(cm)		(sec)	
1	1040	6.28	10.52	173	.08	171	.08	.34	0.0	0
2				172	.08	171	.08	.68	0.38	
3				173	12.3	171	.08	.34	0.47	
4				173	12.3	171	.08	.68	0.43	
5				173	12.3	172	.08	.34	0.53	
6	1561	6.41	10.52	174	.08	176	.08	.51	0.00	0
7				174	.08	175	12.3	.51	0.30	
8				175	12.3	176	.08	.51	0.31	
9	1314	5.02	13.80	271	.10	272	4.0	.21	1.30	
10				271	.10	272	4.0	.38	1.47	
11				271	.10	274	8.0	.21	1.36	
12				271	.10	274	8.0	.38	1.44	
13				271	.10	275	12.0	.38	1.52	
14	697	4.52	15.45	278	12.0	279	12.0	.74	0.00	0

TABLE 5 - 4

(Continued)

		$\Delta\tau$								m
15	903	4.52	15.45	280	12.0	281	12.0	.74	0.00	0
16	1245	4.52	15.45	286	12.0	287	12.0	.25	1.91	3(R)
17				286	12.0	287	12.0	.51	1.52	1(P), 5(R)
18	1451	6.85	15.45	290	12.0	291	12.0	.37	1.19	3(R)
19				290	12.0	291	12.0	.77	0.99	1(P), 5(R)
20	1715	4.52	15.45	284	12.0	285	12.0	.36	1.44	3(R)
21				284	12.0	285	12.0	.74	1.12	1(P), 5(R)

KEY: $\Delta\tau$: Time delay for maximum correlation (Signal A delayed with respect to B)

  m : Azimuthal wave number

  P : Progressive

  R : Retrogressive

CHAPTER VI

Discussion

The results of the previous two chapters showed a remarkable interdependence between the steady and oscillatory motions. We found that the introduction of an Ekman layer instability at some radius in the annulus led to interior wave motions and in certain cases, to a c change of the steady circulation profile. These alterations of the steady flow were found to influence the observed time dependent flow characteristics.

In this chapter, we will attempt to explain some of the more prominent features of the observed flows. In section 6.1, the changes in steady circulation are compared to previous results in differing geometries and to a non-linear modification of geostrophic flow, postulated by Greenspan.

The following section (6.2) discusses the alternate mechanisms available for producing interior disturbances with characteristics similar to those predicted by Stern. In section 6.3, the generation mechanism and the observed frequency of inertial oscillations is related both to the governing flow parameters, and the steady circulation field.

A summary of the boundary layers observed adjacent to both the horizontal and vertical walls in the annulus and their dependence on flow parameters is found in section 6.4.

In section 6.5, the various results are combined into an over-all picture of the flows expected in a rotating source-sink annulus. The observed changes are found to have a critical dependence on flow parameters.

Finally, the relevance of the present work to geophysical phenomena and its possible extensions are discussed in sections 6.6 and 6.7.

6.1.   Interior Circulation Profile

We found in Chapter IV, that for increasing values of flux, the circulation profile at mid-radial positions deviated greatly from theoretical prediction. Ideally, the interior circulation should be constant with radius. In contrast, the present circulation values showed a linear increase with radius, for higher system Rossby numbers (above 0.05). However, this feature was found only between the radial limits of r = 0.35 to 0.70.

Both Fultz (1959) and Malkus (1968) have observed the appearance of similar steady zonal flows, resulting from non-linear effects. Fultz's experiment used an interior disk to force inertial oscillations in a cylindrical tank. The interior motion was observed through the use of dye techniques. A much clearer view of this rectified geostrophic flow was obtained by Malkus in a precessing sphere, using aluminum flakes. In this case, the steady zonal current was observed to change direction several times over the radius of the sphere.

Greenspan (1968) had postulated that this feature may result from a non-linear interaction of a single inertial wave with itself to provide a steady zonal current and an oscillation at twice the basic frequency. However, in a later paper, Greenspan (1969) found that the principal non-linear interaction of inviscid inertial modes does not produce a resonant response in the steady geostrophic circulation. He concluded that only a combination of viscous and non-

linear effects within the boundary layer can provide a mechanism for development of the observed steady interior circulations.

The presently observed circulation changes could be explained by a similar dynamics. However, no definitive analytical work in this area has been reported. The principal cause of the generated steady currents which develop from oscillatory disturbances seems to be non-linear processes within the viscous boundary layers. In the present case, it implies that a linear treatment of the observed flows is valid for $\epsilon_{sys} < 0.05$. In our annular configuration we do not expect the reversing flows observed by Malkus at "critical" latitudes in his sphere. The "critical" latitude in the annulus can be found only in the corner region.

6.2.   Low Reynolds Number Waves at the Outer Radii.

At the outer radial positions (but not adjacent to the source wall) an axi-symmetric wave motion was observed at low Reynolds numbers. The frequency of these waves was found to be slightly greater than Ω (actually 1.04Ω) in all cases. Previous observational work in annular tanks has exhibited slowly moving axi-symmetric instabilities at lower Reynolds numbers. Furthermore, some of their observed wave features corresponded to predictions of Stern's (1960) Ekman layer instability study. Presently, waves with similar characteristics were detected (as discussed in section 5.3) and thought to be the same phenomena. A large attenuation of wave amplitude was noted for the higher Reynolds numbers.

Another possible explanation for the observed structure is found in the shear flow instability work of Busse (1968). He

distinguished between two mechanisms for instability. If the total angular velocity decreases with increasing radius, the Rayleigh (1920) stability criterion for axi-symmetric disturbances can be violated. Taylor vortices in the case of circular Couette flow are an example of this instability. A different kind of instability occurs as a wave propagating in the azimuthal direction and corresponds to the instability of parallel shear flow in a non-rotating system.

In an unpublished work (see Busse [1968]), Hide found that by differentially rotating (at $\Omega(1 + 4\epsilon)$) a concentric disk in the upper wall of a rotating (at Ω) cylinder, non-axi-symmetric disturbances travelled along the resulting shear layer. For the typical Ekman numbers of the present work, Hide found the instability to occur for $\epsilon > .02$. Similar disturbances were not observed in the present experiments.

In the literature, the spin down experiments in a rotating cylinder are the most comparable to the present observations. During spin down, the inner fluid continues to move at the original rotation rate for a short time, thus replicating to some extent the radial profile seen in figures 4.2 - 4.11, at the outer radii. In his spin down experiments, Greenspan (1968) found axially symmetric Taylor vortices near the outer wall in the initial stages. Although some features of the low Reynolds number wave are similar to this instability, a direct analogy to Couette flow is not possible. The lack of a rigid inner cylinder and the characteristic frequency of the waves prohibits an exact comparison.

6.3.   Inertial Oscillations

Inertial waves were frequently observed in the fluid interior. Their detection at a specific radial position was a function of the local Reynolds number, or more specifically the onset of Ekman layer instabilities at an inner radius. When Re_J (Re_L at R = 6.00", see section 5.4) was below 48, no interior waves were observed. However, for Re_J = 50, inertial oscillations were recorded at all interior radii less than 12.5" (r = 0.51). Furthermore, no significant wave motion was observed at R = 15.45" and 21.00" until Re_J had surpassed 61 and 75, respectively. The first appearance of these waves corresponded to the initial instability of the Ekman layer. We observed (in section 5.5) that this instability occurred for $Re_L \sim$ 50. As the maximum Reynolds number for the tank was found to be close in value to Re_J, this generation mechanism is further confirmed. The absence of inertial waves at outer positions can only be attributed to a loss of wave energy, this resulting from reflections at the horizontal walls.

In section 5.6 we found the typical radial wave length of the dominant inertial wave to be 5cm. Incorporating the other cross-correlation results with this value, we obtain the (r, θ, z) wave numbers as (10,3, 1) for the dominant wave and (10, 1, 2) for the secondary peak. Calculating the non-dimensional frequency of such inertial waves gives values of 0.09 and 0.18. Signficantly, these frequencies correspond to the extrapolated (non-advective) wave frequencies in figure 5.14. Although other modes exist (with much lower amplitudes), we find the two dominant waves to be standing inertial oscillations

with the above wave numbers. The axial wave numbers were inferred

from the observed frequencies, as no actual measurements were taken.

Although the wave length of the Class A Ekman layer instabilities

was not measured presently, Tatro (1966) has observed it to be 28δ .

Since δ = 0.18cm for the results of section 5.4, a typical wavelength

is estimated to be 5.2cm. This length corresponds to radial wavelength

of the generated inertial wave. Also, we might expect the azimuthal

wave number of the generated inertial oscillations to be small since

the Class A waves are found by Tatro to be almost axi-symmetric (i.e.,

low azimuthal wave number).

The observed inertial oscillations showed frequency shifts

at different radii, this resulting from Doppler effects. Previous

experimenters have attributed these shifts to the existence of other

waves. The results of figure 5.14 discount this hypothesis.

6.4.   Boundary Layers

In a theoretical work, Lewellen (1965) found that it was not

possible to match an Ekman layer to an interior circulation that de-

creased with increasing radius. He also found that a constant cir-

culation was weakest radial dependence possible for matching. The

presently observed Ekman layers show no consistent change in thickness

for varying interior flow conditions. However, the vertical dependence

of the boundary layer wave characteristics was found to depend on the ra-

dially distributed circulation.

In general, the observed Ekman layer(δ)are found to be 80 - 85%

of the theoretical scale height. Only in the high Reynolds number

range is a significant decrease of boundary layer thickness noted.

Much of the previous work in Ekman layer instabilities has erroneously used thicknesses of two to three times the correct value.

The Ekman layer non-linear modification theories have underlying inconsistencies in their analysis and thus are not subject to comparison.

The existence of sidewall boundary layers at the source and sink confirms theoretical prediction. The characteristic width of these layers was found to be larger than that obtained from linear theory. The boundary layer adjacent to the source is approximately one and a half to two times as wide as that adjacent to the sink. The slight non-linear modification observed on the inner wall boundary layer is not explained by previous non-linear theories. The non-dimensional inner boundary layer width is approximately 0.13, whereas the outer layer is 0.18.

6.5   Flows in a Rotating Source Sink Annulus

The flows observed in a rotating source sink annulus were found to depend critically on the local Reynolds and Rossby numbers. For ϵ_{sys} less than .05 and Re_J less than 40, a constant interior circulation profile was obtained. The Ekman layer thicknesses were 85% of the theoretically predicted value. The width of the sidewall boundary layer adjacent to the sink conformed to linear prediction, whereas the source boundary was 1 1/2 times this value. The only detectable wave motion was the low Reynolds number wave, which was found to extend through the outer half of the annulus.

A marked change became apparent at $Re_J = 50$. At this value, a Class A Ekman instability was observed over a narrow radial range. The introduction of this instability into the flow generated inertial wave motion in the interior with a similar wavelength to that of the Class A waves. These inertial waves were not apparent at the outer radii. However, a small change in the radial dependence of zonal velocity was observed. Through a non-linear interaction of the inertial waves with the Ekman layer, a weak shear layer was produced in the interior. This was evidenced by a linear increase in circulation with radius (over a narrow range). The low Reynolds number waves were found to decrease rapidly in amplitude within the range of this circulation change. The Ekman layer thicknesses were unaltered, except for the area of the instability, in which a decrease was noted. The sidewall boundary layers increased slightly in width for these higher Rossby number flows. The induced Ekman layer divergence produced an immeasurable vertical velocity (1% of zonal velocity).

These changes became more pronounced with increasing Reynolds and Rossby number. For $Re_J > 75$, the inertial wave motion was found in all interior areas of the annulus. Although large changes were apparent in the observed frequency of these waves for the different flow rates, the values could be interpreted by incorporation of Doppler effects. In the interior, only two dominant inertial waves were apparent in most cases. On increasing Re_J past 89, the low Reynolds· number was found to exist only as a secondary peak. For $Re_J > 100$, the wave had an insignificant amplitude. In this Re_J range, the shape of the circulation profile did not change with Re_J.

By greatly increasing the local Reynolds number, an orderly (slow) onset of turbulence was generated within the Ekman layers. However, in the same Re_J range, a similar response was not detected within the Ekman layer of the sink sidewall boundary layer. At this position, only a single wave similar in frequency to the Class A instability, was observed.

At present, the above description represents the most complete analysis of flow characteristics in a rotating source sink annulus, for linear, non-linear and turbulent regimes. Previous work has failed to simultaneously observe the sidewall and horizontal boundary layers, and their influence on the steady and transient motions of the interior. Through the present work, the relation of Ekman layer instabilities to observed changes in circulation and the internally generated wave structure is elucidated. However, the actual forcing of the inertial waves ($\sigma < 2\Omega$) by the instabilities ($\sigma > 2\Omega$) is not readily solvable. The onset of Class A instability occurs at $Re_J \sim 50$. Previous workers have incorporated erroneous Ekman layer thicknesses in calculating the actual value of the critical Reynolds number.

6.6.   Geophysical Relevance

The nature of the present experiments lends itself to applications in the area of strong vortices in nature. The actual structure of the Ekman layer and its influence on the interior flows is also a relevant consideration. The laboratory-produced Ekman layer instabilities excite inertial waves which in turn are found to interact in non-linear fashion with another Ekman layer. This produced a

modification of the interior flow. These alterations of the mean flow may be of importance in both atmospheric and oceanic motions. Recently, Brown (1970) has interpreted secondary flows in the planetary Ekman layer as the cause of some observed atmospheric phenomena (such as cloud patterns).

The instabilities noted at the outer radius, as well as the weak internal shear layers, may find application in the study of the geomagnetic field created by motions in the earth's core (Malkus[1967]).

The influence of stratification and higher frequency motions appears to lessen the direct applicability of the steady and transient Ekman layer observations to related oceanic work. However, Gonella (1968) has observed a boundary layer that closely resembles the predictions of linear Ekman theory, under certain climatic conditions.

6.7.   Future Work

Although time consuming, detailed observations of the actual interior circulation and the radial distribution of Ekman layer thickness for each spectral result, would be beneficial. This would give an improved delineation of the abrupt changes occurring in the observed motions. Also, further work is needed in the area of instability wave structure. The confusion arising from the work of Tatro and Caldwell and van Atta in classifying the two types shows this necessity. This would also allow a clearer view of the actual generation mechanism of inertial waves.

A further analysis of the low Reynolds number at high system Rossby number could be accomplished by filling the inner radial region of the tank with foam, so as to give a tank aspect ratio of 1. With this configuration, inertial waves would be unable to influence these observations over a wide range of ϵ_{sys}.

The onset of turbulence in the Ekman layer and the transient interior response to changes of flux are topics of much interest and require extensive work.

APPENDIX I

Experimental Set-up and Methods

AI.1   The Rotating Source-Sink Annulus

The basic apparatus used in these experiments is a rotating axi-
symmetric annulus with a sink located peripherally on the inner radius.
Similarly, a source is placed on the periphery of the outer radius.
The source and sink are composed of porous reticulated poly-urethane
foam, the latter placed firmly over a porous metal spool and the former
cemented to the upper and lower walls at the outer most radius. The
upper and lower horizontal surfaces are parallel polished aluminum
disks, each of thickness one-half inch. The central spool is attached
to a concentric hollow pipe (and the rotation axis), which in turn
supports the apparatus and provides an exhaust for the induced flow.
A radial pressure gradient is imposed by a vacuum system connected to
the termination of the hollow pipe. A schematic plan of the annulus
and associated hardware was given in figure 3.1.

The annulus shown is designed to rotate about the vertical line
passing through its axis. Careful machining assured that the annulus
was axi-symmetric about its rotation axis, thus eliminating extran-
eous flow disturbances (Thompson, [1968]). The horizontal walls were
maintained parallel by four adjustable connecting spacers located at
the outer radius.

AI.2   The Rotation Control

The tank was rotated by means of a DC motor (1/2 hp) connected

to a speed control unit (Minarik SH-63). Rotation rate could be main-
tained at a constant value for periods up to two hours, with changes

less than that resolvable by the counter circuit (0.5%). For compar-
ative purposes, the rotation rate could.be reproduced at a later date

by use of the fine torque control of the speed unit. As seen under-
neath the tank in figure 3.1, the rotation rate was measured by a

photoelectric counter, tripped by a light source penetrating any one

of the fifty evenly-spaced small holes on an aluminum collar. The

results were displayed on a pre-set counter.

AI.3   The Flux Control

     The technique of obtaining a substantial range in radial pres-

sure gradients was similar to that used by Green (1968). This sub-

system consisted of a calibrated flux meter, baffle, perforated

cylindrical sleeve and an axial fan connected sequentially from the

hollow exhaust pipe of the tank. The calibrated flux meter consists

of a hot wire probe mounted in the wake of a small cylindrical rod

extending across the pipe's diameter. The flow passes through a num-
ber of rectifying screen before impinging on the rod. Above a certain

Reynolds number, a Karman vortex street is formed behind the cylinder,

the shedding frequency of which is measureable by the hot wire. Using

an American Meter Corporation standard bell-type proof meter (accu-
rate to 0.5%) as an absolute volume flux calibrator, Green (personal·

communication) found the flux was linearly related ($\pm$ 1.5%) to the

shedding frequency. The relation, $S = 218 + 13.7\eta$, gave the volume

flux S in cc/sec., when η (shedding frequency) was measured in hertz

(for rod diameter 0.182cm). Changes in flux were obtained by altering

the vacuum suction mechanically or by changing the covered area of the

perforated sleeve at a constant suction, the latter resulting in a

change of the differential pressure provided by the fan. A discussion

of the advantages and disadvantages of such a system is found in

Green (1968).

AI.4   Probe Configurations

For all the veolcity measurements, hot wire anemometer probes

were used. A great variety of probe configurations were employed, as

seen in figure AI.1. The simple (single) hot wires are similar to

those used by many previous experimenters. The boundary layer probe,

is of similar nature but has a small leg which protects the wire from

damage by collision with the boundary and gives an exact vertical ref-

erence height. The vertical distance between the hot wire and the

bottom of the leg was measured optically with a toolmaker's compara-

tor (accurate to the nearest one-thousandth of an inch). The extend-

ed arm probe was built to allow measurements of interior velocity for

a wide range of radius under identical operating conditions. The

plug-in probes were similar hot wires to those above, but were mounted

in plexiglass inserts, which could be positioned in the bottom of

the tank. The probe positions noted in figure 3.1 readily shows the

possible positions of the different designs. The mobility of the

top-mounted probes is seen in figure AI.2, as well as their relative,

position to those mounted on the bottom plate.
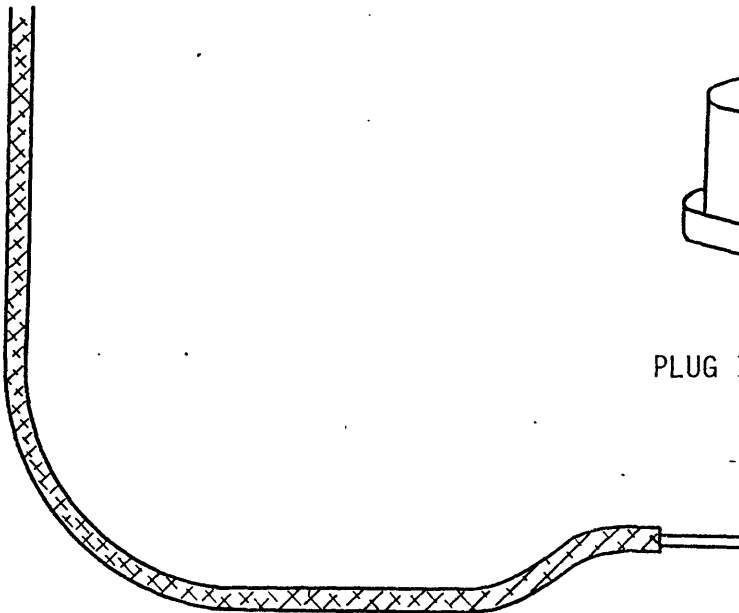
Through the use of mechanical sliprings, small motors were ut-

ilized to change the orientation of the top-mounted probes through

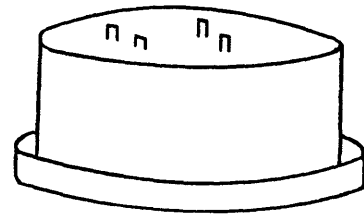360° about their own axis while the tank is rotating. A tank mounted

SIMPLE HOT WIRE

BOUNDARY LAYER PROBE
WITH PROTECTOR

PLUG IN HOT WIRES

EXTENDED SINGLE HOT WIRE

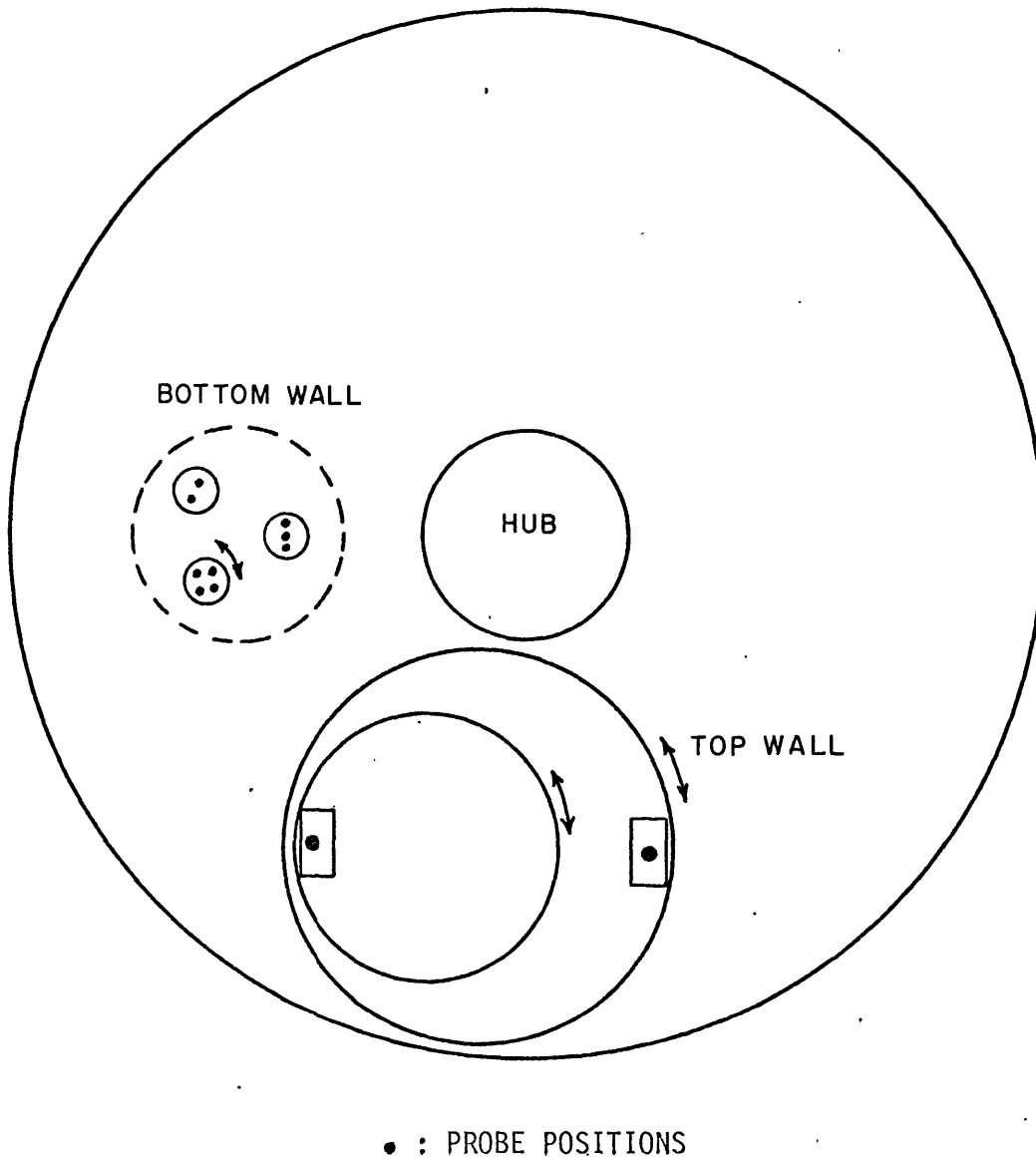FIGURE APPENDIX I.1 - PROBE DESIGNS

FIGURE APPENDIX I.2 - PROBE MOBILITY

potentiometer was used to measure the angular changes. In a similar fashion, the probes may be vertically raised or lowered, with the height changes measured by a trip switch, each pulse being equivalent to 3.31 x 10^{-3}mm. This allowed for a thorough examination of the vertical boundary layers, although their thickness was only of order 2mm.

The radial position of the top-mounted probes was calculated using the angular position of the probes relative to the tank surface. The two eccentric inset plates were each divided into 360 degrees, and the angular position of the inner disk relative to a reference point on the outer disk recorded. The position of the outer plate relative to the tank surface was determined by a similar technique. With this set-up, it was possible to calculate an accurate position for both probes knowing the geometrical constants of the tank and the two reference angles. Comparison of these values with those measured manually demonstrated the geometrical method to be far superior, especially at large radii. Positioning of the bottom plug-mounted probes was not amenable to this technique, although their low profile facilitated mechanical measuring. In spite of their mobility, the probes do have limitations in their relative positions. Consequently the top probes cannot occupy identical radii for certain comparative flow studies (cross-correlations). All probe sensors were self-manufactured using 9 micron tungsten wire and have typical cold resistances of order 2 ohms.

AI.5   Hot Wire Anemometers and Related Equipment

Throughout this work, DISA Type 55D05, battery operated constant temperature anemometers have been used. These units measured

the amount of power required to keep the probe sensor temperature constant. The forced convective heat loss by flow of air around the probe sensor was calibrated against the velocity of the incident flow. For flow speeds greater than 30 cm/sec. in air, a linear relation was found between the square of the bridge voltage (needed to keep temperature constant) and the square root of the flow velocity. In this velocity range, it was possible to calibrate the probes in a manner similar to Tatro (1966), using a large wind tunnel (figure AI.3). By observing the shedding frequency of various cylindrical rods placed in front of the sensor at different flow velocities, a calibration curve was obtained. This procedure failed in the lower velocity range frequently obtained during the present experiments. Using the basic idea of Almquist and Legath (1965), a new and different type of low velocity wind tunnel was built, as shown in figure AI.4. Essentially, a water and ethyl glycol mixture was forced by a constant pressure head into a sealed erlenmeyer flask, and the evacuated air from the flask was then passed through a number of rectifying straws and screens in a small test section. The sensor to be calibrated was positioned at the end of this section. Baffles were placed at a sizable distance around the sensor and test section to prevent extraneous flows from interfering with the forced flow. By measuring the volume of fluid deposited in the flask during a given time interval, one obtained the flow rate of air through test section. Significantly, this technique gave much more consistent calibrations for velocities of 1 cm/sec. to 100 cm/sec. than other methods. Furthermore, this technique showed that the anemometers can consistently resolve better than 1 cm/sec. in the range of 1 to 25 cm/sec. in air. According to the manufacturers, the DISA units have
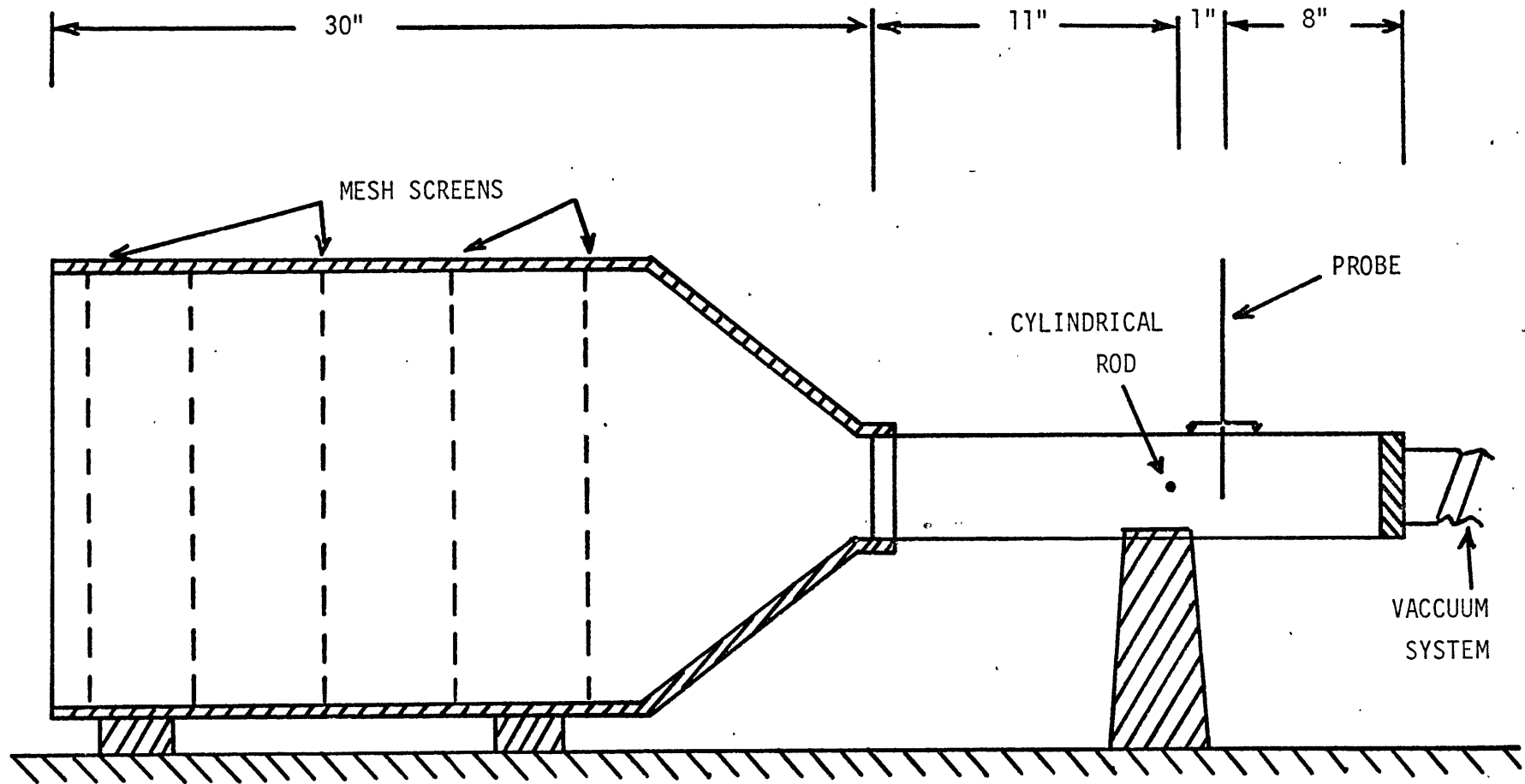
FIGURE APPENDIX I.3 – HIGH VELOCITY WIND TUNNEL
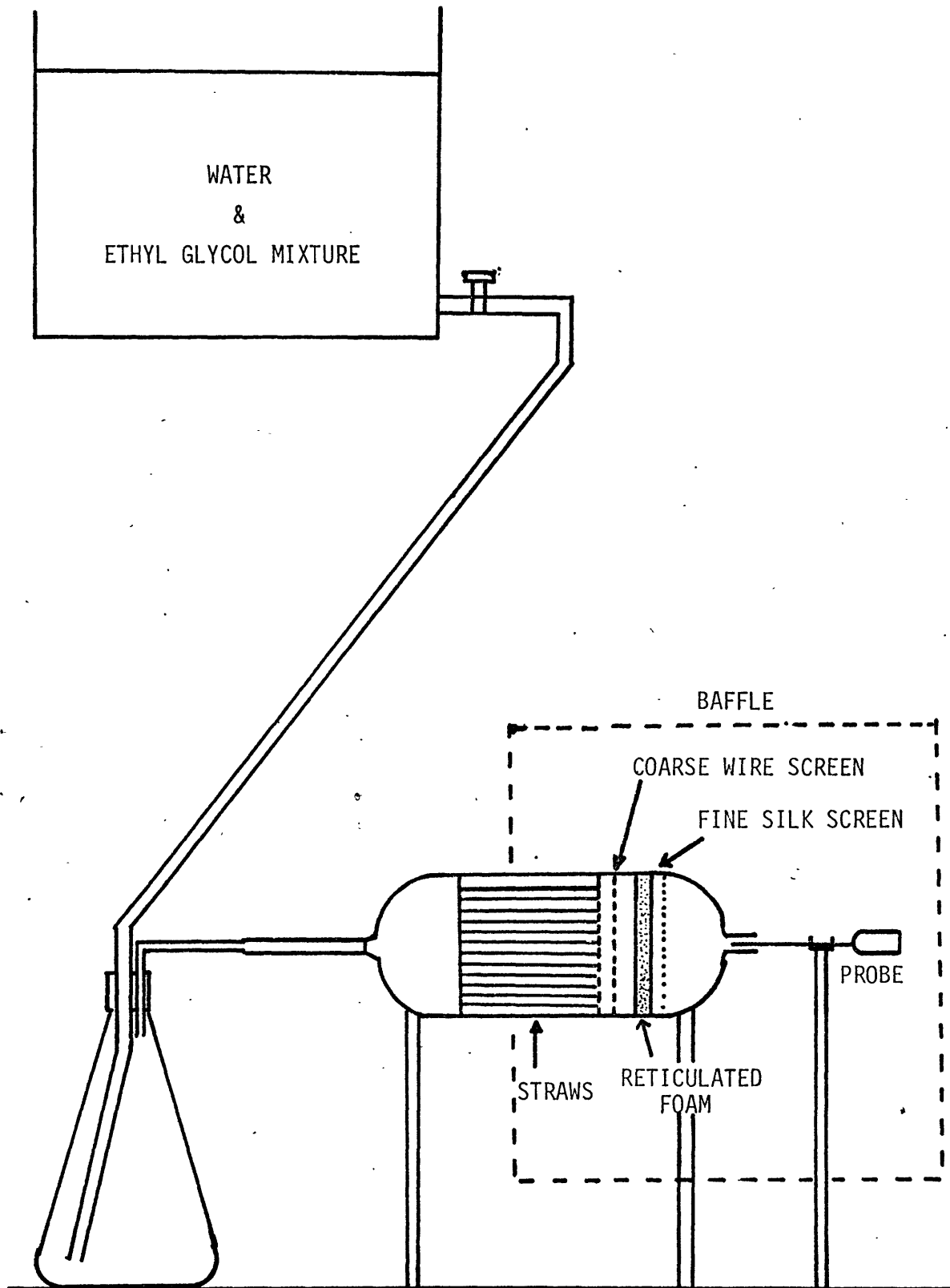
FIGURE APPENDIX I.4 - LOW VELOCITY WIND TUNNEL

an upper frequency limit in the range of 50 kHz for the configu-
ration employed in these experiments.

A schematic representation of the equipment used was given in
figure 3.2. The twelve mercury wetted sliprings (Rotocon type MKD13)
were electrically noiseless (virtually), which assured that the probe
signal was relayed from the rotating frame to that of the laboratory
with no loss of clarity.

In order to discriminate small velocities, it was necessary that
the zero velocity output of the anemometer (DC voltage) be removed
prior to signal amplification. This was accomplished through the use
of the bias units. Two types of DC amplifiers were used in these ex-
periments - the Kintel model 190 (six units) and four DANA units.
The former have an amplification range of 20 to 1000, whereas the
latter, 30 to 1000.

AI.6   Auxiliary Equipment

Filters: Five simple low pass R-C filters (40 Hz) were used at
the output of the amplifiers and prior to recording stage.

Two Rockwell 1010F Operational Filters were used for
low frequency band pass work connected with auto- and cross-correla-
tions.

Correlation Function Computer: The Princeton Applied Research
model 101 was used, which allowed a great deal of flexibility and para-
meter range. Both auto- and cross-correlations were computed. The
computer had a frequency range from DC to 250 Hz with an error of less
than 1/2%.

Fourier Analyzer: Princeton Applied Research model 102, which

operates in conjunction with the correlation function computer to pro-
duce quadrature and co-spectra of the input waves used. The useful
frequency range was dependent on the correlator setting, but was of
order 0.25 to 495 Hz with less than 1% error.

Tape Recorders: An 8-Channel, Precision Instrument, Model PI-
6200, magnetic tape recorder, with three recording speeds was em-
ployed. The data were read into the correlator at a speed ten times
greater than that of the recording rate. The usual mode of infor-
mation storage was a tape loop which contained 5 minutes (minimal-
ly) of data at the lowest recording speed (.375 inches/sec.).

Function Generator: A low-frequency function generator (Hewlett-
Packard model 202A) was used to produce a Lissajous figure, for mea-
suring the shedding frequency of the flux monitoring system for var-
ying rates. It was also employed in calibration tests of the cor-
relator and fourier analyzer.

Pre-Set Counter: A Universal Pre-set counter, model 2019 was
used to display the rotation rate and period count, the latter being
more accurate.

Oscilloscope: A Tektronix Model 502A Dual Beam Oscilloscope was
used to monitor velocity fluctuations and some of the mean velocity
data.

X-Y Plotter: A Mosley model 2D-2 X-Y Plotter graphed final
spectra, auto- and cross-correlations, as well as the output of the
extended probe versus sensor orientation.

Pen Recorder: A Sanborn Model 67-300 four channel pen recorder
was used to record voltage fluctuations, transient responses, hyster-
esis effects, and to check for any long term D.C. drifts in the output.

APPENDIX II

Data Collection Methods

AII.1 Recording of Variables

Typically, the data recorded for each experimental run con-
sisted of the following (see also fig. AI.5),

(a) Instantaneous voltage output of operating hot wire ane-
     mometers, each having a known overheat ratio.

(b) Rotation rate of the tank.

(c) Flux rate, as indicated by the "flux" hot wire.

(d) Ambient temperature of laboratory, to be compared to
     calibration values.

(e) Angular position (local coordinates) of top-mounted
     probes and radial position of those bottom-mounted.

(f) Orientation of all probes relative to a perpendicularly
     impinging flat plane tangent to the local radius vector
     (by potentiometer output).

(g) Angular separation of all probes in azimuthal direction
     of annulus.

(h) Vertical separation of all sensors from the inner side of
     the bottom aluminum disk.

(i) Time of measurement.

AII.2 Mean Velocity Levels

AII.2.1 Interior and Side-wall Layers
         (a) General characteristics: the measurements of in-
         terior flows, with fixed probes, were found to have a cri-
         tical dependence on ambient temperature. To avoid this un-
         wanted variability, a continuous profile scheme was effected.

(b) Probe location: These runs were made at a height
of 12cm from the bottom (i.e., at the vertical midpoint
of the tank for numerous radii. The aim was twofold:
to quantify the influence of various flow configura-
tions in altering the interior velocity structure, and
to describe the side-wall layers. The usual method was
to run an experiment at a constant rotation rate for a
series of fluxes, and alternately at a constant flux for
varying rotation. In this manner, the effect of systema-
tically altering the Reynolds, Rossby and Taylor number
could be interpreted.

(c) DC drift: For all probe calibrations and measure-
ments, the output voltage was initially adjusted to zero
for a "no flow" condition (i.e., free convection). After
the completion of a run, velocity output was rerecorded
to verify that no significant dc drift had occurred from
the original zero position.

(d) Ambient temperature changes: The influence of
ambient temperature changes on any individual series,
with single fixed probes, was insignificant. The recor-
ded differences did not exceed 0.2°C. The major diffi-
culty came on comparing a particular series against
another set, at a different radius, taken at a later time.
In this case, the influence of temperature change was
important for the lower velocities, obtained at the outer
radii (Rasmussen, 1965). The temperature range experien-
ced over all runs was ± 1.5°C from the mean. According

to Rasmussen, such a fluctuation can introduce.
changes of approximately 5-10% for the lower velocities,
and a smaller difference at higher magnitudes (of velo-
city). These errors in the radial distribution of velo-
city were avoided by use of the extended single probe.
This sensor allowed for complete mapping of the interior
velocity field within a relatively brief time. The influ-
ence of temperature change was insignificant during each
series. Obviously, the probe must always have a shaft
component directed upstream to avoid any spurious wake
effects.

(e) Flow direction: The interior mean velocities
measured were azimuthally directed. Using a single fixed
probe, numerous tests verified that the interior flow
was zonal in nature, within the error bounds of the
directional sensor (potentiometer). In a more defin-
itive experiment, Tatro (1966) found the interior <u>radial</u>
transport to be less than 2% of that predicted for the
Ekman layer transport, using an annular configuration.

AII.2.2 Ekman layer

(a) General flow characteristics: The steady-state
observations taken in the bottom boundary layer were
very similar in nature to those of the interior, and
thus subject to the same errors. Of course, the impor-
tance of vertical positioning in the determination of
boundary layer structure was paramount. The Ekman layer

measurements differed from those in the interior, in
that the velocities near the bottom of the layer were
small, and secondly, the influence of an aluminum plate
in close proximity to the probe caused it to respond in
an anomalous fashion.

(b)   Flow speeds: In a majority of experiments using
constant temperature anemometers the velocities were of
a much higher magnitude than those encountered presently.
Figure 4 of the DISA manual (1969) shows the mean response
of tungsten hot wire probe to flows at a varying angle
of incidence for a flow of 3000 and one of 6000 cm/sec.
On careful analysis of the response for incidence angles
approaching $\pm$ 90° from the perpendicular, the output was
found not to be zero, but instead 7 or 8% of the maximum
output (for 3000 cm/sec and an overheat of 0.8). This
response was due to a "side-wise" forced convection, and
became quite influential at lower velocities. At the
low speeds encountered in the boundary layer, this dis-
crepancy may account for a "velocity" of up to 40% of
the maximum value, recorded at perpendicular incidence
with corrections for free convection. This effect was
found by using the high-velocity wind tunnel (figure AI.3).
The distortion greatly complicated the detection of the
small radial component in the Ekman flow. At greater
heights in the boundary layer accurate separation of the
flow velocity into two directions was a critical function
of probe orientation. The small angle formed with zonal

direction was difficult to estimate. For these reasons
a majority of the results shown display only the azimu-
thal component's structure within the Ekman layer. Al-
though it was possible to calibrate each probe for a
known flow at a variety of incidence angles in the high
velocity tunnel, the low velocity wind tunnel design
did not allow such modifications. Thus, in the present
case, the low velocities inherent in an Ekman layer
were not amenable to calibration as a function of probe
direction for small fluxes and/or large radii.

(c)   Low speed calibration: The influence of cali-
brating a probe in a flow, parallel to the probe shaft
(top mounted) and thereafter using the sensor to detect
flows perpendicular to the holder was unimportant. The
differences found by Rasmussen (1965) resulted from the
impinging flow (forming various angles with respect to
gravity. However, in the present case, the flow was
perpendicular to the local gravitational field for all
top-mounted·probes, both in calibration and operation.

(d)   Boundary heat losses: Another influence on record-
ed voltages in the boundary layer was the proximity
effect of the wall. Wills (1962) made an extensive
study of such effects as a function of wire diameter,
overheat ratio and flow rate. In the present case, the
ratio of minimum distance from the wall (leg length) to
that of wire radius was 140, and for this value the influ-
ence of velocity on the corrections was negligible for

flows greater than 4.5cm/sec. Nevertheless, there was

an "extra heat loss", as applied by Dryden (1936), inde-

pendent of velocity. This influence was felt at distan-

ces less than 1.35mm from the plate (for an overheat of

0.7 and wire of diameter 9μ) and was largest at the

smallest heights. The normal routine for boundary layer

observations included running the probe with no flux

or rotation from the lowest position to a height, at

which changes in apparent heat loss ceased. This cor-

rection (in voltage) was then applied to the values ob-

tained under operating conditions. Failure to do this,

resulted in an anomalous velocity structure which in-

creased with decreasing height, as found by Green and

Mollo-Christensen (1970). Since other workers have

used a variety of materials as horizontal walls in

their annuli, a short comparative study of the various

heat losses is presented in Appendix III.

AII.3 Wave Motion Analysis·

(a) Signal decomposition: The structure of the fluctuating

component was usually complex, consisting of a number of

different waves. These signals were decomposed, using an

analog fourier analyzer. In these cases, the mean velocity

was removed from the signal before amplifying the wave com-

ponent. Using this method, spectra of wave motions for num-

erous Reynolds and Rossby number combinations were possible.

Similar techniques were employed for readings both within

the boundary layers and the interior. For each recording, · the tank was allowed to run for fifteen minutes prior to a five and a half minute recording interval. The spin-up time for the tank was of order thirty seconds. A comparison of spectra taken sequentially for the same flow, showed that after an initial period of ten minutes, the spectra were invariant with time.

(b) External influences: External influences were significant, and their minimization was crucial for the reliability of spectra. Two prevalent disturbances were quick motions of the experimenter in close proximity to the tank and secondly, the slamming of doors and similar motions. These disturb the flows by producing an abrupt pressure fluctuation on the outer wall. None of the results in the present work were subject to these disturbances.

(c) Cross-correlations: The signals to be cross-correlated were recorded simultaneously on an 8-track tape recorder. Subsequently, the individual signals were analyzed for their dominant wave energies as a function of frequency. Using accurate Rockwell band-pass filters, waves of a certain frequency were isolated at the various sensors and cross-correlated separately. A description of wave structure was accomplished using this technique.

AII.4 Transitory Experiments

In Appendix IV some spin-up and "flux-up" experiments are presented. The time required to change both rotation and flux were short in

duration (usually one second), as compared to the spin-up time

(Ts = $[H^2/\nu\Omega]^{1/2}$, where H was tank height). The flux was altered using

the vacuum motor control, whereas the rotation changes were applied

through speed control brake and external mechanical means. This method

was limited to "spin down to" or " spin up from" rest, both with and

without a superimposed flux. The response was recorded on the four chan-

nel pen recorder, each transient being monitored at two different

radii. The large inertia of the tank prevented incremental rotation

changes.

AII.5 General Comments

The segments recorded on a tape loop over an interval of five

minutes were analyzed at a speed greater than the recording rate by

a factor of ten. This technique had two advantages: greater pre-

cision in filtering the signals (i.e. at higher frequencies) and

utilzation of the fourier analyzer at frequencies much larger than

its low cut-off.

All wave traces obtained had voltage rather than velocity as

ordinate. Similarly, the fourier analyzed signal was the fluctua-

ting voltage component with the dc level removed. Although there was

a non-linear relation between voltage and velocity, the wave size was

sufficiently small to preclude any extraneous peaks greater than 4%

of the dominant wave amplitude.

All final data were punched onto data cards for use in the

IBM 360 digital computer. Both steady and unsteady results were so

analyzed, and corrections applied if necessary (i.e., wall losses).

APPENDIX III

Wall Proximity Effects

As discussed in appendices I and II, anomalous velocity profiles were
obtained when using a hot wire probe in close proximity to a solid boundary.
The Exman layer results of both Tatro (1966) and Green (1968) showed this
influence to be significant for vertical distances comparable to the boun-
dary layer thickness (2 mm). In contrast, Caldwell and van Atta (1970)
observed no heat losses above a height of 0.2 mm. Including the present
annulus, we found that three different materials have been used as horizon-
tal walls. Since the substances have differing thermal properties, a com-
parison of individual influence on a hot wire probe was made.

Table AIII-1 shows the voltage change (from zero) resulting from a
hot wire probe positioned 0.64 mm from a flat piece of each test material.
The relevant authors are mentioned with the appropriate wall materials.

TABLE AIII-1

Proximity Losses for Various Boundary Materials

Arbitrary Constant Signal Amplification (X50).

z = 0.064 cm

Material	Voltage Change	Thermal Conductivity (CGS)
(Air)	(0.0)	(.0006)
Plywood (Caldwell & Vanatta)	0.20	.003
Plexiglass (Tatro)	0.32	.002
Aluminum (Ingram, Green)	0.39	.500
Masonite	0.26	.001
Stone	0.44	.056

Although the plywood walls produce the least distortion of those

compared, corrections are still necessary. The most surprising result is the minor difference in losses between plexiglass and aluminum. The contrasting conductive properties of these two materials dictates a different mode of heat loss. Aluminum, being a good conductor, must take the heat away from the area immediately under the probe. On the other hand the plexiglass wall is heated locally and forms a "hot-spot". The free convection field generated by this zone distorts the velocity observations above it. From Tatro's work the influence is found to exist at a height of minimally 2 mm, even with a horizontal velocity field.

From Caldwell and van Atta's findings, it can be surmised that plywood responds in a completely different manner than plexiglass to the presence of a heated probe.

In summary, no systematic difference in heat loss is attributable to the conductive properties of the boundary wall. It should be remarked, however, that the above measurements were taken with no flow. According to Wills (1962), for the typical velocities observed, the results should not differ substantially in heat losses.

APPENDIX IV

Transient Response Times

Table AIV-1 shows the experimental data obtained under conditions of changing flux and rotation. The time intervals (ΔT) were measured between consecutive steady state interior mean flows. As a means of comparison, the spin up time (Greenspan and Howard [1963]) for each configuration is included in the chart. The arrows indicate the direction of parameter change.

TABLE AIV-1

System Response to Step-Function Changes

Flux (cc/sec)	ROT (rad/sec)	Spin Time (sec)	ΔT(R=12.4")(sec)	ΔT(R=18")(sec)
0	0 → 2.70	37	40	40
0	2.70 → 0	37	56	48
902	0 → 2.70	37	25	27
902	2.70 → 0	37	64	58
1848 → 1141	2.65	38	37	39
1114 → 1848	2.65	38	37	38
1630 → 1081	3.89	31	26	29
998 → 1630	3.89	31	26	26
1526 → 941	5.52	26	24	24
1040 → 1526	5.52	26	21	20
2136 → 2410	2.65	38	24	25
1753 → 2136	2.65	38	23	23

$$\text{Spin Time} = \left(\frac{H^2}{\nu\Omega} \right)^{1/2} = \frac{H}{.394\Omega^{1/2}}$$

For spin up from rest, no significant difference in response time was detected at the two probe positions. With no imposed flux, the measured delay time was comparable to the spin-up time (T_s), whereas with a constant flux, much shorter lags were observed. A much longer response time (than T_s) was recorded in the spin down to rest experiments (no flux). The influence of an imposed flux was to increase ΔT.

Only for low rotation and flux were the "flux-up" and "flux-down" times similar to T_s. Other combinations of the system parameters consistently gave smaller values of ΔT (than T_s). The observed differences are not readily related to either the Rossby or Reynolds number.

REFERENCES

Almquist, P. and E. Legath (1965): The hot wire anemometer at low air velocities. DISA Information No. 2, 3-4.

Arons, A.B., A.P. Ingersall and T. Green (1961): Experimentally observed instability of a laminar Ekman layer in a rotating basin. Tellus 13, 31-39.

Barcilon, V. (1965): Stability of Anon Divergent Ekman layer. Tellus, 17, 53-68.

Barcilon, V. (1970): Some inertial modifications of the linear viscous theory of steady rotating fluid flows. Phys. of Fluids, 13, 537-544.

Brennecke, W. (1921): Die ozeanographischen Arbeiten der Deutschen Antarktischen Expedition, 1911-1912. Arch. dt. Seewarte, 39, 208.

Brown, R. (1970): A secondary flow model for the planetary boundary layer. J. Atmos. Sci. 27, 742-757.

Busse, F. (1968) Sheer flow instabilities in rotating systems. J. Fluid Mech. 33, 577-589.

Caldwell, D. and C. van Atta (1970): Characteristics of Ekman boundary layer instabilities. J. Fluid Mech. 44, 79-95.

Chandrasekhar, S. (1961): Hydrodynamic and hydromagnetic stability. The Clarendon Press, Oxford.

Coles, D. (1965): Transition in Circular couette flow. J. Fluid Mech. 21, 385-425.

Day, C. and F. Webster (1965): Some current measurements in the Sargasso Sea. Deep Sea Res. 12, 805-814.

Dryden, H. (1936): Air flow in the boundary near a plate. NACA Tech. Report No. 562.

Dudis, J. and S. Davis (1971): Energy stability of the Ekman boundary layer. J. Fluid Mech. 47, 405-413.

Ekman, V.W. (1905): On the influence of the earth's rotation on ocean currents. Ark. Mat. Astr. FYS 2, 1-52.

Faller, A. (1963): An experimental study on the instability of the laminar Ekman later. J. Fluid Mech. 15, 560-576.

Faller, A.J. and R.E. Kaylor (1966): A numerical study of the laminar Ekman boundary layer. J. Atmos. Sci. 23, 466-480.

Ffwocs Williams, J., S. Rosenblat and J. Stuart (1969): Transition from laminar to turbulent flow. J. Fluid Mech. 39, 547-559.

Fultz, D. (1959): A note on overstability and the elastoid-inertia oscillations of Kelvin, Solberg and Bjerkness. J. Meteorol. 16, 199-208.

Gonella, J. (1969): Analyse des mesures de courant et de vent a la bouee-laboratoire (position B). Cahiers Ocean. 19, 855-862.

Green, A. (1968): An experimental study of the interactions between Ekman layers and an annular vortex. Massachusetts Institute of Technology, Ph.D. thesis.

Green A. and E. Mollo-Christensen (1970): Laboratory observations of Ekman layer flow. Dept. of Meteorology, Massachusetts Institute of Technology, Report No. 70-4.

Greenspan, H. (1968): The theory of rotating fluids. Cambridge Univ. Press.

Greenspan, H. (1969): On the non-linear interaction of inertial modes. J. Fluid Mech. 36, 257-264.

Greenspan, H. and L. Howard (1963): On a time dependent motion of a rotating fluid. J. Fluid Mech. 17, 385-404.

Gregory, N., J.T. Stuart and W.S. Walker (1955): On the stability of three dimensional boundary layers with application to the flow due to a rotating disc. Phil. Trans. A 248, 155-199.

Gustafson, J. and B. Kullenberg (1936): Untersuchungen von Tragheits-stromungen in der Ostee. Sven. Hydr.-Biol. Kom. Sicr. Ny. Ser. XIII. Lund.

Hide, R. (1968): On source-sink flows in a rotating fluid. J. Fluid Mech. 32, 737-764.

168.

Hunkins, K. (1966): Ekman drift currents in the Arctic Ocean. Deep Sea Res. 13, 607-620.

Kelvin, Lord (1880): Vibrations of a columnar vortex. Phil. Mag. 10, 155-168.

Knauss, J. (1965): A technique for measuring deep ocean currents close to the bottom with an unattached current meter, and some preliminary results. J. Marine Res. 23, 237-245.

Lewellen, W.S. (1965): Linearized vortex flows. AIAA Journal 3, 91-98.

Lilly, D.K. (1966). On the instability of the Ekman layer boundary. J. Atmos. Sci. 23, 481-494.

Malkus, W. (1968). Precession of the earth as the cause of geomagnetism. Science 160, 259-264.

Pollard, R.T. and R. Millard Jr. (1970): Comparison between observed and simulated wind-generated inertial oscillations. Deep Sea Res. 17, 813-821.

Rasmussen, C. (1965): The air jet hot wire microphone. DISA Information No.2, 5-13.

Rayleigh, Lord (1917): On the dynamics of revolving fluids. Proc. Roy. Soc. London, A 93, 148-151.

Smith, N.H. (1945): Exploratory investigation of laminar boundary oscillations on a rotating disc. NACA Tech. Note 1227.

Stern. M.E. (1960): Instability of Ekman flow at large Taylor numbers. Tellus 12, 399-417.

Stewartson, K. (1957): On almost rigid rotations. J. Fluid Mech. 3, 17-26.

Swallow, J. and G. Bruce (1966): Current measurements off the Somali coast during the southwest monsoon of 1964. Deep Sea Res. 13, 861-888.

Tatro, P. (1966): Experiments of Ekman layer instability. Center for Space Research, M.I.T. Report No. CSR-TR-66-2.

Theodorsen, T. and A. Regies (1944): Experiments on drag of revolving discs, cylinders and streamline rods at high speeds. NACA Report No.793.

Thompson, R. (1967): An instability of the flow in a slightly tilted rotating glass of water. Geo. Fluid Dynamics (Woods Hole Oceanographic Institution) Report No. 67-54.

Webster, F. (1963): A preliminary analysis of some Richardson current meter records. Deep Sea Res. 10, 389-396.

Wills, J. (1962): The correction of hot wire readings for proximity to a solid boundary. J. Fluid Mech. 12, 388.

BIOGRAPHICAL NOTE

The author was born in Winwick, England on February 15, 1945. After immigrating to Canada, he graduated from St. Johns High School in June, 1961. Thereafter he received a B.S. degree in physics, June, 1965, and an M.S. in marine sciences, June, 1967, from McGill University in Montreal, Canada. His master's thesis work was a model for predicting the motion of sea ice in the Gulf of St. Lawrence. In the summer of 1967, he obtained Summer Student fellowship from the Woods Hole Oceanographic Institution. The following fall, he enrolled in the Department of Meteorology, at M.I.T. In May of 1970, he married the former Beatrix Wanke.